

410

PREPRINT / IN-42
AVAIL. CASE
112 322

Submitted to
JGR

Multiple GISS AGCM Hindcasts and MSU Versions
of
1979-1998

~~138p~~
138p
3994/3

Kathryn Pierce Shah, David Rind¹, Leonard Druyan, Patrick Lonergan² and Mark Chandler

Center for Climate Systems Research, Columbia University
NASA Goddard Institute for Space Studies
2880 Broadway, New York, NY 10025

¹ NASA Goddard Institute for Space Studies, Goddard Space Flight Center, New York, NY.

² Science Systems and Applications, New York, NY.

Abstract

Multiple realizations of the 1979-1998 time period have been simulated by the GISS AGCM to explore its responsiveness to accumulated forcings, particularly over sensitive agricultural regions. A microwave radiative transfer postprocessor has produced the AGCM's lower tropospheric, tropospheric and lower stratospheric brightness temperature (T_b) time series for correlations with the various Microwave Sounding Unit (MSU) time series available. MSU maps of monthly means and anomalies were also used to assess the AGCM's mean annual cycle and regional variability. Seven realizations by the AGCM were forced by observed sea surface temperatures (sst) through 1992 to gather rough standard deviations associated with internal model variability. Subsequent runs hindcast January 1979 through April 1998 with an accumulation of forcings: observed ssts, greenhouse gases, stratospheric volcanic aerosols, stratospheric and tropospheric ozone and tropospheric sulfate and black carbon aerosols. The goal of narrowing gaps between AGCM and MSU time series was complicated by multiple MSU time series, by T_b simulation concerns and by unforced climatic variability in the AGCM and in the real world. Lower stratospheric T_b correlations between the AGCM and MSU for 1979-1998 reached as high as 0.91 ± 0.16 globally with sst, greenhouse gases, volcanic aerosol, stratospheric ozone forcings and tropospheric aerosols. Mid-tropospheric T_b correlations reached as high as 0.66 ± 0.04 globally and 0.84 ± 0.02 in the tropics. Oceanic lower tropospheric T_b correlations similarly reached 0.61 ± 0.06 globally and 0.79 ± 0.02 in the tropics. Of the sensitive agricultural areas considered, Nordeste in northeastern Brazil was simulated best with mid-tropospheric T_b correlations up to 0.75 ± 0.03 . The two other agricultural regions, in Africa and in the northern mid-latitudes, suffered from higher levels of non-sst variability. Zimbabwe had a maximum mid-tropospheric correlation of 0.54 ± 0.11 while the U.S. Cornbelt had only 0.25 ± 0.10 . Precipitation and surface temperature performance are also examined over these regions. Correlations of MSU

and AGCM time series mostly improved with addition of explicit atmospheric forcings in zonal bands but not in agricultural regional bins each encompassing only six AGCM gridcells.

1. Introduction

The extreme El Nino of 1998 has spurred research and funding agencies to sponsor cross-disciplinary work on climate impacts, particularly on agricultural, societal and economical impacts. Various groups have begun hindcasting and forecasting climate modeling efforts geared towards interaction with regional interests. The Climate, Agriculture, Fisheries and Environment (CAFE) group at the Goddard Institute for Space Studies (GISS) has hindcasts of the 1969-1998 period from an AGCM initially forced with observed sea surface temperatures (sst) and then with additional atmospheric forcings. The goal is to optimize hindcasting over agricultural regions sensitive to El Nino events, drive off-line agricultural, fishery and economic models and begin to integrate a forecasting sea-surface temperature model. One of the initial steps is to gauge the AGCM involved and determine agricultural regions that could be successful forecasts. Correct temperature and precipitation over the agricultural regions are needed to drive crop models. Three agricultural regions are considered: Nordeste in northeastern Brazil, within the tropical (20S-20N) zone and adjacent to the Pacific Basin; Zimbabwe in southern Africa, in the equatorial (30S-30N) zone and distanced by a continental landmass and the Atlantic Basin from ENSO forcing; and the U.S. Cornbelt, in the difficult, highly variable northern mid-latitudes (30N-50N). The synoptic mechanisms and precipitation responses to sst forcing over these regions were detailed in Druyvan et al. (1999). Cane et al. (1994) correlated Zimbabwe's maize yield production to ENSO ssts and Phillips et al. (1999) determined correlations of regional US cornbelt data to ENSO ssts. The AGCM's responses to sst and other forcings over these regions are assessed herein primarily with the well-publicized Microwave Sounding Unit (MSU) data, with in-house GISS global surface air temperature analyses (GISTEMP) and NOAA/NCDC archived station observations of precipitation values.

The MSU brightness temperature (T_b) datasets have caused controversy as temperature trends derived from it lack the warming trend found in meteorological station surface temperatures, other datasets and results of some climate models. The latter disagreement is at least partly due to climate models not incorporating known forcings. The AMIP I AGCM simulations, for example, occurred without variable ozone and greenhouse gas levels and without volcanic aerosol forcings. Work with a fast idealized-geography climate model (Hansen et al., 1995) began accounting for neglected forcings and found improved climate model and MSU agreement as simulated tropospheric temperatures cooled more than the surface temperatures with inclusion of observed lower stratospheric ozone depletion. Subsequent studies by Hansen et al (1997) included the forcings of stratospheric volcanic aerosols, ozone distribution changes and solar irradiance for the 1979-1996 period. This work builds on their study by using a slightly more developed AGCM, incorporating tropospheric aerosol impacts, extending the time period to April of 1998 and occasionally back to 1969, creating AGCM's T_b time series with explicit radiative transfer calculations, examining sensitive agricultural regions and considering the various MSU time series versions available.

Deep convection over warm, tropical sst forcing in a climate model is translated into a change in the tropical upper tropospheric flow and then translated into an extratropical tropospheric response. Boyle (1998) argues that different mean states of an AGCM will affect the extratropical responses to tropical ssts through varying planetary wave propagation and the mean winds. Tribbia (1991) points to the nonlinear dependence of the extratropical response on the subtropical jets' strength and position. Yulaeva and Wallace (1994) warn that some GCMs, dominated by baroclinic adjustment for dispersal of excess tropical warmth, will not create teleconnections correctly. They outline the necessary simulation of the observed reduced static stability of the upper troposphere equatorward of the jet streams due to the

El Nino-warmed tropical troposphere. This reduced static stability would enhance the potential vorticity across the subtropical jet streams and strengthen them. The Hadley Cell could be amplified by increased tropical uplift and provide the needed eastward acceleration to the jet streams. Concurrently, the lower stratospheric pressures should undergo observed zonal mean cooling with uplift of the tropopause and negative correlations with warmed ssts. With inclusion of volcanic and tropospheric aerosols and variable ozone distributions forcings, the CAFE AGCM should combine radiative and dynamical conditions and communicate the tropical sst forcing to higher latitudes. [This also relates to two schools of thought on the source of stratospheric trends wherein either radiative impacts from ozone loss explain the lower stratospheric cooling or whether circulation changes driven by alteration of the troposphere and, perhaps, greenhouse gases are necessary.]

This exploration of the performance of a typical climate model forced by known atmospheric and sea surface temperature events at global, zonal and regional levels used a coarse 9-vertical layer version of the GISS AGCM (Figure 1) with a 4° latitude by 5° longitude resolution. The coarse resolution of this AGCM makes the needed computer time for a transient run bearable, considering that the standard simulations alone required an ensemble of seven runs with sst forcing through 1992 for statistical results. Subsequent individual runs, still forced at the lower boundary by observed ssts, added in changing greenhouse gases, volcanic aerosol opacities, tropospheric and lower stratospheric ozone and tropospheric black carbon and sulfate aerosols through April of 1998. This coarse resolution model has performed extremely well in climate model comparisons to observations, being tied for the top US climate model and fifth out of 29 models in an AMIP examination of the hydrological cycle, for example (Lau et al., 1996).

The goal of perfectly hindcasting 1978 through 1998, as defined as a perfect agreement between an AGCM and the MSU's T_b time series, has obstacles. Neither

an ensemble of AGCM realizations nor the MSU data are perfect. First, the past year has produced numerous papers on calibration and processing concerns with the MSU data. Several versions of the MSU data are publically available, as criticisms are addressed and as longer baselines become available. Second, an AGCM may produce a good simulation by chance so multiple simulations are necessary in order to assess a potential of correct hindcasting. But how many simulations are appropriate for a particular model? The AGCM's own internal variability sources can prompt extratropical responses that overpower boundary-layer responses such as ENSO sst. Boyle (1998) refers to this as 'the chaotic nature of the midlatitude dynamics'. Third, this AGCM was forced by observed AMIP I ssts, volcanic aerosol opacities, ozone levels and tropospheric aerosols each of whose specification has its own weaknesses. Fourth, the time period of the 1980s had two extremely strong ENSO events only surpassed by the recent 1998 event. Good simulation of these odd events does not insure correct simulation of ENSO events in other decades. Fifth and lastly, an AGCM simulation of an anomaly is likely to be dependent upon its mean-observations-based parameterizations and its mean climate.

Hopefully the following analysis of these multiple AGCM simulations can begin to answer some of these questions:

- Does the AGCM simulate the mid-tropospheric temperature dumbbell pattern of Yulaeva and Wallace (1994) in response to El Nino sst forcing? Does the AGCM's tropopause rise and the lower stratospheric channel 4 temperatures cool in localized response to tropospheric warmth during El Nino (Reid et al., 1989; Yulaeva and Wallace, 1994; Randel and Cobb, 1994)?
- Is there reduced static stability in the tropical upper troposphere over the Pacific due to warm equatorial sst?? Do the upper tropospheric, subtropical jet streams and the Hadley Cell circulation strengthen promoting teleconnections?
- How well can the AGCM correlate with the oceanic lower tropospheric,

mid-tropospheric and lower stratospheric temperature time series of MSU? Do the correlations improve with additional atmospheric forcings? Do the correlations change with use of different MSU versions?

- How good is the AGCM's response over sensitive agricultural regions? Finally, does the AGCM's response over these agricultural regions improve with inclusion of atmospheric forcings?

Section 2 describes the AGCM, the applied forcings of the individual transient runs and the off-line microwave radiative transfer model. Section 3 discusses the various MSU data versions and reviews recent published concerns with MSU calibration and processing. It also compares different means of calculating the T_b from AGCM diagnostics and the resultant impact on time series and monthly mean values. Section 4 begins to look at the microwave analysis of the GCM runs, focusing upon the monthly mean climate simulated and the associated regional variability. Section 5 explores the different AGCM zonal responses to ENSO and other forcings in terms of the AGCM microwave temperature time series and their correlations to MSU time series in the lower troposphere, mid-troposphere and lower stratosphere and in terms of regional maps. Section 6 focuses on the sensitive agricultural regions and their responses to sst and additional atmospheric forcings relative to precipitation, surface temperature and MSU observations. Section 7 concludes this paper with replies to the above questions and discussion on weaknesses in the analyses and, thus, future work planned.

2. The AGCM, Forcings and the Microwave Model

Table 1 lists the GISS CAFE AGCM runs, their applied forcings and the length of time analyzed. The actual start to these runs is January 1, 1969, but analyses in this work focuses primarily on the 1979-1998 period. The seven sst-forced runs (255A-G) differ in terms of their initial conditions and are treated as individual realizations

of the 1979-1992 period. Subsequent climate model runs have explicit atmospheric forcings added in cumulatively. All of the runs in Table 1 have sea ice coverage specified climatologically due to issues over the spatial and temporal continuity of current sea ice datasets. The sea ice coverage is based on the 1979-1993 period and the version released for usage with the Atmospheric Model Intercomparison Project I (AMIP-I) (Gates, 1992) but with slight modifications.

a. AGCM

The AGCM version employed is roughly referred to as ‘SI96’ as it includes model development for the 1996 GISS “Summer Institute” . The coarse resolution of 9 vertical layers and 4° latitude by 5° longitude works with a quadratic upstream scheme for moisture and heat advection and a fourth-order scheme for momentum advection. Both of these schemes imply finer resolution for horizontal and vertical advection. The rigid top of the AGCM occurs in the lower stratosphere at roughly 31 km or 10 mb (see Figure 1). This climate model has the typical collection of climate feedback parameterizations, such as cloud formation and snow cover. The cloud parameterizations are described in Del Genio et al. (1996), the land surface parameterizations in Rosenzweig and Abramopoulos (1997) and the planetary boundary layer in Hartke and Rind (1997). The radiation package employed by the AGCM has compared quite well with line-by-line calculations and with radiation code in other AGCMs (Cess et al., 1993). The SI96 version of the AGCM differs from the SI95 version used in Hansen et al (1997) only in a newer cloud scheme; an improved orbital calculation of solar irradiation and an associated solar constant change to 1367 W/m^2 from 1362 W/m^2 ; small changes of increasing puddling on sea ice, snow melting before ice and associated hydrology adjustments; increased radiation time steps; additional dependence on surface type for radiation fluxes; and consolidation of relationships between cloud cover, threshold relative humidity and background relative humidity to reduce

unwanted shortwave absorption in middle and high latitudes.

b. Forcings

The sst observations used to force the climate model are monthly values over 1969 to 1998 from the analysis of Reynolds and Smith (1994). The latter's dataset was distributed at 2° by 2° resolution and so was interpolated to the necessary 4° by 5° grid size using the ETOPO5 dataset as a land reference. The monthly sea surface temperature anomalies inherently contain some portion of the atmospheric forcings. Figure 2 shows the ssts after a 3-month smoothing across the tropical Pacific, the northern hemisphere and the southern hemisphere. The northern hemispheric averages, in particular, show a warming trend perhaps derived from anthropogenic forcing.

The explicit atmospheric forcings begin in AGCM run 281 with observed variation in greenhouse gas forcings by CO₂, CH₄, N₂O, CFC-11 and CFC-12. The specified CO₂ increases are similar to observations and IPCC scenarios (IPCC, 1992) with a concentration of 323 ppm in 1969 and 368 in 2000. Increases match observations up to 1994. Then increases are fixed at 1.5 ppm annually from 1994-95 and 1.4 ppm from 1996 onward for CO₂, at 10 ppb from 1994-95 and at 8 ppb from 1996 onward for CH₄ and at 0.7 ppb from 1994-95 and at 0.6 ppb from 1996 onward for N₂O. Table 2 lists the trace gas concentrations used to force the experiments. While the CO₂ increases are uniform with height, the other trace gases only increase up to 16 km and, at higher levels, have diminishing increases with a 10 km scale height.

The AGCM run 307 adds in zonal stratospheric aerosol optical depth forcings (Sato et al., 1993; Hansen et al., 1996) as shown in Figure 3. These aerosol optical depths change the net radiation entering the troposphere and warm in situ stratospheric temperatures which affects dynamics. This stratospheric warming is clearly seen in the MSU channel 4 T_b of Figure 6 due to that channel's center around 80 mb

(Figure 1). A background optical depth of 0.0001 serves as a lower limit for aerosol forcing after 1979. The optical depths were derived from the Stratospheric Aerosol and Gas Experiment (SAGE) occultation data available from 1979-1980 and then 1985 onwards as detailed in Hansen et al (1996). SAGE occultation data was not available after the 1982 El Chichon eruption and the optical depths of Sato et al (1993) with a 10% increase based on comparison with multiple data analyses (Hansen et al., 1996; Hansen et al., 1997). Optical depths due to the 1991 Pinatubo eruption were derived via four wavelengths measurements in the solar occultation data by SAGE II with extrapolations applied during saturation events and with constraints from 12.1 micron Improved Stratospheric and Mesospheric Sounder (ISAMS) measurements (Hansen et al., 1996). The optical depths for the January 1995 to December 1999 period were extrapolated assuming an exponential decay with a time constant of 1 year across all latitudes. Figure 3 shows that the resultant optical depth forcing at $0.55\ \mu\text{m}$ peaks at 0.30 in northern tropical latitudes after the 1982 El Chichon eruption, with an associated global mean maximum of 0.09, and peaks at 0.26 just south of the equator after the 1991 Mt Pinatubo eruption, with an associated global mean maximum of 0.15.

Severe ozone depletion has occurred in the lower stratosphere and upper troposphere from 1970 onward. The atmosphere responds to vertical redistributions of ozone in a complex fashion given its influence on solar and IR radiation and the tropospheric-stratospheric energy balance. Loss occurred most deeply in ambient ozone abundances near 17 km with trends of -1.5 to -3% per year from February 1979 to April 1991 (McCormick et al. 1992). These negative trends were near zero at the equator, but increased toward the poles with strongest values in the Southern Hemisphere's spring (Stolarski et al., 1991). Randel and Cobb (1994) found strong positive correlations between MSU lower stratospheric channel 4 T_b and total ozone column data from TOMS. Hansen et al. (1995), in turn, found ozone cooling of the

surface air level ($0.03^{\circ}\text{C}/\text{decade}$) to be less than cooling in the lower troposphere at 800 mb ($0.06^{\circ}\text{C}/\text{decade}$) with their idealized-geography climate model. Inclusion of ozone depletion into real-world-geography GCM integrations may thus draw together regional AGCM forecasts and the MSU channel 2 and 4 observations.

The background level of ozone in the AGCM is based upon the ozone climatology of McPeters (1993) which are 1979-1980 levels. Zonal stratospheric ozone trends have already been derived from the Solar Backscatter Ultraviolet (SBUV) measurements of ozone total column amounts and profiles above 32 mb (Hollandsworth et al., 1995) and the SAGE stratospheric ozone profiles between 125 and 32 mb (McCormick et al., 1992) by Hansen et al. (1997). AGCM run 334 adds in such stratospheric ozone trends. Figure 4 shows the total ozone change from its specified zonal, stratospheric inputs in panel a and the ozone time series at different pressure levels over Washington, D.C.(38N) in panel b

The tropospheric ozone changes added separately into AGCM run 321 are much more uncertain than the stratospheric ozone changes. Tropospheric ozone levels, roughly 10% of the total column ozone amount, are specified geographically as shown in Figure 4c. Specified ozone increases occur primarily in the mid-troposphere and across the northern hemisphere by up to 20 Dobson Units (DU) since the pre-industrial year 1850 and by up to 8 DU between 1995 and 1970 (Hansen et al., 1997). This northern hemispheric enhancement agrees with IPCC estimates (IPCC, 1996) but the southern hemispheric changes of Figure 4c are not negative over the southern high latitudes as suggested by IPCC. Rates of increase for the tropospheric ozone forcing remain fixed after 1985 in rough agreement with observations showing slowing or stopping of its upward trend (IPCC, 1996). Tropospheric ozone observations are sparse. Therefore the global and vertical tropospheric ozone changes of Figures 4c and 4d have little regional or fine-scale structure. AGCM run 339 has both the tropospheric and stratospheric ozone forcings included.

Tropospheric aerosols are the last added atmospheric forcing in Table 1 and the most uncertain in terms of background distribution and trends. Their distributions, despite a short lifetime of a few days in the troposphere, arise from continual combustion of fossil fuels, biomass burning, desert dust uplift and other sources. Sulfur, in AGCM run 332, and black carbon (soot), in AGCM run 349, aerosols force the AGCM radiation package. The indirect impact of tropospheric aerosols influencing cloud condensation nuclei is not incorporated. While scattering off of tropospheric sulfuric aerosols cools local temperatures, tropospheric soot aerosols absorb radiation and primarily warm local temperatures. Background sulfur distributions were provided by D. Koch (Koch et al., 1999) and a background carbon distribution by I. Tegen (personal communication, 1999). The 1970 and 1995 December geographical distributions of sulfuric and soot tropospheric aerosols are shown in Figure 5. Trends for sulfuric aerosols are specified in nine regions from 1950 to the present and are based on CO₂ emissions (Robertson et al., 1999). Thus, the US, Europe and eastern Asia have stronger emission rates than Africa. Given the fewer observations available on tropospheric soot aerosols, these sulfuric trends are applied to the background soot distribution.

In summary, the last AGCM run, 350, has all of the atmospheric forcings applied (see Table 1). The earlier AGCM run, 334, incorporates the least uncertain forcings since it excludes tropospheric ozone and tropospheric aerosols from its specified forcings.

c. Microwave Model

The microwave radiative transfer model employed in the following analyses produces maps of microwave brightness temperatures based on the AGCM's simulated, monthly-mean global fields of atmospheric and surface diagnostic parameters. The climate model's T_b maps are calculated assuming a nonscattering, refracting atmosphere

containing absorbing molecular oxygen and water vapor in local thermodynamic equilibrium above a spectrally gray, Lambertian surface. Non-negligible scattering from precipitation and large convective ice particles is ignored as such scattering events were filtered out of the MSU climatologies. Interaction with the surface is characterized by an emissivity. Snow-free land has the highest emissivity of 1.0, snow-covered land an emissivity of 0.85, ice-covered oceans an emissivity of 0.70, and oceans an emissivity of 0.50. The snow-free land provides a very warm background and the oceans a cold background for microwave channels sensitive to the surface. For example, in the tropics, roughly 20% of the full signal or 58 K comes from surface emission over land and 10% or 29 K from surface emission over ocean for lower tropospheric channel 2R T_b (Shah and Rind, 1995). Changing the surface emissivity by 0.1 alters channel 2 T_b by 0.4 K and channel 2R T_b by 0.8 K over tropical low topography areas. For this reason, channel 2R values from the AGCM are masked over land and only values over the less-variable ocean surfaces are considered. Channel 2 T_b values are similarly masked over high topography, the Himalayas, the Andes, the Greenland Plateau and Antarctica.

This microwave postprocessor has favorably contrasted radiosonde and the NCEP/NCAR Reanalysis climatologies with the MSU tropospheric and stratospheric monthly mean climatologies (Shah and Rind, 1998). It has also produced zenith attenuations in agreement with available observations (Shah and Rind, 1995). While Hansen et al (1995, 1997) used a quicker weighting functions method to calculate MSU T_b from AGCM diagnostics, the full radiative transfer model is employed herein to ensure sensitivity to changing profiles of temperature, humidity and refraction and to changing snow and ice coverage. The microwave radiation code is available from K. Shah.

3. MSU Data: Versions and Processing

The MSU brightness temperature (T_b) climatologies have been successfully used in AGCM validation (Shah and Rind, 1995; Rind et al., 1999; Druryan et al., 1995, Hansen et al., 1997). Also well known is the usage of tropospheric channel 2 to examine ENSO phenomena (Yulaeva and Wallace, 1994) and tropospheric channels to spur temperature trend research (Hansen et al., 1995; Christy et al., 1997). The upper tropospheric channel 3 T_b has also been used to estimate mid-tropospheric vorticity (Spencer et al., 1995) while the lower stratospheric channel 4 T_b has been used to regress solar cycle, linear trend, quasi-biennial oscillation (QBO) and El Nino-Southern Oscillation ENSO signals (Randel and Cobb, 1994).

There are various MSU data versions publically available. The versions differ in terms of duration, limb-darkening corrections, monthly-mean climatologies employed to determine anomalies, and intersatellite calibrations. There are also numerous recent papers critiquing MSU brightness temperatures in terms of their calibration, processing or neglect of satellite orbital changes. The following subsections review both subjects and their relevance to this paper's microwave analysis.

a. MSU versions

Two characteristics of MSU data are very attractive for climate research: global coverage and consistent instrumentation. The MSU channels, 2 (53.74 GHz or 5.58 mm), 3 (54.96 GHz or 5.46 mm), and 4 (57.95 GHz or 5.18 mm), simultaneously measure atmospheric temperatures across the mid-troposphere, the tropopause region and the lower stratosphere, respectively. These channels have 200 MHz bandwidths on the low-frequency side of the 60 GHz molecular oxygen band. Synthesized channels 2R and 3R were designed to sense narrower atmospheric layers with vertical centers dependent upon their source. Channel 2R is a mixture of channel 2 T_b at different view angles: four times the average of channel 2 T_b at 28.41° and 18.94° minus three times

the average of T_b at 47.35° and 37.88° . Channel 3R is a combination of frequency channels: 1.35 times a nadir channel 3 T_b minus 0.35 times a nadir channel 4 T_b . Sometimes labeled as MSU channel 3/4, channel 3R's climatology is an experimental product generated despite difficult calibration due to channel 3's straddling of the tropopause and with avoidance of NOAA 6 and NOAA 9 channel 3 radiances which drifted by up to 1 K. (Spencer, 1995; Spencer et al., 1995). Shah and Rind (1998) proposed zonal additions to the magnitude of channel 3R monthly-means to bring them into agreement with NCEP/NCAR Reanalysis channel 3R magnitudes.

The MSU has collected radiances continuously since 1978 in 11 footprints in a 2300-km swath having a nadir, 110 km-circular footprint and an elliptical, 179x323-km wide footprint at the extreme viewing angle of 47.35° (Wu and McAvaney, 1998; Schwalb, 1978). These footprints accumulate to global coverage every several days given a particular satellite's precession rate. Data from NOAA polar-orbiting satellites were merged having local equator crossing times at 0230 and 1430 LT for a 'morning satellite' and 0730 and 1930 LT for an 'afternoon satellite'. The morning and afternoon satellites alternate and sometimes overlap in the NOAA series of satellite launches (see Wu and McAvaney (1998) and Christy et al., (1998) for further details)

The MSU channels' broad vertical weightings are shown in Figure 1. The broadness of these weightings is actually useful in our AGCM assessments as the MSU vertical sensitivities encompass several vertical AGCM layers. While mid-tropospheric channel 2 and lower tropospheric channel 2R derive roughly 10% and 20% of their full signal from land-surface emission, channel 3R has a small surface input only over high topography and channel 4 has no surface input. The impact of surface emissivity variations on the tropospheric channels' T_b is discussed in further detail in the Microwave Model section and in Shah and Rind (1995, 1998). Atmospheric humidity is the next, but much more minor, influence, adding opacity to tropospheric channels

and warmth over an ocean background. These microwave channels are nearly insensitive to the presence of non-precipitating clouds (see Shah et al. (1996) and Shah and Rind (1995)). Precipitation influences, which would cool T_b values by several degrees, were filtered from the climatologies.

These MSU climatologies of monthly mean T_b maps and complementary monthly anomaly T_b maps were created by Spencer and Christy (1992ab, 1993, 1998) at a 2.5° resolution. The climatologies are designated as the 'limb90 a' set if they have the initial processing applied (e.g., limb darkening correction 'limb90') as described in Spencer and Christy (1992ab, 1993). This 'a' version covered 1979 through 1994. Subsequent versions of the MSU data, 'b' (available on the anonymous ftp site roughly since 4/95), 'c' (1/97) and 'd' (3/99), differ in terms of longer time periods, the intercalibration of the satellite platforms, additional satellite radiances, attention to orbital influences and/or new limb darkening corrections (Christy et al., 1998). The majority of this paper uses the 'c' version of the MSU data since 'd' is currently being created and only partially available as monthly global and hemispheric averages. Any excursions from usage of the c version are clearly noted in the following text.

Figure 6 shows the MSU channel 2 and channel 4 time series, globally averaged, from the c dataset version. ENSO warmings and coolings are apparent in the mid-tropospheric channel (and in the lower tropospheric channel not shown) while the volcanic aerosol warming events associated with the El Chichon and Mt Pinatubo dominate the lower stratospheric time series. Also apparent in the lower stratospheric T_b anomalies is a cooling trend positively correlated with in situ ozone depletion. Panels b and c of Figure 6 compare the older a version to the recent c version for the mid-tropospheric channel 2 and lower stratospheric channel 4. The monthly-mean T_b for these anomalies changed between version a and version c from a 1982-1991 baseline for both channels to only 1984-1990-baseline means for channel 4. There is little significant change to the midtropospheric MSU channel 2 anomalies between the

a and c versions. Even in the tropics where the mid-troposphere displayed the largest anomalies associated with sst forcing, the differences between the a and c versions' channel 2 time series were less than 0.07 K. However the lower stratospheric channel 4 time series altered notably. The new version of the channel 4 anomalies emphasized the cooling of the lower stratosphere and differed from the older version by up to 0.60 K. Its new 1984-1990 monthly-mean climatology base excluded volcanic events and had different sampling of the high latitudes' sudden stratospheric warmings and other variability (see also Figure 4 of Christy and Drouilhet (1994)). Figure 7 shows the difference between monthly-mean channel 4 T_b from the c and a versions with maximum changes in the northern high latitudes up to -8 K in March. The differences between monthly-mean channel 2 T_b from the c and a datasets were similarly examined but magnitudes were barely above 1 K and limited regionally to latitudes over Antarctica, northern Greenland and the Arctic Ocean.

Figure 6d shows the global, northern hemispheric and southern hemispheric time series of the MSU version 'd'. Processing of this latest MSU version is detailed in Christy et al (1998). This new processing focused on removing individual radiometer biases, intersatellite biases, orbital drift biases, and artificial variations due to the annual cycle assumptions. The baselines, as with the c version, are again 1982-1991 for mid-tropospheric channel 2 and 1984-1990 for the lower stratospheric channel 4. Larger differences are seen in channel 2 anomalies between the c version and the d version than between the c and a versions. These mid-tropospheric time series changes maximize in October of 1997 at 0.25 K for the northern hemispheric time series. The lower stratospheric time series also differs by up to 0.39 K for the northern hemispheric average in March of 1997. Most of the larger differences in the lower stratospheric time series occur in the mid- to late- 1990s. Differences in the mid-tropospheric anomalies occur throughout the time series. In general the channel 4 anomalies had larger differences between the c and d versions than the channel 2 anomalies.

b. MSU Processing Concerns

The year of 1998 had a small flood of papers on MSU temperatures and how the dataset has been skewed by either calibration, processing or satellite orbit changes. Every data product has some built-in problem from either coverage, instrumentation or calibration. However any dataset used to monitor the politically-sensitive determination of atmospheric temperature trends will receive considerable scrutiny. Spencer and Christy (1992ab, 1993, 1998) have done considerable work translating raw MSU radiances into mean values (the climatology) and anomalies (the time series). These MSU's anomalies have created controversy as their lower tropospheric (channel 2R) temperature time series did not point to warming of near-surface temperatures unlike meteorological stations surface temperature time series, unlike the MSU mid-tropospheric (channel 2) temperature time series, and unlike radiosonde time series which all indicate warming of tropospheric and surface temperatures.

Two particularly notable problems were uncovered by the 1998 papers which impact the MSU T_b time series and the T_b climatologies. First, the NOAA satellite series that flew the MSU radiometers experienced uneven orbital decay. This decay was extreme over the 1979-1983 and the 1989-92 period. Hurrell and Trenberth (1998) had noticed inexplicable discontinuities in the MSU's lower tropospheric time series around mid-1981 and mid-1991. Wentz and Schabel (1998) proposed a physical source for these discontinuities. When the NOAA satellite dropped in altitude, the MSU footprints which were pointed off-nadir saw higher altitudes. The more off-nadir a footprint was, the more its radiance cooled as higher altitudes were measured in the troposphere. Since the channel 2R, lower tropospheric MSU T_b s were created from a combination of off-nadir footprints, they are sensitive to the satellite's orbital height. Wentz and Schabel determined that the orbital decays of the various NOAA satellites skewed the MSU lower tropospheric time series. Their correction turned the

channel 2R trends from a cold trend of -0.05 K per decade to a warm trend of 0.07 K per decade (though the error on this trend is placed at ± 0.05 K per decade). So the decay of the satellite orbit pointed off-nadir MSU footprints to sense higher altitudes and cooler temperatures and artificially cooled MSU channel 2R T_b by a few tenths of degree (for further discussion see Gaffen (1998) and Hansen (1998)). For the mid-tropospheric channel 2 and lower stratospheric channel 4 MSU temperatures, this satellite altitude changes amounts to an absolute temp change of up to 0.01 K and 0.002 K respectively. These negligible impacts were calculated with the microwave radiative transfer model assuming an off-nadir view angle of 18.94 degree (to mimic the averaging of 7 footprints as discussed below) and a satellite orbit varying from 870 to 810 km

The second concern published in 1998 addressed the non-nadir nature of the MSU channel 2 and channel 4 T_b due to the averaging of footprints radiances used to generate a 'nadir' T_b (Spencer and Christy, 1992a; Christy et al., 1993, 1998). Wu and McAvaney (1998) published work that examined this processing wherein the inner 7 footprints in a MSU swath are used to create a single 'nadir' T_b value. The 6 off-nadir and 1 nadir footprint (f) values are scaled and averaged via empirically-derived factors. This method is called limb correction and is a common practice of lowering noise in a dataset. Wu and McAvaney used the NCEP Reanalysis and determined that the MSU products actually represented a 21.6 zenith angle (or, equivalently, an 18.94 viewing angle from the satellite) rather than a nadir view. Therefore, the MSU climatology and time series measure a slightly higher altitude and less surface input. Spencer and Christy had rescaled the magnitude of MSU products to be a nadir magnitude but those MSU product still inherently measured atmospheric variability at a higher altitude. In addition, Wu and McAvaney also detailed the homogenization of the Spencer and Christy MSU products since 7 footprints were equivalent to 950 km or 3-4 grid meridians at the equator, 7-8 grid meridians at 60° latitude and 3-4

latitudinal grids at the poles. The impact of the 950 km spanned by these footprints is particularly damaging across topography and in the troposphere.

Figure 8 shows view angle influence on midtropospheric and lower stratospheric monthly-mean T_b from a 31-vertical layer AGCM's January and July. A higher vertical resolution AGCM was used to heighten sensitivity to multiple view angles or, equivalently, footprints making up a T_b value. These maps of the AGCM January and July were calculated assuming a nadir view angle and then assuming that 7 footprints of the AGCM site were viewed and then rescaled with the limb-correction determined by Wu and McAvaney (1998). The general cooling of land surfaces for the mid-troposphere is -0.5 K and warming of oceanic values 0.1 K equatorially to 0.4 K at high latitudes. The mid-tropospheric differences closely resemble the influences shown in Figure 4a of Wu and McAvaney (1998). The lower stratospheric differences, due to incorporation of 7 footprints or view angles averaged and then rescaling, is new in Figure 8. The nadir channel 4 T_b are cooler, particularly over the summer pole where discrepancies reach up to 1 degree and the lapse rate would be steeper over the tropopause. Lower stratospheric T_b impacts have little structure or regional form. The exception to this is any region where wave activity dominates spatial variance, such as the Aleutian High. Mean lower stratospheric values may be off by up to 0.9 K in regions of wave-activity.

Figure 9 shows the minimal difference from calculating a mid-tropospheric and a lower stratospheric time series with nadir values or with the 7 footprints view angles with magnitudes rescaled. Most of the 7-footprints averaging impacts of Figure 8 are systematically removed when looking at the anomalies (at least with a 9-vertical layers AGCM run). Differences in the mid-tropospheric time series is generally ± 0.01 K and in the lower stratospheric time series ± 0.02 K.

The current microwave radiative transfer model and the AGCM create a few of the MSU processing problems. The emissivity specified for tropospheric channels

is simplistic. This limits the spatial variability of the simulated MSU temperatures. The AGCM's coarse vertical resolution limits the sensitivity to off-nadir viewing. The AGCM also has a coarse horizontal resolution and this diminished the sensitivity to cross-gridcell sampling by the MSU footprints.

4. AGCM Mean Annual Cycles and Variability

As discussed in Boyle (1998), perhaps the very different mean states of the initial atmosphere (real or simulated) will affect the extratropical responses to tropical ssts with varying planetary wave propagation and the mean winds. Tribbia (1991) also discusses the nonlinear dependence of the extratropical response on the subtropical jets' strength and position. Kiladis and Diaz (1986) documented observational evidence of midlatitude teleconnections in terms of the Aleutian Low magnitude during the winter of 1983. Hoerling et al (1997) also detail wave trains which shape teleconnections during ENSO events. These dynamical responses and the background wind profiles will be dependent on the background temperature structure. So, the following discussion examines the AGCM's mean annual cycle and its interannual variability.

Baselines for T_b anomalies do vary depending on the AGCM run and the MSU data versions considered. The monthly-mean T_b baseline, 1982-1991 for tropospheric channels and 1984-1990 or 1982-1991 for the lower stratospheric channel depending on which MSU data version is used for comparisons, is from the AGCM control run for sst forcing runs, experiments 255A to 255G, or from the individual atmospheric forcing run, experiments 281 to 350 (see Table 1).

a. Monthly-Mean AGCM Temperatures

A 10-year average from the AGCM control run 255 produced monthly T_b values in good agreement with the MSU mean climatology (Figure 10). The AGCM control run had mean ssts from AMIP data over the 1982-1987 period and mean ice coverage from

the 1979-1993 period as a lower boundary. The resultant tropospheric temperatures generally match MSU observations but are too cool over the mid-to-high latitudes by several degrees. Lower tropospheric T_b are also significantly cool (based on ratios to MSU interannual standard deviations in Figure 10) over the equatorial oceans. These weaknesses may be related to insufficient high cloud coverage in the northern latitudes and insufficient upper tropospheric atmospheric moisture, both of which are difficult to confirm. However, the tropical lower tropospheric coolness and the higher latitudes' tropospheric coldness are common, tenacious flaws in AGCMs (IPCC, 1996). In terms of impacts on the subtropical jets, the latitudinal temperature gradients in the mid-tropospheric T_b , which influence the strength of the jets, are only slightly amplified (Figures 10 and 11).

The lower stratosphere of the AGCM exhibits some weaknesses. The presence of the model top at 10 mb and the lack of gravity wave parameterizations in the model distort the annual cycle of mean temperatures. The AGCM's T_b s differ from MSU observations by over 10 degrees over the southern pole and at wave centers and by several degrees over the tropics (see Figure 10 and Figure 11b). The excess tropical warmth in the lower stratosphere, is another common, unwelcome AGCM flaw (IPCC, 1996). Rind et al. (1999) detail the need for gravity wave parameterizations and a high altitude for the model top in order to correctly simulate the lower stratosphere. Currently, the low height of the model top (at 10 mb or roughly 32 km) reflects energy back into the troposphere. This artificial, unavoidable top had originally set up strong wind and temperature deviations in early 9-layer GCMs (Hansen et al., 1983). As a solution, a specified stratospheric drag was placed in the top vertical layer to bring wind and temperature deviations down to acceptable levels. However, this artificial drag in the model's top layer sets up divergence over the summer pole and convergence over the winter pole, as seen in the temperatures of Figure 11, and in the meridional and vertical upper-layer winds. Unrealistic conditions near the model

top may affect tropospheric features and impact the AGCM's teleconnections; this aspect will be explored in a subsequent paper.

b. Mean Seasonal AGCM Variability

Initial examination of the AGCM does find appropriate, stronger variability over high latitudes, winter seasons, and continents in the AGCM's T_b maps. Figure 12 shows the seasonal maps of MSU variability and of AGCM variability from the sst-forced run 255F over the 1980-1997 period. The MSU's mid-troposphere has a bit more northern winter (DJF) equatorial Pacific ocean variability and a bit more variability over northern winter and spring landmasses. The AGCM actually produces more mid-tropospheric variability over the continental US during the northern winter and over the Asian continent during northern summer (JJA).

The lack of gravity wave parameterizations in the model's lower stratosphere sensibly limits variability comparisons with MSU channel 4 observations in Figure 12b. Placement of variability in the AGCM is appropriate with maxima over the northern winter high latitudes and minima across equatorial latitudes. The AGCM's lower stratosphere does not have wave-related variability at mid-to-high latitudes in both the northern and southern hemispheres. The MSU maps also show more variability over the northern winter pole from sudden stratospheric warmings. [Sudden stratospheric warmings are simulated in the 23-layer version of this AGCM.] Thus, the 9-layer AGCM's lower stratospheric variability peaks at 4 K when MSU observations peak at nearly 8 K in February and just over 8 K in March over northern high latitudes.

5. AGCM Zonal and Regional Responses

The regional and zonal responses of the AGCM to sst and other forcings are examined in terms of anomaly maps and time series correlations. Warm ENSO sst

anomalies should: prompt strong precipitation and deep convection over the eastern equatorial Pacific; strengthen the Hadley Cell and the subtropical jets; induce changes to the tropical troposphere's static stability; create warm (cold) centers of tropospheric (stratospheric) temperature anomalies; and spur extratropical teleconnections. These teleconnections may or may not be properly engaged and positioned in order to spur temperature and precipitation impacts over sensitive agricultural regions in the AGCM.

Again, the monthly-mean T_b baseline, 1982-1991 for the tropospheric channels and 1984-1990 or 1982-1991 for the lower stratospheric channel, depends on the MSU data version used for comparisons. The AGCM control run 255 supplies the baseline for the sst-forced runs 255A to 255G while the individual atmospheric forcing run, runs 281 to 350, supply their own baselines (see Table 1). The individual AGCM atmospheric forcing runs are treated as single realizations of the past climate. Maps of T_b anomalies or AGCM diagnostics are monthly anomalies without any smoothing applied. Correlation coefficients between AGCM and observational anomaly time series are labeled as significant if the associated student's t-test is greater than 99%. Changes to correlation coefficients with introduction of additional forcings are labeled as significant if the change is greater than the correlations' standard deviation and if the associated Fisher's z-transformation significance of the change is greater than 90%. Time series of both the MSU and AGCM T_b anomalies have been smoothed. The 3-month smoothing of MSU and AGCM T_b anomalies emphasizes the low-frequency component of the climate response, which the GISS AGCM does well.

a. AGCM Teleconnective Responses

Figure 13 shows regional changes to relevant AGCM diagnostics from an sst-forced run, its sea surface temperatures, precipitation and sea level pressure, for January 1983 and January 1998. These months were selected due to the size of the

warm sst anomalies over the eastern Pacific cold tongue (see Hoerling et al, 1997, on ENSO nonlinearities). Also these winter months are characterized with stronger teleconnections to the northern extratropics given the more favorable temperature gradient (see Trenberth, 1991).

AGCM sea level pressures in Figure 13a do shift during these El Nino months with decreases over the eastern Pacific and increases over the tropical South Pacific ocean. As anticipated, the very warm sst anomalies prompt precipitation increases over the eastern equatorial Pacific in the AGCM. The AGCM's maximum precipitation anomalies over the eastern Pacific appears concentrated more tightly over latitude than normal and precipitation diminishes over the southeastern Pacific.

There is associated strengthening of the AGCM's northern winter Hadley Cell and the subtropical jet as detailed in Table 3. During January, 1983, and January, 1998, the winter Hadley Cell strengthens and vertical motion increases by 300% in its southern branch's uplift. Its upper tropospheric meridional winds and column stream function concentrate about an 8°N center and increase. The AGCM's subtropical jet strengthens by 2.0 m/s in January 1983 and 4.2 m/s in January 1998.

Concurrently, local compensation and cooling in response to movement of the tropopause can be seen in both the MSU and AGCM lower stratospheric T_b . These T_b values are an integrated temperature across a broad pressure layer (as shown in Figure 1) and lifting of the tropopause brings cooler temperatures into the peak sensitivity of channel 4. In the maps of Figure 13b and 13c, changes to the tropical troposphere's static stability create warm (cold) centers of tropospheric (stratospheric) temperature anomalies. MSU observations show east-west gradients to the mid-tropospheric warming and lower stratospheric cooling across the Pacific. This gradient is also present in the maps of AGCM T_b . The 'dumbbell-shaped' centers of warming and cooling straddling the equator over the eastern Pacific in the MSU maps, however, are not always discrete in the AGCM T_b maps. The AGCM could generate

discrete, cool lower stratospheric peaks while not having discrete warm peaks in its mid-tropospheric T_b .

Over the North Pacific, Kiladis and Diaz (1986) documented the enhancement and southward displacement of the Aleutian Low pressure system due to northward flux of angular momentum during January of 1983. The deeper center moved the North Pacific storm systems southward, bringing hard winter storms to the western US coast. The intense strength of the Aleutian Low reached sea level pressure anomalies of -20 mb while the AGCM run in Figure 13a reaches anomalies of -14 mb southwest of Alaska. The associated, observed decrease of sea level pressures over the Greenland Sea and increase of pressures for the Azores High which led to milder winters over western Europe are not apparent in the AGCM winter sea level pressure anomalies. Thus, while tropical tropospheric changes in the AGCM do occur, it is uncertain if the AGCM creates all the extratropical teleconnections sufficient for responses over extratropical agricultural regions .

b. AGCM Mid-tropospheric T_b Time Series

Time series of T_b anomalies over 1979-1992 were first calculated from the sst-forced series, the seven transient runs forced by ssts alone (255A - 255G in Table 1). The seven runs are identically forced by observed ssts but differ in terms of initial conditions. They provide rough standard deviations due to model internal variability and a rough range of predictability by this AGCM for the agricultural regions of interest. These standard deviations are used to judge the significance of changes to correlations with addition of explicit atmospheric forcings (see Table 1). Figure 14 shows the unsmoothed mid-tropospheric T_b time series across the tropical Pacific, the AGCM T_b time series from the average of the 7 runs (255AG in Table 1) and the range of the individual AGCM time series for each month. These mid-tropospheric MSU and AGCM channel 2 anomalies clearly capture the warming and coolings of

the troposphere due to ENSO events in the 1980s. The average AGCM time series, 255AG, has a strong correlation coefficient of 0.78 with the tropical Pacific MSU time series over the 1979-1992 time period. Figure 14 shows the scatter of individual runs' values in the highly-responsive area of the tropical Pacific over 14 years.

3-month smoothing emphasizes the low-frequency component of the T_b response, which the GISS AGCM does well, and, thus, correlations between the model and observations' T_b improve. Tables 4 and 5 contrast the mid-tropospheric correlations between MSU and AGCM which rose from a mean of 0.75 ± 0.02 to 0.84 ± 0.02 across the tropics (20S-20N) for the 1979-1992 period with smoothing. Smoothed mid-tropospheric correlations were highest in the tropics (20S-20N) even though the magnitude of the response during an El Nino event was stronger in the tropical Pacific (20S-20N, 80W-100E) (see Figure 15). Usage of the MSU a dataset versus the c dataset had no significant impact on correlations. The average of seven runs, sst AG, generally had significantly higher correlations than the individual runs or the mean of the individual correlations (see Table 4). Its smoothed 1979-1992 global correlation was 0.72 and tropical pacific correlation 0.85 while the mean correlation of the individual sst runs was 0.64 ± 0.04 globally and 0.80 ± 0.03 across the tropical Pacific (see Table 5).

The presence of teleconnections in the AGCM temperatures are shown in Figure 15, with delayed, shrinking responses from the tropical pacific (PacTr, 80W-100E, 20@-20N), the tropics (Tr, 20S-20N), the equatorial latitudes (Eq, 30N-30S) into the northern midlatitudes (30N-50N). Figures 15a, 15b and 15c shows these responses to the 1983 and 1998 El Ninos in the MSU and AGCM mid-tropospheric T_b and their lag relative to the tropical Pacific sst. Magnitudes of the mid-tropospheric temperature response to warm sst anomalies diminish and increasingly lag with distance into the northern (or southern) high latitudes in both the MSU and AGCM channel 2 T_b . The chaotic nature of the northern midlatitudes is also displayed, obscuring the El Nino

mid-tropospheric responses.

Consequently, correlations degrade and standard deviations increase with distance from the tropics. As shown in Table 4, the 1979-1992 correlations of AGCM and MSU time series become insignificant, based on a student's t-test, for one of the sst-forced runs in the northern mid-latitudes (30N-50N) and for most of the runs in the southern midlatitudes (30S-50S) and both the northern and southern high latitudes (50N-70N and 50S-70S). Correlations of the mid-troposphere were consistently better in the northern than the southern hemisphere. The northern hemisphere has many stationary wave features unlike the southern hemisphere which may explain this strong hemisphere differences in correlation between the AGCM and MSU channel 2 time series. The AGCM's southern high latitudes (50S-70S) have little of the variability seen in the MSU observation, as discussed in the previous section and Figure 12, unlike the AGCM's northern high latitudes (50N-70N).

Table 5 lists the 3-month smoothed, 1979-1992 mid-tropospheric T_b correlations for the sst-forced run series and the additional atmospheric forcing runs. Globally, the best individual AGCM run had sst, greenhouse gases, volcanic aerosols, stratospheric ozone changes and tropospheric sulfate forcings (run 332) and a correlation of 0.73 ± 0.04 with the MSU channel 2 time series. Two other runs, though, were not significantly different and their forcings either also had black carbon aerosols (run 349) or lacked the tropospheric aerosols and the stratospheric ozone depletion (run 307) (see Table 5). Similarly, across the tropics over the 1979-1992 period, six individual runs did best with AGCM forcing ranging from only ssts to every forcing except tropospheric ozone changes. These best tropical mid-tropospheric correlations were within the 0.87 ± 0.02 level.

Interestingly stronger correlations between the AGCM and MSU mid-tropospheric T_b are found over the 1979-1992 time period (Table 5) than the 1979-1998 time period (Table 6). The 1990-97 period of sst anomalies, as shown in Figure 2, does not provide

enough of a strong signal to dominate the atmospheric temperature anomalies. The introduction of explicit atmospheric forcings over 1979-1998 does improve the strength of AGCM El Nino mid-troposphere responses globally and over the tropical Pacific as shown in Figure 16a. The associated correlations over the full time period in Table 6, however, show slightly smaller correlations in all latitudinal zones than seen for 1979-1992 in Table 5.

Inclusion of stratospheric volcanic aerosols significantly improve the 3-month smoothed, 1979-1998 mid-tropospheric correlations over the northern hemisphere in Table 6 (and in Table 5). Sensibly, tropospheric ozone forcing mostly impacted correlations in the northern mid- and high latitudes and hemisphere for 1979-1998 (see its distribution in Figure 4cd). This impact was generally not a positive one, pulling down northern hemispheric correlations significantly from 0.62 ± 0.05 to 0.51 ± 0.05 for example. Inclusion of stratospheric ozone depletion, on the other hand, significantly improved the correlations over low latitude zones rather than the high latitudes where depletion was greatest (Figure 4a and Tables 5 and 6). Tropospheric sulfates did not make a strong impression on the correlations. The most uncertain forcing of tropospheric soot, however, made a significant, favorable impression on northern mid-latitude correlations, rising from 0.30 ± 0.10 to 0.64 ± 0.10 . Over the southern mid- and high latitudes the correlations generally remain poor or insignificant regardless of the imposed forcings except for the average sst run, AG, which had a southern mid-latitude correlation of 0.31. Lastly, imposed atmospheric forcing generally do not improve performance over the southern hemisphere where there is little land and sea surface temperatures appear to dominate tropospheric forcing.

Globally, for 1979-1998, the best agreement in mid-tropospheric temperatures occurs at 0.66 ± 0.04 with the AGCM run which includes sst, greenhouse gases, volcanic, stratospheric ozone and tropospheric sulfate forcings (run 332). It is not significantly different, though, from the AGCM run which included tropospheric ozone forcing

instead of tropospheric sulfate forcing in Table 6. Both AGCM runs had similar, relatively high correlations also in low latitude zones, the northern high latitudes and the northern hemisphere. For the tropics, most of the atmospheric forcing runs in Table 6 runs have 1979-1998 correlations close to the maximum of 0.84 ± 0.02 .

The AGCM hindcasts seem less influenced by atmospheric forcings within the low latitudes of 30S-30N than in the extratropics. The only exception, as already mentioned, was the stratospheric stratospheric ozone forcing. The northern high latitudes, in particular, benefited from the addition of explicit atmospheric forcings in mid-tropospheric correlations of 1979-1998 of Table 6.

This result is no doubt partly due to the land-ocean effect of imposed forcings on top of specified ssts: the ocean-dominated, southern hemispheric correlations were indifferent to imposed atmospheric forcings while the land-dominated northern hemispheric correlations did respond to imposed atmospheric forcings. Though the known atmospheric forcings often improved hindcasts, a single realization with sst-forcing and, by chance, with favorable internal variability could hindcast almost as well globally and as well with the tropics.

c AGCM Lower Stratospheric T_b Time Series

The AGCM's lower stratospheric channel 4 T_b s from the sst-forced runs, 255A-255G, appropriately show no volcanic warmings from the 1982 El Chichon and 1991 Mt Pinatubo eruptions. Also the AGCM channel 4 time series does not exhibit the in situ cooling due to ozone depletions or the presence of QBO effects. Obviously the sst record cannot force the AGCM to produce those temporal signatures in its lower stratosphere. Correlations of the MSU and AGCM channel 4 time series are therefore less than 0.20 and insignificant for the 1979-1992 series of sst-forced runs. Only the standard deviations derived from these runs are presented in Table 7. The two 1979-1998 sst-forced runs, 255F and 255G, show the typical, insignificant correlations of

the sst-forced runs with MSU lower stratospheric observations. Thus, the AGCM lower stratospheric T_b do not appear to be significantly, negatively correlated with ssts over the 1979-1998 period. This result is despite observational evidence of such a relationship when only sst anomalies are present to provide non-chaotic forcing (Reid et al., 1989; Yulaeva and Wallace, 1994; Randel and Cobb, 1994). This result is also despite the maps of the AGCM's channel 4 cooling over the Pacific in Figure 13b. Apparently the AGCM's lower stratosphere cannot generate a sufficient zonal cooling in response to its lower boundary forcing though it can generate localized cooling over the eastern Pacific in a compensating response to the extra, El Nino tropospheric warmth.

The AGCM's lower stratospheric temperatures improve significantly with inclusion of explicit atmospheric forcings. Table 7 shows the improvement of AGCM and MSU channel 4 time series correlations primarily with addition of greenhouse gases, volcanic aerosols and stratospheric ozone depletion forcings. Tropospheric ozone forcing has a positive impact on correlations when added to run 307 but not when it is added to the penultimate run 349. Contrary to results in the mid-troposphere, tropospheric sulfate aerosols have a beneficial impact on most correlations while tropospheric soot significantly diminishes the northern midlatitude correlation and had little influence elsewhere. Also unlike the troposphere, the AGCM's lower stratosphere does equally well in both hemispheres in its correlations with MSU time series. Figure 16b shows individual runs' time series against the MSU observations. The AGCM's lower stratosphere even appears to cool over the 1978 to 1998 time period with introduction of the greenhouse gases forcing. The volcanic aerosol optical depths on top of this greenhouse gas cooling introduce warm events at roughly a third of the magnitude of the El Chichon warming and at almost all of the Mt. Pinatubo warming observed by MSU's channel 4 in the Tropics. The simulation of the El Chichon warming is slightly improved with introduction of the stratospheric ozone depletion

which cools the lower stratospheric T_b , alters its baseline and improves correlations in every zonal band (see Figure 16 and Table 7).

Globally the AGCM lower stratospheric hindcasts can correlate up to 0.91 ± 0.16 with the MSU time series over the 1979-1998 period and with 3-month smoothing. The large standard deviations derived from the sst-forced runs, which did not generate strong signals in the lower stratosphere, make it difficult to discriminate between individual atmospheric forcing runs. Nonetheless, the forcing runs which had sst, greenhouse gases, and volcanic aerosols (with or without tropospheric aerosols) achieve a grouping of high correlations in Table 7 in both low latitude, mid-latitude and hemispheric zones. Lower stratospheric correlations across the northern hemisphere reached 0.83 ± 0.12 levels, across the southern hemisphere 0.76 ± 0.05 levels and across the tropics 0.63 ± 0.13 levels.

d. AGCM Lower Tropospheric T_b Time Series

The AGCM's oceanic, lower tropospheric temperature time series (like its mid-tropospheric time series) are influenced by inclusion of atmospheric forcings but not to the degree that its lower stratospheric time series are impacted. Table 8 lists the 1979-1998 correlations of the AGCM and MSU T_b time series. Only oceanic values could be considered due to the lack of observations available to specify AGCM microwave land emissivities with confidence. Figure 16c shows several of the individual, atmospheric-forcing runs against the observed MSU time series. The AGCM time series for the lower troposphere did not reproduce the warm anomalies prior to mid-1981 seen in the MSU c dataset. Unfortunately version d of the MSU lower tropospheric data, which addresses critiques outlined in section 3, is not yet available.

ENSO variability dominates lower tropospheric temperatures at the low latitudes as it did for mid-tropospheric temperatures. T_b anomaly maps for January 1983 and 1998 in Figure 13c show the strong, Pacific El Nino warmth observed by MSU and

hindcast by the AGCM run sst F. The tropical Pacific (20S-20N, 80W-100E) and the full tropical zone (20S-20N) yielded the highest correlations between 3-month smoothed MSU and AGCM time series. This differs from the mid-tropospheric values in Table 6 in which 30S-30N correlations were often as high or higher and may be due to the larger magnitude of the tropical Pacific anomalies in MSU channel 2R than channel 2 (see Figure 16 and Figure 13). Correlations again diminish and standard deviations increase with distance from the tropics in Table 8. Lower troposphere correlations were again consistently better in the northern than the southern hemisphere. As with the mid-troposphere, correlations with observations over the southern mid- and high latitudes are often insignificant or extremely low. Unlike the mid-troposphere, however, correlations between AGCM and MSU lower tropospheric temperatures were less swayed by atmospheric forcings. Only in a few locations are there significant changes to correlations: the decrease over northern midlatitudes and the increases over the southern midlatitudes, the southern hemisphere and the globe with addition of tropospheric sulfates. Thus, the oceanic, lower tropospheric T_b are mostly shaped by the AGCM's lower boundary ssts.

Globally, the best correlation between oceanic AGCM and MSU channel 2R time series for 1979-1998 was 0.59 ± 0.06 from one of the sst-forced runs, sst F. Over the tropical Pacific and across the tropical zone, lower tropospheric temperature correlations reached maxima of 0.80 ± 0.02 and 0.78 ± 0.02 respectively.

6. Agricultural Regions' Responses

Three agricultural regions are examined in the following text in terms of their mid-tropospheric and lower-stratospheric T_b time series, their surface temperature time series and their precipitation. The first one, Nordeste in northeastern Brazil, lies within the tropical belt and on a landmass adjacent to the Pacific Basin. Zimbabwe in Africa lies within the subtropics but distanced by the South American landmass

and the Atlantic Basin from the ENSO sst forcings. The last region, the U.S. cornbelt, lies in the notoriously chaotic northern mid-latitudes.

Ropelewski and Halpert (1987) found 9 out of 11 extreme droughts over northeastern South America from 1911 to 1983 to coincide with El Nino years. Nordeste has lower annual rainfall amounts than most of Brazil, with rainfall highs only over March until May because of the southernmost movement of the Inter-Tropical Convergence Zone (ITCZ). Droughts and famines over Nordeste have caused several large migrations of the population (Chu, 1991). Druryan et al. (1999) details the El Nino years' enhanced subsidence, warmer surface air temperatures and drought events over Nordeste due to compensation for the anomalous strong convection over the Pacific coast of South America. However, sst anomalies over the tropical Atlantic Ocean correlate even more strongly with Nordeste precipitation. The ITCZ follows the latitude of the warmest sst. So, warm ssts in the tropical North Atlantic tend to cause less of a southward migration of the ITCZ. The reverse is true: cool ssts north of the equator and warm ssts south of the equator in the Atlantic promote further southward placement of the ITCZ and wetter years over Nordeste.

Matarira (1990) found that Zimbabwe similarly suffers rainfall deficits during El Nino years based on correlations of meteorological station precipitation data with sst anomalies. Cane et al (1994) extended these relationships with strong correlations between NINO3 ssts and maize yield in Zimbabwe. Normally Zimbabwe receives 80-90% of its precipitation from November to March due to the presence of the ITCZ over the area. The country's topography features high mountains along its eastern border with Mozambique, topography higher than the other two agricultural regions considered herein. During El Nino years there appeared to be an eastward shift of rainfall towards Madagascar and the Indian Ocean related to the eastward shift of convection areas in most of the tropical belt (Matarira, 1990; Druryan et al., 1999). However, interannual variability of Zimbabwe's climate is only partly shaped by ENSO

events and is strongly shaped by land surface conditions, ssts of the Atlantic and Indian oceans, and other sources of atmospheric variability.

Phillips et al., (1999) examined relationships between ENSO sst anomalies and the maize yields from the USDA/NASS Crops Count Data and the monthly observed precipitation and surface temperature from NOAA. They determined that roughly 15% of the interannual maize yield variability in the US cornbelt was due to ENSO forcing. The positive impact of cooler temperatures and enhanced rainfall during El Nino years was less influential than the La Nina years' warmer and drier summers. They found highest correlations between winter, NINO3 sst anomalies (5S-5N, 90W-180W) and the following summer's surface air temperatures with an r value of 0.41 over the 1950-1995 period.

a. MSU Atmospheric Temperatures

The MSU observations shown in Figure 17 clearly indicate ENSO signals which become hidden and delayed with separation from the equatorial to subtropical to the northern midlatitude zonal bands. The mid-tropospheric temperature signal over the U.S. cornbelt is consequently extremely noisy unlike the strong signals over Nordeste and Zimbabwe. These agricultural regions each only span 6 gridcells in this 4° by 5° AGCM. Figure 18 shows the MSU and AGCM mid-tropospheric time series over these two agricultural regions. Just as Zimbabwe has greater variability than Nordeste in the MSU record, the AGCM's hindcast is more lucid and coherent over Nordeste than Zimbabwe.

Table 9 lists the MSU and AGCM sst-forcing runs' mid-tropospheric correlations for the 1979-1992 period over the relevant zonal bands and the three regions. Nordeste's highest individual run's correlation is 0.81 ± 0.03 and its mean correlation from the seven sst-forced runs 0.78 ± 0.03 . Its correlation from the average of the seven sst-forced runs, sst AG, on the other hand was 0.86. Zimbabwe's mid-tropospheric

correlations between the MSU and the average, sst AG run is 0.64 and significantly greater than its individual run values. The individual, sst-forced correlations reach as high as 0.50 but the mean is 0.39 with a considerable standard deviation of ± 0.11 . While the U.S. cornbelt has a similar standard deviation of 0.10, it does not have a strong signal to correlate to. Most of the correlations between MSU T_b and AGCM T_b over the US cornbelt are not significant, including the mean of 0.11 ± 0.10 .

Though additional atmospheric forcings generally improve the mid-tropospheric performance of the AGCM hindcasts in zonal bands, the atmospheric forcings do not consistently improve the agricultural regions. Correlations in Table 10a of the monthly mid-tropospheric temperatures for Nordeste do not change significantly with addition of forcings unlike correlations for the tropical zone. The AGCM hindcast of mid-tropospheric temperatures over Nordeste remains within the level of 0.73 ± 0.03 . While the performance over Nordeste by the AGCM is consistently good, the addition of known forcings does not alter the veracity of the response in its 6 gridcells.

Zimbabwe, on the other hand, had a highest correlation of mid-tropospheric temperatures at 0.54 ± 0.11 with the addition of greenhouse gases. Further additions of explicit atmospheric forcings actually worsen the correlation. This behavior is particularly notable when tropospheric ozone is added to the accumulated forcings in the last AGCM experiment, run 350. Changes to Zimbabwe's correlations do not reflect the changes to correlations in the equatorial zone. The equatorial zone correlations are no doubt dominated by the AGCM simulation over the Pacific Basin.

Finally, mid-tropospheric temperatures barely achieved a significant correlation of 0.25 ± 0.10 with one of the atmospheric-forced AGCM runs in Table 10 for the US cornbelt. These poor correlations may be partly due the unusually high variability of the model over the continental US (Figure 12). The relatively high variability of the midlatitudes certainly obscures even the observed MSU signal over the US cornbelt. While the northern mid-latitude zone of 30N-50N can reach correlations of 0.50 ± 0.10

with particular atmospheric forcings, the US cornbelt does not respond similarly in its 6 gridcells.

If 1979-1998 seasonal time series are correlated, there is no improvement to the US cornbelt's mid-tropospheric correlations. Nordeste and Zimbabwe's highest seasonal correlations are not larger than the full time series correlations discussed above. However, the AGCM does have seasonal differences in its hindcast performance over Brazil and southern Africa as shown in Table 10b. Nordeste's AGCM T_b match MSU observations best in the winter (JJA) and spring (SON) with maximum correlations at 0.76 and 0.74 respectively. Its fall performance, when northeastern Brazil receives most of its rain, is moderately good with mid-tropospheric temperature correlations ranging from 0.48 to 0.66. AGCM hindcasts over Zimbabwe do better in the summer (DJF) and fall (MAM) months and much worse in the winter (JJA) months. This seasonal response by the AGCM is preferable since Zimbabwe receives most of its rain from November to March. Zimbabwe's seasonal AGCM T_b correlations, however, exhibit much more scatter than Nordeste. Its summer (DJF) correlations range from 0.54 to 0.10, its fall (MAM) from 0.38 to 0.14, its winter (JJA) from -0.12 to 0.34 and its spring (SON) from 0.06 to 0.46. The following sections discuss concurrent precipitation and surface air temperatures over these agricultural regions.

b. GISTEMP Surface Temperatures

The GISTEMP observations shown in Figure 19 clearly show ENSO signals which become hidden by other forcings with concentration from the global to the north hemispheric to the northern hemispheric land averaging. Also these surface temperature time series clearly show a warming trend, particularly over northern hemispheric land (Hansen et al., 1999). The surface air temperature signal over the U.S. cornbelt is extremely noisy unlike the strong warm signal over Nordeste of 1.3 degrees during the 1980's El Ninos and the less clear, but strong signal over Zimbabwe of over 1.5 degrees.

Again, these agricultural regions each only span 6 gridcells in this 4° by 5° AGCM. Figure 20 shows the GISTEMP and AGCM surface air temperature time series over northern hemispheric land and the two agricultural regions. The AGCM time series is from the average of the seven sst-forced runs, sst AG. As with the mid-tropospheric temperatures, the AGCM's surface air temperature hindcast is more coherent over Nordeste than Zimbabwe. This average of the seven sst-forced runs cannot generate the surface air temperature warming seen in the observed northern hemispheric land time series.

Table 11 lists the GISTEMP and AGCM sst-forcing runs' correlations for the 1979-1992 period over the three agricultural regions and over northern hemispheric land. Nordeste's highest individual run's correlation is 0.49 ± 0.04 is not significantly different from the average run, sst AG, correlation of 0.51. The mean correlation over Nordeste, though, is significantly weaker at 0.42 ± 0.04 than the ensemble average. Zimbabwe and the US cornbelt's surface air correlations from individual runs are mostly insignificant. Only the ensemble average, sst AG, and one of the sst-forced runs achieve significant correlations over Zimbabwe of 0.33 and 0.43 respectively. This again underlines the possibility of a good simulation by chance and the necessity of multiple simulations to ensure a reliable hindcast.

Table 12a again shows that though additional atmospheric forcings generally improve performance of the AGCM hindcasts over large areas, the forcings do not consistently improve responses over small agricultural regions. Only the northern hemispheric land correlations over the 1979-1998 period show significant improvement with addition of certain atmospheric forcing, increasing to 0.55 ± 0.07 for the run with greenhouse gases and volcanic aerosols (run 307) and 0.62 ± 0.07 for the run with greenhouse gases, volcanic aerosols and tropospheric ozone changes (run 321). While addition of tropospheric ozone forcing improves northern hemispheric land correlations between the AGCM and GISTEMP when added onto greenhouse gas and

volcanic aerosol forcings, it diminishes this correlation significantly when added to the penultimate combination of forcings.

The AGCM hindcast of surface air temperatures over Nordeste remain close to the maximum level of 0.46 ± 0.04 throughout Table 12a, indifferent to introduced atmospheric forcings. Correlations over 1979-1998 for Zimbabwe and the US corn-belt are mostly insignificant. The AGCM hindcast of surface air temperatures over Zimbabwe does reach 0.37 ± 0.16 with greenhouse gases, volcanic aerosols and stratospheric ozone depletion forcing (run 334), but the scatter in the AGCM performance demands cautious interpretation and multiple realizations of this agricultural region.

If 1979-1998 seasonal time series are correlated, there is no improvement to the US cornbelt's or Zimbabwe's surface air temperature correlations. Nordeste's and the northern hemispheric land's correlations exhibit strong seasonal dependence and do reach higher correlations with observations than seen from the full time series. Table 12b shows that the AGCM hindcasts surface air temperatures over both Nordeste and northern hemispheric land much better during the JJA and SON seasons. Crop production over the US relies on germination and establishment during the spring (MAM) months and tasselling and grain fill during the summer months (JJA) so the stronger performance during northern hemispheric land's summer is encouraging.

c Precipitation

AGCM precipitation anomalies in the agricultural regions were validated against NOAA/NCDC archived station observations (Druryan et al., 1999). Different model and observational means were used to form the anomalies. The ensemble of five runs with globally-specified observed sst, without any additional atmospheric forcings (sst AE), was examined over the time period of 1969-1991. Precipitation anomalies over the agricultural regions from experiments with atmospheric forcings of greenhouse gases and aerosols were similarly validated over the same period to gauge the impact

of the added forcings.

As in the case of tropospheric temperature, AGCM precipitation anomalies for Nordeste also exhibit interannual responses that parallel observations. Druyan et al. (1999) showed that the AGCM time series of Nordeste precipitation anomalies were much better correlated with observations when running means were applied. Thus, the 5-run ensemble mean, sst AE, achieved a 0.63 correlation with observations (significant at the 1% level) from 5-month running means, but only 0.35 from unsmoothed monthly means.

Correlation coefficients between time series of observed and simulated Nordeste precipitation anomalies were comparable with and without the additional atmospheric forcings, except when the combined effects of greenhouse gases, volcanic aerosols and stratospheric ozone were added (run 334). The 5-month smoothed time series of Nordeste precipitation for this run achieved a 0.72 correlation with observations. This is much stronger than the average correlation of 0.49 (with a standard deviation ≈ 0.08) from the five individual, sst-forced correlations. This improvement to the correlation coefficient has only a 6% probability of being a chance occurrence. Inclusion of forcing from tropospheric aerosols did not improve the simulation of Nordeste precipitation anomalies.

Because of the seasonality of Zimbabwe's climate, usually 80-90% of its annual rainfall is concentrated in the months of November to March. Even when the correlation between AGCM and observed time trends of Zimbabwe precipitation anomalies is nil for monthly means, it can be positive for November-March totals (Druyan et al., 1999). For the ensemble average of 5 simulations (sst AE), the correlation between model and observed November-March Zimbabwe precipitation anomalies for 1969-1991 was 0.23. This result is not significant since only 22 seasons are considered. Seasonal precipitation time series for only three of the five individual sst runs were positively correlated with observations, the highest being 0.31. The average of

the five individual correlation coefficients was a mere 0.12 with a standard deviation of 0.14.

Correlations of Zimbabwe seasonal precipitation anomalies showed no benefit from the additional atmospheric forcings, except when the combined effects of greenhouse gases, volcanic aerosols and stratospheric ozone were added (run 334). The Zimbabwe November-March rainfall anomalies for that simulation achieved a correlation of 0.54 with observations, a correlation that is significantly different from the precipitation results of the other experiments. Since only twelve seasons are included, the probability that the positive correlation of 0.54 is a chance occurrence is roughly 7%. The simulation of Zimbabwe precipitation anomalies did not benefit from inclusion of the effects of tropospheric aerosols.

Druyan et al. (1999) found that even with a 5-month smoothing of the ensemble time series of US Corn Belt precipitation was still uncorrelated with the corresponding observational time series. The impact of additional atmospheric forcings, individually or collectively, did not improve the correlation of modeled rainfall anomalies for the US Corn Belt. This is not surprising, considering our finding above that the rather chaotic nature of mid-latitude atmospheric variability also prevented any significant correlation between model and observed tropospheric temperatures in this region.

However, in terms of seasonal precipitation responses, Ropelewski and Halpert (1986) identified typical spatial patterns of precipitation and temperature anomalies over North America associated with the ENSO cycle. The southeastern US and northern Mexico had positive precipitation anomalies for 18 of 22 warm events. Composites of US precipitation anomalies for seven ENSO warm events by Livezey et al. (1997) similarly showed that January through March saw anomalous rain along the Gulf coast from Texas to Florida. In addition, the same months, particularly January, experience large negative precipitation anomalies over the US Midwest and Lower Mississippi Valley (excluding Louisiana). Wang et al. (1999) also found sta-

tistical correlations between positive sst anomalies in the Pacific and positive winter precipitation anomalies for southern California eastward to Texas. Cold Pacific SST anomalies, on the other hand, were correlated with drought in the southeast US and rainy conditions in the Midwest.

Therefore, patterns of the simulated December-February (DJF) precipitation anomalies over North America were examined from the the sst-forcing ensemble and from two individual atmospheric-forcing runs. AGCM DJF precipitation anomalies were computed relative to each experiment's multi-year mean but compared to observed anomalies relative to 1950-1995. For the sst-forcing ensemble, the average of five runs 255A-E, DJF anomalies were computed relative to the 1970-1991 mean. For the single runs, DJF anomalies were computed relative to 1980-1997 means. The first of these runs (run 334) accounts for atmospheric forcing from greenhouse gases, volcanic aerosols and stratospheric ozone and the second (run 350) adds in tropospheric sulfates, carbon aerosols and ozone forcings. Both of these simulations achieved comparable or better correlations with observed time series of Nordeste and Zimbabwe rainfall anomalies compared with the sst ensemble. However, the sst-forcing ensemble results inherently had more coherent responses than the individual atmospheric-forcing runs and so caution is necessary in their comparisons.

The spatial distribution of observed, rain gauge precipitation anomalies over the US for the DJF 1982-83 El Nino season includes large positive rainfall anomalies of more than 200 mm across the Pacific and Gulf coasts. A strip of heavy rainfall extends from the Mississippi Valley delta northward. The northeast US is the only area experiencing significant negative precipitation anomalies. Negative departures in the Ohio Valley overlap the area identified for below normal precipitation by the Livezey et al. (1997) El Nino composite for January-March.

Results from the sst ensemble, 255 AE, include large positive anomalies over the southeastern US and the Lower Mississippi Valley, matching the observational evi-

dence. Also there is agreement regarding smaller rainfall surpluses over the Southwest and the Great Plains. The additional forcings in run 334 and 350 gave comparable anomalies over the southeastern and southwestern US. However, accounting for greenhouse gases and volcanic aerosols (run 334) does not achieve realistic precipitation anomalies over the West Coast or elsewhere over the US. Adding the effect of tropospheric aerosols (run 350) created a more realistic pattern of precipitation over the West Coast but not over the Northeast.

The El Nino season of DJF 1986-87 also featured positive precipitation anomalies along the mid-Atlantic coast, the Gulf coast and much of Texas. Contrasting dry conditions prevailed along the West Coast and in the Midwest. The AGCM ensemble, sst AE, was appropriately rainy over the mid-Atlantic states but not along the Gulf coast. Negative anomalies over the western US were much smaller than observed and the Midwest was not particularly dry in the simulations. Thus, the added forcings for this season in runs 334 and 350 did not produce precipitation anomalies more realistic than the sst ensemble over most regions.

Lastly, the La Nina season of DJF 1988-89 featured drought along the Gulf, Atlantic and Pacific coasts. A single contiguous area of excessive rainfall extended from the Lower Mississippi Valley northeastward into the Tennessee and Ohio Valleys. The AGCM sst ensemble, 255 AE, does indicate a drier than average regime over the southeastern US which overlaps the area of the observed drought. It does not represent the dry conditions in the west or the heavy rains observed in Tennessee/Kentucky. The simulations with the added forcings did not improve on these sst ensemble results.

7. Summary

Multiple realizations of the 1979-1998 time period have been hindcast by the GISS AGCM to examine its performance, particularly over sensitive agricultural regions. While the initial ensemble of seven runs was only forced by ssts, subsequent runs incor-

porated atmospheric forcings from greenhouse gases, stratospheric volcanic aerosols opacities, stratospheric ozone, sparsely observed tropospheric ozone and even more poorly observed tropospheric sulfate and black carbon aerosols. Several questions can be answered:

- Does the AGCM simulate the mid-tropospheric temperature dumbbell pattern of Yulaeva and Wallace (1994) in response to El Nino sst forcing? Yes. However, the AGCM's warmings in the troposphere do not always occur in discrete, off-equator centers as observed. Does the AGCM's tropopause move and the stratospheric temperatures cool and compensate locally for tropospheric warmth during El Nino (Reid et al., 1989; Yulaeva and Wallace, 1994; Randel and Cobb, 1994)? Yes. Despite the coarse vertical resolution of this 9-layer AGCM, its lower stratospheric temperatures responded locally to the specified lower boundary forcing of El Nino sst anomalies with cool anomalies over the eastern Pacific.

- Is there reduced static stability in the tropical upper troposphere over the Pacific due to warm equatorial sst? Yes. Do the upper tropospheric, subtropical jet stream and the Hadley Cell circulation strengthen promoting teleconnections? Yes. In January 1983 and January 1998, for instance, the upward vertical motion in the southern branch of the Hadley Cell tripled, its associated stream functions increased by up to 18%, the associated meridional flow in the upper troposphere increased in speeds by up to 10% and the subtropical jet's zonal wind speeds increased by up to 28%.

- How well can the AGCM correlate with the oceanic lower tropospheric, mid-tropospheric and lower stratospheric temperature time series of MSU? Correlations for 1979-1998 between AGCM and MSU temperature time series reach as high as 0.91 ± 0.16 globally for the lower stratosphere, as high as 0.66 ± 0.04 globally and 0.84 ± 0.02 in the tropics for the mid-troposphere and 0.61 ± 0.06 globally and 0.79 ± 0.02 in the tropics for the oceanic lower troposphere. The AGCM consistently

disagreed with warm, lower tropospheric MSU channel T_b anomalies prior to mid-1981 reminiscent of concerns with anomalous MSU 'c' channel 2R discontinuities (see Figure 6) found by Hurrell and Trenberth (1998) in comparisons of MSU to sst observations.

- Do the correlations improve with additional atmospheric forcings? Yes. This result is especially true in the lower stratosphere and often true in the mid-troposphere but less true in the lower troposphere. Figure 16 shows the MSU and AGCM time series from the runs forced by the most certain observations. Tropospheric T_b anomalies during warm El Nino events, in particular, achieved higher magnitudes with inclusion of known atmospheric forcings. The run which incorporated the least uncertain collection of atmospheric forcings, run 334 with greenhouse gases, stratospheric aerosols and stratospheric ozone depletion, appears to yield most of the top correlations for the lower stratospheric, mid-tropospheric and lower-tropospheric temperatures and for surface air temperatures and precipitation anomalies.

This result is complicated by the land-ocean bias of responsiveness to imposed atmospheric forcings on top of specified ssts: the ocean-dominated, southern hemispheric correlations were relatively indifferent to imposed atmospheric forcings while the land-dominated northern hemispheric correlations responded to imposed atmospheric forcings. Southern hemispheric correlations between AGCM values and observations were smaller in magnitude or insignificant compared to their northern hemispheric counterparts. Only lower stratospheric T_b correlations were similar in both the northern and southern hemispheres and equally responsive to the addition of known atmospheric forcings.

Comparisons between the individual atmospheric forcings is difficult given single hindcasts, given the varying land amounts in latitudinal zones, given the forcings' differing regional and vertical distributions and given the AGCM's redistribution of a forcing's impact. For instance, while stratospheric ozone depletion is specified primar-

ily in the mid- to high latitudes, the AGCM's mid-tropospheric and lower tropospheric temperatures improve significantly across equatorial latitudes. Addition of the most uncertain forcing of tropospheric carbon aerosols notably improves mid-tropospheric, lower tropospheric and surface air temperatures in the northern mid-latitudes while lowering global correlations for the tropospheric temperature time series. Tropospheric sulfates, oppositely, worsen northern mid-latitude performances but improve global correlations in the mid-troposphere and lower troposphere. Lastly, addition of the tropospheric ozone forcing had variable impacts on the AGCM hindcasts. While this forcing improved correlations when added to the run already forced by ssts, greenhouse gases, volcanic aerosols and stratospheric ozone, it worsened the AGCM hindcast forced by the penultimate combination of atmospheric forcings. This variable impact from inclusion of tropospheric ozone forcing opens the door to questions concerning the necessity of other forcing's presence in order to obtain the desired outcome or hindcast. This result also draws into question the tropospheric ozone distribution employed as similar experiments by Folland et al. (1998) in comparison with radiosonde upper air temperatures found strong improvement with inclusion of tropospheric ozone changes.

- Do the correlations change with use of different MSU versions? No, or at least not yet. Table 13 shows 1979-1992 and 1979-1998 correlations between mid-tropospheric and lower stratospheric T_b time series from an sst-forced run and an atmospheric-forced run and from the three MSU versions. Little change occurs with use of a different MSU version. Unfortunately the much-discussed lower tropospheric MSU time series is not available yet in the most recent, most sophisticated version 'd'.

- How good is the AGCM's response over sensitive agricultural regions? The AGCM's mid-tropospheric temperature response is quite good over Nordeste, northeastern Brazil, at maximum correlation with observations of 0.75 ± 0.03 , moderate

over Zimbabwe at 0.54 ± 0.11 and weak over the US cornbelt at 0.25 ± 0.10 . The latter two agricultural regions, in Africa and in the northern mid-latitudes, suffered from higher levels of non-sst variability. Finally, does the AGCM's response over these agricultural regions improve with inclusion of atmospheric forcings? The AGCM's response remains mostly the same over the agricultural regions irrespective of the introduced atmospheric forcings. Only the combination of greenhouse gases, volcanic aerosols and stratospheric ozone depletion (run 334) seem to provide surface air temperature and precipitation anomalies over Zimbabwe notably better than the sst-forced ensemble. The correlation of 0.54 between Zimbabwe AGCM and observational November-March seasonal values, for example, had only a 6% probability of being a chance occurrence

The AGCM's hindcasts do have a seasonal dependence. Nordeste's mid-tropospheric temperatures from the AGCM match MSU observations best in the winter (JJA) and spring (SON) with maximum correlations at 0.76 and 0.74 respectively. Surface air temperature performances improve over both Nordeste and northern hemispheric land during the JJA and SON seasons. As crop production over the US relies on germination and establishment during the spring (MAM) months and tasselling and grain fill during the summer months (JJA), the stronger performance during northern hemispheric land's summer is encouraging. Each region encompasses 6 AGCM gridcells and, while atmospheric forcings improve hindcasts over hemispheric or zonal areas, the space of 6 gridcells is susceptible to variability and more sensitive to synoptic mechanisms. For hindcasts or forecasts over such small areas, this AGCM's diagnostics should probably be used to initialize and update regional models whose diagnostics could then be given to agricultural, fishery and economic models.

In future work the influence of higher vertical and horizontal resolution in the climate model will be examined. Also, the number of runs needed with these resolution for a sound ensemble average will be addressed. Table 14 shows the impact on

correlations with observations when the number of runs for an ensemble below seven runs. For this coarse, 9 vertical layers and 4 degrees latitude by 5 degrees longitude, AGCM it appears that 5 runs may have sufficed for the sst ensemble. The failure of the observed sst forcing to prompt the AGCM to produce high correlations in the southern hemisphere suggests that the specified sst data may be wrong in areas. This is certainly possible given the sparseness of such observations particularly over southern mid- to high latitudes and may be addressed by future AMIP II ssts. Forcings due to solar variability and the QBO will also be incorporated into future work. Finally, the CAFE project plans to run these forcing experiments in three lower boundary tests: for the “ideal” match with use of observed sea surface temperatures (sst) and observed sea ice extent, for the “less-than-ideal” match of OAGCM-calculated ssts and sea ice; and, for the “forecasting” mode into the early-2000’s. These different phases would test the capability of an interactive ocean to produce the observed sst trends given the atmospheric forcings.

Acknowledgments

The CAFE work was supported by a NASA Earth System Science Grant NCC5-117. K Shah was also supported by NSF Grant ATM-96-28843. L. Druyan was also supported by NSF Grant ATM-97-25142. NASA GISS climate work was also supported by NASA Climate and Earth Observing System Programs.

References

- Boyle, J. S., Intercomparison of interannual variability of the global 200-hPa circulation for AMIP simulations, *J. Climate*, **11**, 2505-2529, 1998.
- Cane, M. A., G. Eshel and R. W. Buckland, Forecasting Zimbabwe maize yield using eastern equatorial Pacific sea surface temperature, *Nature*, **370**, 204-205, 1994.
- Cess, R. D. et al., Uncertainties in Carbon Dioxide Radiative Forcing in Atmospheric General Circulation Models, *Science*, **262**, 1252-1255, 1993.
- Christy, J. R. and S. J. Drouilhet, J., Variability in daily zonal mean lower stratospheric temperatures, *J. Chm*, **7**, 106-120, 1994.
- Christy, J. R., R. W. Spencer, and E. S. Lobl, Analysis of the merging procedure for the MSU daily temperature time series, *J. climate*, **11**, 2016-2041 1998.
- Christy, J. R., R. W. Spencer, and W.D. Braswell, How accurate are satellite 'thermometers'?, *Nature*, **389**, 342, 1997.
- Chu, P., Brazil's climate anomalies and ENSO, in *Teleconnections Linking Worldwide Climatic Anomalies*, Glantz, Katz and Nicholls, eds, Cambridge Univ. Press, NY, 43-72, 1991.
- Del Genio, A.D., M-S Yao , W. Kovari and K-W. Lo , A prognostic cloud water parameterization for global climate models, *J.Chm.*, **9**, 270-304, 1996.
- Druyan, L., K. Shah, M. Chandler, and D. Rind, GCM Hindcast of sst-forced climate variability over agriculturally intensive regions, . *Chm. Change*, In press.
- Druyan, L. , K. P. Shah, K. Lo, J. Marengo and G. Russell, Impacts of Model Improvements on General Circulation Model Sensitivity to Sea Surface Temperature Forcing, *Inter. J. Chm.*, **15**, 1061-1086, 1995..
- Folland, C. K., D. M.H. Sexton, D. Karoly, C. Johnson, D. Rowell and D. Parker, Influences of Anthropogenic and Oceanic Forcings on Recent Climate Change, *GRL*, **25**, 353-356, 1998.

- Gaffen, D., Falling satellites, rising temperatures?, *Nature*, **394**, 615-616, 1998.
- Hansen, J. et al. Efficient Three-Dimensional Global Models for Climate Studies: Models I and II. *Mon Wea. Rev.*, **111**, 609-662, 1983.
- Hansen, J., H. Wilson, M. Sato, R. Ruedy, K. Shah, and E. Hansen , Satellite and Surface Temperature Data at Odds? *Chmatic Change*, **30**, 103-117, 1995.
- Hansen, J., R. Ruedy, J. Glascoe and M. Sato, GISS Analysis of Surface Temperature Change, Submitted to *JGR* , 1999.
- Hansen, J., R. Ruedy, M. Sato and R. Reynolds, Global surface air temperatures in 1995: Return to pre-Pinatubo levels, *GRL*, **23**, 1665-1668 , 1996.
- Hansen, J. et al., Forcings and chaos in interannual to decadal climate change, *JGR*, **102**, 25679-25720, 1997 .
- Hansen, J , M Sato, R. Ruedy, A. Lacis and J. Glascoe, Global Climate Data and Models: A reconciliation, *Science*, **281**, 930, 1998.
- Hartke, G. and D. Rind, Improved surface and boundary layer models for the GISS GCM, *JGR*, **102**, 16407-16422, 1997.
- Hollandsworth, S. M., R D. McPeters, L.E. Flynn, W. Planet, A.J.Miller, and S. Chandra, Ozone trends deduced from combined Nimbus 7 SBUV and NOAA-11 SBUV/2 data, *GRL*, 905-908, 1995.
- Hurrell, J. and K. Trenberth, Difficulties in obtaining reliable temperature trends: Reconciling the surface and satellite microwave sounding unit records, *J. Chmate.*, **11**, 945-967, 1998.
- Hoerling, M. P. and A. Kumar, Origins of Extreme Climate States during the 1982-83 ENSO Winter, *J. Clm.*, **10**, 2859-2870, 1997.
- Hoerling, M. P., A. Kumar and M. Zhong, El Nino, La Nina and the Nonlinearity of their Teleconnections, *J. Clm.*, **10**, 1769-1786, 1997.
- IPCC, *Chmate Change, 1992*, Houghton, Callander and Varnay eds, Cambridge Univ. Press, U.K., 1992.

- IPCC, *Climate Change*, 1995, Houghton, Filho, Callander, Harris, Kattenberg and Maskell eds, Cambridge Univ. Press, U.K., 1996.
- Kiladis, G. N. and H. Diaz, An Analysis of the 1877-1878 ENSO Episode and Comparison with 1982-83, *Mon. Wea. Rev.*, **114**, 1035-1047, 1986.
- Koch, D., D. Jacobs, I. Tegen, D. Rind and M. Chin, Tropospheric sulfur simulation and sulfate direct radiative forcing in the GISS GCM, *JGR*, In press, 1999.
- Lau, K.-M, J.H. Kim, and Y. Sud, Intercomparison of Hydrologic Process in AMIP GCMs, *Bull. Am. Soc.*, **77**, 2209-2228, 1996.
- Livezey, R., M. Masutani, A. Leetmaa, H. Rui, M. Ji and A. Kumar, Teleconnective response of the Pacific-North American region atmosphere to large Central Equatorial Pacific SST anomalies. *J. Climate*, **10**, 1787-1820, 1997.
- Logan, J. A. (1994) Trends in the Vertical Distribution of Ozone: An Analysis of Ozonesonde Data. *JGR*, **99**, 25553-25585.
- Matarira, C. (1990) Drought over Zimbabwe in a regional and global model, *Int. J. Clim*, **10**, 609-625.
- McCormick, M. P., R. E. Veiga, and W. P. Chu (1992) Stratospheric Ozone Profile and Total Ozone Trends Derived from the SAGE I and SAGE II Data. *Geo. Res. Lett.*, **19**, 269-272.
- McPeters, R. D. Ozone profile comparison, in *The Atmospheric Effects of Stratospheric Aircraft*, Prather and Remsberg, eds, NASA Reference Publication 1092, NASA, MTPE, Washington, D. C., D1-D37, 1993.
- Miller, A.J. et al. (1992) Comparison of Observed Ozone and Temperature Trends in the Lower Stratosphere. *Geo. Res. Lett.*, **19**, 929-932.
- Phillips, J., B. Rajagopalan, M. Cane, and C. Rosenzweig, The role of ENSO in determining climate and maize yield variability in the U.S. cornbelt, *Inter, J. Clim.*, In review, 1999.
- Randel, W. J. and J. B. Cobb (1994) Coherent Variations of Monthly Mean Total

- Ozone and Lower Stratospheric Temperature. *JGR*, **99**, 5433-5447.
- Reid, G. C., K.S. Gage and J.R. McAfee, The thermal response of the tropical atmosphere to variations in equatorial Pacific sea surface temperature, *JGR*, **94**, 14705-14716, 1989.
- Reynolds, R. W. and T. M. Smith, Improved global sea surface temperature analysis, *J. Climate*, **7**, 929-948, 1994.
- Rind, D., J. Lerner, K. Shah and R. Suozzo, Use of on-line tracers as a diagnostic tool in GCM development. 2. Transport between the tropospheric and stratosphere, *JGR*, In press, 1999.
- Robertson, A. D., J.T. Overpeck, E. Mosley-Thompson, G.A. Zielinski, J. L. Lean, D. Koch, J.E. Penner, I. Tegen, D. Rind and R. Healy, Hypothesized Climate Forcing Time Series for the Last 500 Years, in preparation for submission, 1999.
- Ropelewski, C.F. and M.S. Halpert, North American precipitation and temperature patterns associated with the El Niño-Southern Oscillation, *Mon. Wea. Rev.*, **114**, 2352-62, 1986.
- Ropelewski, C. F. and M. S. Halpert, Global and regional scale patterns associated with the El Niño/Southern Oscillation (ENSO), *Mon. Wea. Rev.*, **115**, 2352-2362, 1987.
- Rosenzweig, C. and F. Abramopoulos, Land-Surface Model Development for the GISS GCM, *J. Climate*, **10**, 2040-2054, 1997.
- Santer, B. D., J.J. Hnilo, T.M.L. Wigley, J.S. Boyle, C. Doutraux, M. Fiorino, D. E. Parker, and K.E. Taylor, Uncertainties in observationally based estimates of temperature change in the free atmosphere, —it *JGR*, **104**, 6305-6333.
- Sato, M., J. Hansen, M. P. McCormick and J. B. Pollack, Stratospheric Aerosol Optical Depths, 1850-1990, *JGR*, **98**, 22987-22994, 1993.
- Schwalb, A., The TIROS-N/NOAA A-G satellite series, NOAA Technical Memorandum NESS 95, Washington D.C., 1978.

- Shah, K.P. and D. Rind (1995) Use of Microwave Brightness Temperatures With a General Circulation Model. *JGR*, **100**, 13841-13874.
- Shah, K. P. and D. Rind, Comparison of Upper Tropospheric and Lower Stratospheric Temperatures: MSU, Radiosonde, CIRA, and NCEP/NCAR Reanalysis Climatologies, *JGR*, **103**, 31569-31592, 1998.
- Spencer, R., 1995, personal communication.
- Spencer, R., W. M. Lapenta, and F. Robertson, Vorticity and vertical motions diagnosed from satellite deep-layer temperatures, *Mon. Wea. Rev.*, **123**, 1800-1810, 1995.
- Spencer, R. W. and J.R. Christy, Precision Lower Stratospheric Temperature Monitoring with the MSU: Technique, Validation, and Results 1979-1991, *J. Chm.*, **6**, 1194-1204, 1993.
- Spencer, R. and J. Christy, Precision and radiosonde validation of satellite gridpoint temperature anomalies, I, MSU channel 2, *J. Chm.*, **5**, 847-857, 1992a.
- Spencer, R. and J. Christy, Precision and radiosonde validation of satellite gridpoint temperature anomalies, II, A tropospheric retrieval and trends during 1979-1990, *J. Chm.*, **5**, 858-866, 1992b.
- Stolarski, R. S., P. Bloomfield, and R. D. McPeters (1991) Total Ozone Trends Deduced from Nimbus 7 TOMS Data. *Geophys. Res. Lett.*, **18**, 1015-1018.
- Trenberth, K, General Characteristics of El Nino-Southern Oscillation, , in *Teleconnections linking worldwide climate anomalies*, Glantz, Katz and Nicholls, eds, Cambridge Univ. Press, 1991.
- Tribbia, J, The rudimentary theory of atmospheric teleconnections associated with ENSO, in *Teleconnections linking worldwide climate anomalies*, Glantz, Katz and Nicholls, eds, Cambridge Univ. Press, 1991.
- Wang, H., M. Ting and J. Ming, Prediction of seasonal mean US precipitation based on El Nino SST, *GRL*, **26**, 1341-1344, 1999.

- Wentz, F. J. and M. Schabel, Effects of orbital decay on satellite-derived lower-tropospheric temperature trends, *Nature*, **394**, 661-664, 1998.
- Wu, Z.-J. and B. McAvaney, Simulations of impacts of climatological MSU data processing methods using NCEP/NCAR reanalysis data, *JGR*, **103**, 19495-19508, 1998.
- Yulaeva, E. and J. M. Wallace, The signature of ENSO in global temperature and precipitation fields derived from the microwave sounding units, *J. Clm.*, **7**, 1719-1736, 1994.

Table 1. CAFE AGCM Transient Experiments

AGCM Run	Description	Years Analyzed
255m9	Control Run, Mean ssts	10 years
255Am9	Obs ssts	Jan 1979 - Nov 1992
255Bm9	"	"
255Cm9	"	"
255Dm9	"	"
255Em9	"	"
255Fm9	"	Jan 1979 - Apr 1998
255Gm9	"	"
255ACm9	Average of 3 runs, 255A-255C	Jan 1979 - Nov 1992
255AEm9	Average of 5 runs, 255A-255E	Jan 1979 - Nov 1992
255AGm9	Average of 7 runs, 255A-255G	Jan 1979 - Nov 1992
281m9	Obs ssts + CO ₂ & Trace Gases	Jan 1979 - Apr 1998
307m9	Obs ssts + CO ₂ & Trace Gases + Volcanic Aerosols	"
334m9	Obs ssts + CO ₂ & Trace Gases + Volcanic Aerosols + ΔO_3 strat	"
321m9	Obs ssts + CO ₂ & Trace Gases + Volcanic Aerosols + ΔO_3 trop	"
339m9	Obs ssts + CO ₂ & Trace Gases + Volcanic Aerosols + ΔO_3 strat & trop	"
332m9	Obs ssts + CO ₂ & Trace Gases + Volcanic Aerosols + ΔO_3 strat + trop Sulfate Aerosols	"
349m9	Obs ssts + CO ₂ & Trace Gases + Volcanic Aerosols + ΔO_3 strat + trop Sulfate & Carbon Aerosols	"
350m9	Obs ssts + CO ₂ & Trace Gases + Volcanic Aerosols + ΔO_3 strat & trop + trop Sulfate & Carbon Aerosols	"

Table 2. Trace Gas Concentrations used as AGCM Forcings

Year	CO ₂ ppm	N ₂ O ppb	CH ₄ ppb	CFC-11 ppt	CFC-12 ppt
1969	323.4	294.4	1389.7	51.1	106.5
1972	327.0	296.2	1429.7	78.1	150.0
1975	330.7	298.0	1475.5	116.0	207.0
1978	334.6	300.4	1522.7	147.4	257.1
1981	341.3	303.4	1581.0	283.5	330.5
1984	345.7	305.8	1620.0	445.0	383.0
1987	350.1	306.8	1659.0	612.5	436.0
1990	354.8	309.8	1687.0	780.0	489.5
1993	357.9	312.0	1709.0	928.5	524.0
1996	362.2	313.9	1737.0	1065.5	528.0
1999	366.4	315.7	1761.0	1185.5	528.0

Table 3. Zonally-averaged AGCM Diagnostics: Control Run versus Peak El Ninos

Diagnostic	Control	sst F	sst F
	Ave 10 Januarys	January 1983	January 1998
Subtropical Jet			
Zonal Wind			
32°N			
103 mb	40.3	42.5	45.1 m/s
201 mb	39.5	41.5	43.7 m/s
Hadley Cell			
Meridional Wind			
201 mb			
8°S	0.78	-0.10	0.06 m/s
8°N	2.46	2.66	2.70 m/s
24°N	0.53	0.28	0.34 m/s
Vertical Motion			
Column average			
6°S	12	10	4 10^{-5} mb/s
2°N	11	33	33 10^{-5} mb/s
10°N	3	-5	-3 10^{-5} mb/s
Stream Function			
Column max			
8°S	-62	23	22 10^9 kg/s
0°	-149	-99	-73 10^9 kg/s
8°N	-178	-210	-197 10^9 kg/s
16°N	-144	-150	-140 10^9 kg/s

Table 4. Correlations of sst-Forced AGCM and MSU Trop Ch 2 T_b Time Series: 1979-1992

Run	PacTr 20S-20N 80W-100E	PacTr	Tr 20S-20N	Equa 30S-30N	NH ml 30N-50N	NH hl 50N-70N	SH ml 30S-50S	SH hl 50S-70S	SH	NH	G
	MSU 90a	MSU c									
sst A	0.75	0.75	0.79	0.73	0.20	0.21	<i>0.18</i>	<i>-0.09</i>	0.37	0.53	0.56
sst B	0.70	0.69	0.73	0.68	0.32	<i>0.14</i>	<i>0.12</i>	<i>0.08</i>	0.22	0.58	0.54
sst C	0.74	0.74	0.76	0.67	0.28	<i>0.10</i>	<i>0.10</i>	<i>-0.05</i>	0.24	0.46	0.45
sst D	0.66	0.65	0.73	0.67	0.37	<i>0.12</i>	<i>0.14</i>	<i>-0.11</i>	0.25	0.55	0.51
sst E	0.72	0.72	0.73	0.66	0.35	<i>0.10</i>	0.21	<i>-0.05</i>	0.36	0.52	0.52
sst F	0.71	0.69	0.75	0.69	0.32	<i>-0.04</i>	<i>0.17</i>	<i>0.08</i>	0.37	0.45	0.54
sst G	0.69	0.69	0.73	0.66	<i>0.18</i>	<i>-0.05</i>	<i>0.08</i>	<i>-0.02</i>	0.36	0.43	0.51
sst AG	0.79	0.78	0.83	0.77	0.42	<i>0.15</i>	0.21	<i>-0.05</i>	0.41	0.64	0.63
r mean	0.71	0.70	0.75	0.68	0.29	<i>0.08</i>	<i>0.14</i>	<i>-0.02</i>	0.31	0.50	0.52
r std	0.03	0.03	0.02	0.02	0.07	0.10	0.05	0.08	0.07	0.06	0.04

Italicized correlations are not significant

Table 5. Correlations of AGCM and MSU 3-month-smoothed Ch 2 Trop T_b Time Series: 1979-1992

Run	PacTr 20S-20N 80W-100E	Tr 20S-20N	Equa 30S-30N	NH ml 30N-50N	NH hl 50N-70N	SH ml 30S-50S	SH hl 50S-70S	SH	NH	G
sst A	0.84	0.87	0.83	0.33	0.29	0.25	<i>-0.18</i>	0.48	0.65	0.67
sst B	0.79	0.82	0.77	0.42	0.23	<i>0.17</i>	<i>0.07</i>	0.30	0.69	0.65
sst C	0.82	0.84	0.77	0.42	<i>0.18</i>	0.23	<i>-0.09</i>	0.35	0.59	0.57
sst D	0.76	0.82	0.78	0.50	0.24	0.21	<i>-0.16</i>	0.34	0.69	0.64
sst E	0.79	0.81	0.75	0.49	<i>0.15</i>	0.28	<i>-0.11</i>	0.47	0.66	0.65
sst F	0.82	0.85	0.81	0.44	<i>-0.01</i>	0.29	<i>0.13</i>	0.49	0.62	0.68
sst G	0.80	0.83	0.78	0.23	<i>-0.06</i>	<i>0.18</i>	<i>-0.06</i>	0.48	0.56	0.62
sst AG	0.85	0.89	0.85	0.55	0.25	0.31	<i>-0.12</i>	0.50	0.74	0.72
r mean	0.80	0.84	0.78	0.41	<i>0.14</i>	0.23	<i>-0.06</i>	0.41	0.64	0.64
r std	0.03	0.02	0.03	0.10	0.13	0.05	0.12	0.08	0.05	0.04
sst + gg	0.80	0.84	0.80	0.47	0.12	0.23	-0.01	0.45	0.61	0.65
sst + gg + vol	0.81	0.82	0.79	0.52	0.27	0.25	0.05	0.49	0.68	0.69
sst + gg + vol + O3 s	0.86	0.87	0.84	0.40	0.16	0.24	-0.22	0.55	0.65	0.67
sst + gg + vol + O3 t	0.83	0.85	0.80	0.38	0.23	0.17	0.12	0.43	0.59	0.61
sst + gg + vol + O3 s&t	0.86	0.87	0.85	0.49	0.29	<i>0.05</i>	-0.24	0.44	0.68	0.68
sst + gg + vol + O3 s + S	0.82	0.86	0.84	0.30	0.40	<i>0.16</i>	<i>-0.13</i>	0.55	0.68	0.73
sst + gg + vol + O3 s + S&C	0.82	0.85	0.80	0.64	0.40	<i>0.13</i>	<i>-0.14</i>	0.42	0.72	0.70
sst + gg + vol + O3 s&t + S&C	0.81	0.84	0.77	0.51	0.36	<i>0.14</i>	<i>-0.04</i>	0.33	0.69	0.60

Italicized correlations are not significant

Table 6. Correlations of AGCM and MSU 3-month-smoothed Ch 2 Trop T_b Time Series: 1979-98

Run	PacTr 20S-20N 80W-100E	Tr 20S-20N	Equa 30S-30N	NH ml 30N-50N	NH hl 50N-70N	SH ml 30S-50S	SH hl 50S-70S	SH	NH	G
r std	0 03	0 02	0 03	0 10	0 13	0 05	0 12	0.08	0.05	0.04
1979-1998										
sst F	0 77	0 81	0 77	0 40	<i>-0 06</i>	0.26	<i>0 07</i>	0 43	0.57	0 60
sst G	0 76	0 79	0 75	0.20	<i>0.04</i>	0.17	<i>-0.10</i>	0 42	0 51	0.55
sst + gg	0 71	0 76	0 70	0 33	<i>0 12</i>	<i>0.13</i>	<i>0.00</i>	0 34	0 48	0 49
sst + gg + vol	0 74	0 76	0 72	0 50	0 31	0.21	<i>0 05</i>	0 40	0 62	0 58
sst + gg + vol + O3 s	0 82	0 84	0 80	0 35	0 18	0 18	<i>-0 03</i>	0 50	0 58	0 60
sst + gg + vol + O3 t	0 79	0 81	0 74	0 39	0 20	<i>0 14</i>	<i>-0 01</i>	0 35	0 51	0 51
sst + gg + vol + O3 s&t	0 82	0 83	0 80	0 42	0 33	<i>0 03</i>	-0 15	0 39	0 65	0 62
sst + gg + vol + O3 s + S	0 79	0 83	0 79	0 25	0 39	0 19	<i>-0 10</i>	0 50	0 62	0 66
sst + gg + vol + O3 s + S&C	0 78	0 80	0 74	0 50	0 36	<i>0 11</i>	<i>-0.06</i>	0 33	0 63	0 59
sst + gg + vol + O3 s&t + S&C	0 77	0 78	0 72	0 40	0 30	<i>0 11</i>	<i>-0 04</i>	0 26	0 57	0.50

Italicized correlations are not significant

Table 7. Correlations of AGCM and MSU 3-month-smoothed Ch 4 Lower Strat T_b Time Series

Run	PacTr 20S-20N 80W-100E	Tr 20S-20N	Equa 30S-30N	NH ml 30N-50N	NH hl 50N-70N	SH ml 30S-50S	SH hl 50S-70S	SH	NH	G
1979-92										
sst AG	<i>-0 15</i>	<i>-0 01</i>	<i>0 07</i>	<i>-0 20</i>	<i>0 13</i>	0 21	0 26	<i>0 09</i>	<i>-0 19</i>	<i>-0 17</i>
r mean	<i>-0 10</i>	<i>-0 01</i>	<i>0 04</i>	<i>-0 12</i>	<i>0 07</i>	<i>0 12</i>	<i>0 12</i>	<i>0 05</i>	<i>-0 14</i>	<i>-0 15</i>
r std	0 10	0 13	0 13	0 11	0 09	0 06	0 13	0 05	0 12	0 16
1979-98										
sst F	<i>-0 12</i>	<i>-0 15</i>	<i>-0 05</i>	<i>-0 12</i>	<i>0 16</i>	<i>0 08</i>	0 17	<i>0 05</i>	<i>-0 11</i>	<i>-0 20</i>
sst G	<i>-0 07</i>	<i>-0 10</i>	<i>-0 13</i>	<i>-0 14</i>	<i>0 07</i>	<i>0 02</i>	<i>0 08</i>	<i>-0 17</i>	<i>-0 11</i>	<i>-0 28</i>
sst + gg	0 07	0 15	0 17	<i>-0 17</i>	0 18	<i>0 09</i>	<i>0 01</i>	<i>0 09</i>	0 31	0 32
sst + gg + vol	0 48	0 52	0 60	<i>0 12</i>	<i>0 04</i>	0 51	<i>0 12</i>	0 71	0 59	0 81
sst + gg + vol + O3 s	0 60	0 62	0 68	0 48	0 26	0 60	0 31	0 75	0 83	0 90
sst + gg + vol + O3 t	0 51	0 51	0 58	0 49	0 30	0 55	<i>0 01</i>	0 61	0 67	0 79
sst + gg + vol + O3 s&t	0 55	0 56	0 66	0 24	0 26	0 38	0 20	0 73	0 62	0 82
sst + gg + vol + O3 s + S	0 59	0 63	0 70	0 50	<i>0 14</i>	0 59	0 29	0 76	0 83	0 91
sst + gg + vol + O3 s + S&C	0 53	0 56	0 62	0 29	<i>0 16</i>	0 37	0 37	0 71	0 78	0 91
sst + gg + vol + O3 s&t + S&C	0 45	0 49	0 53	0 33	<i>0 13</i>	0 30	<i>0 05</i>	0 60	0 61	0 80

Italicized correlations are not significant

Table 8. Correlations of AGCM and MSU 3-month-smoothed Oceanic Ch 2R Lower Trop T_b Time Series

Run	PacTr 20S-20N 80W-100E	Tr 20S-20N	Equa 30S-30N	NH ml 30N-50N	NH hl 50N-70N	SH ml 30S-50S	SH hl 50S-70S	SH	NH	G
1979-92										
sst AG	0.83	0.83	0.76	0.73	0.39	0.46	<i>0.12</i>	0.44	0.77	0.68
r mean	0.80	0.79	0.72	0.62	0.21	0.34	<i>0.06</i>	0.36	0.68	0.61
r std	0.02	0.02	0.03	0.04	0.08	0.08	0.09	0.11	0.04	0.06
1979-98										
sst F	0.76	0.75	0.70	0.58	0.22	0.24	<i>0.10</i>	0.40	0.66	0.59
sst G	0.77	0.78	0.73	0.54	0.36	0.23	<i>-0.09</i>	0.33	0.64	0.56
sst + gg	0.72	0.72	0.63	0.52	0.24	0.26	<i>0.07</i>	0.23	0.61	0.46
sst + gg + vol	0.77	0.74	0.67	0.60	0.28	0.26	<i>0.05</i>	0.33	0.65	0.54
sst + gg + vol + O3 s	0.80	0.78	0.72	0.56	0.25	0.24	<i>-0.02</i>	0.36	0.62	0.54
sst + gg + vol + O3 t	0.78	0.77	0.67	0.57	<i>0.03</i>	0.32	<i>0.14</i>	0.25	0.57	0.45
sst + gg + vol + O3 s&t	0.79	0.77	0.71	0.62	<i>0.12</i>	<i>0.12</i>	-0.21	0.22	0.62	0.49
sst + gg + vol + O3 s + S	0.76	0.77	0.70	0.52	<i>0.06</i>	0.33	<i>0.06</i>	0.40	0.64	0.56
sst + gg + vol + O3 s + S&C	0.73	0.70	0.61	0.59	0.32	<i>0.16</i>	<i>0.01</i>	0.25	0.63	0.47
sst + gg + vol + O3 s&t + S&C	0.78	0.76	0.67	0.57	0.24	0.29	0.03	0.26	0.67	0.52

Italicized correlations are not significant

Table 9. Regional Correlations of sst-Forced AGCM and MSU 3-month-smoothed Ch 2 Trop T_b Time Series: 1979-92

Run	Tr 20S-20N	Equa 30S-30N	NH ml 30N-50N	Nordeste 4S-12S 37W-48W	Zimbabwe 16S-24S 22 5E-32.5E	US Cornbelt 36N-44N 87 5W-97 5W
sst A	0 87	0 83	0 33	0 76	0 44	<i>-0.02</i>
sst B	0 82	0 77	0 42	0 80	0 49	<i>0.16</i>
sst C	0 84	0 77	0 42	0 81	0.38	<i>-0.03</i>
sst D	0 82	0.78	0 50	0 75	0.39	<i>0.14</i>
sst E	0 81	0 75	0 49	0 80	<i>0.19</i>	<i>0.17</i>
sst F	0 85	0 81	0 44	0 73	0 50	0 23
sst G	0 83	0 78	0 23	0 79	0 36	<i>0.09</i>
sst AG	0 89	0.85	0 55	0 86	0 64	<i>0 18</i>
r mean	0 84	0 78	0 41	0 78	0 39	<i>0 11</i>
r std	0 02	0 03	0 10	0 03	0 11	0.10

Italicized correlations are not significant

Table 10a. Regional Correlations of AGCM and MSU 3-month-smoothed Ch 2 Trop T_b Time Series: 1979-98

Run	Tr 20S-20N	Equa 30S-30N	NH ml 30N-50N	Nordeste 4S-12S 37W-48W	Zimbabwe 16S-24S 22.5E-32 5E	US Cornbelt 36N-44N 87 5W-97 5W
r std	0 02	0 03	0 10	0 03	0 11	0 10
1979-98						
sst F	0 81	0 77	0 40	0 68	0 42	0 21
sst G	0 79	0 75	0 20	0 71	0 34	<i>0.01</i>
sst + gg	0 76	0 70	0 33	0 73	0 54	<i>-0 05</i>
sst + gg + vol	0 76	0 72	0 50	0 70	0 39	<i>0 08</i>
sst + gg + vol + O3 s	0 84	0 80	0 35	0 72	0 27	<i>0 08</i>
sst + gg + vol + O3 t	0 81	0 74	0 39	0 74	0 40	<i>0.00</i>
sst + gg + vol + O3 s&t	0 83	0 80	0 42	0 75	0.26	0 17
sst + gg + vol + O3 s + S	0 83	0 79	0 25	0 74	0 40	0 25
sst + gg + vol + O3 s + S&C	0 80	0 74	0.50	0 73	0 38	0 03
sst + gg + vol + O3 s&t + S&C	0 78	0 72	0 40	0 73	0 16	0 01

Italicized correlations are not significant

**Table 10b. Regional Correlations of AGCM and MSU 3-month-smoothed
Ch 2 Trop T_b Time Series: Seasons, 1979-98**

Run	Nordeste				Zimbabwe			
	4S-12S 37W-48W				16S-24S 22.5E-32.5E			
	DJF	MAM	JJA	SON	DJF	MAM	JJA	SON
sst F	0.40	0.52	0.64	0.61	0.22	0.20	0.16	0.34
sst G	0.51	0.48	0.69	0.66	0.08	0.37	-0.11	0.37
sst + gg	0.40	0.60	0.69	0.71	0.16	0.38	0.34	0.46
sst + gg + vol	0.50	0.53	0.76	0.59	0.10	0.21	0.27	0.31
sst + gg + vol + O3 s	0.43	0.65	0.66	0.61	0.10	0.34	0.17	0.05
sst + gg + vol + O3 t	0.52	0.56	0.68	0.68	0.37	0.37	0.27	0.19
sst + gg + vol + O3 s&t	0.49	0.57	0.69	0.71	0.14	0.24	0.12	0.17
sst + gg + vol + O3 s + S	0.46	0.66	0.71	0.65	0.54	0.32	0.21	0.10
sst + gg + vol + O3 s + S&C	0.36	0.66	0.76	0.74	0.22	0.14	-0.03	0.25
sst + gg + vol + O3 s&t + S&C	0.40	0.57	0.74	0.68	0.23	0.14	-0.12	0.06

Table 11. Regional Correlations of sst-Forced AGCM and GISTEMP 3-month-smoothed Surface Air Temperature Time Series: 1979-92

Run	Nordeste 4S-12S 37W-48W	Zimbabwe 16S-24S 22 5E-32 5E	US Cornbelt 36N-44N 87.5W-97 5W	NH land
sst A	0.45	<i>0 04</i>	<i>-0 03</i>	0 26
sst B	0 40	0 23	<i>0.05</i>	0 44
sst C	0 42	<i>0.17</i>	<i>0.10</i>	0 46
sst D	0.35	<i>0.11</i>	<i>0.03</i>	0 40
sst E	0 49	<i>0 00</i>	<i>0.16</i>	0 34
sst F	0 42	<i>-0.02</i>	<i>0.16</i>	0 39
sst G	0 44	0 43	<i>0.03</i>	0.38
sst AG	0 51	0 33	<i>0 06</i>	0 55
r mean	0 42	<i>0 14</i>	<i>0 04</i>	0 38
r std	0 04	0 16	0 10	0 07

Italicized correlations are not significant

**Table 12a. Regional Correlations of sst-Forced AGCM and GISTEMP
3-month-smoothed Surface Air Temperature Time Series: 1979-98**

Run	Nordeste 4S-12S 37W-48W	Zimbabwe 16S-24S 22.5E-32 5E	US Cornbelt 36N-44N 87 5W-97 5W	NH land
r std	0 04	0 16	0 10	0 07
1979-98				
sst F	0 36	<i>-0 03</i>	<i>0 09</i>	0.28
sst G	0 46	0 31	<i>0.01</i>	0 41
sst + gg	0 42	<i>- 0 05</i>	<i>-0 04</i>	0 32
sst + gg + vol	0 38	<i>0 00</i>	<i>0 08</i>	0.55
sst + gg + vol + O3 s	0 38	0 37	<i>0 08</i>	0 50
sst + gg + vol + O3 t	0 33	0 18	<i>-0 14</i>	0 62
sst + gg + vol + O3 s&t	0 39	<i>0 00</i>	<i>0 04</i>	0 60
sst + gg + vol + O3 s + S	0 46	<i>0 10</i>	0 12	0 51
sst + gg + vol + O3 s + S&C	0 43	0 20	<i>-0 08</i>	0 59
sst + gg + vol + O3 s&t + S&C	0 40	<i>0 15</i>	<i>-0 06</i>	0 45

Italicized correlations are not significant

Table 12b. Regional Correlations of sst-Forced AGCM and GISTEMP 3-month-smoothed Surface Air Temperature Time Series: Seasonal, 1979-98

Run	Nordeste 4S-12S 37W-48W				NH land			
	DJF	MAM	JJA	SON	DJF	MAM	JJA	SON
sst F	0 19	0 40	0 61	0 28	0 26	-0 01	0 02	0 32
sst G	0 33	0 56	0 49	0 33	0 19	0 26	0 07	0 45
sst + gg	0 19	0 41	0 30	0 41	0 09	0 16	0 11	0 49
sst + gg + vol	0 24	0 43	0 37	0 24	0 29	0 37	0 49	0 58
sst + gg + vol + O3 s	0 25	0 44	0 33	0 26	0 50	0 34	0 33	0 40
sst + gg + vol + O3 t	0 08	0 26	0 42	0 33	0 24	0 35	0 47	0 54
sst + gg + vol + O3 s&t	0 09	0 39	0 40	0 57	0 29	0 39	0 56	0 46
sst + gg + vol + O3 s + S	0 27	0 48	0 51	0 25	0 33	0 34	0 42	0 53
sst + gg + vol + O3 s + S&C	0 21	0 48	0 50	0 31	0 25	0 45	0 62	0 62
sst + gg + vol + O3 s&t + S&C	0 17	0 41	0 43	0 48	0 26	0 20	0 39	0 57

Table 13. Impact of MSU Versions on Unsmoothed Time Series Correlations with AGCM runs

Variable	r std	sst F 1979-92			sst+gg+vol+O3st 1979-92			sst F 1979-98		sst+gg+vol+O3st 1979-98	
		ver 90a	ver c	ver d	ver 90a	ver c	ver d	ver c	ver d	ver c	ver d
Ch 2 T _b											
Glob	0 04	0 54	0 54	0 44	0 56	0 57	0 50	0 48	0 41	0 52	0 48
NH	0 06	0 45	0 45	0 39	0 54	0 56	0 53	0 43	0 39	0 52	0 52
SH	0 07	0 37	0 37	0 24	0 30	0 28	0 21	0 32	0 24	0 27	0 21
Ch 4 T _b											
Glob	0 14	-0 19	-0 22	-0 21	0 77	0 78	0 81	-0 17	-0 18	0 80	0 82
NH	0 10	-0 13	-0 14	-0 14	0 51	0 52	0 54	-0 10	-0 12	0 55	0 56
SH	0 05	-0 10	0 09	0 10	0 47	0 65	0 66	0 02	0 03	0 65	0 64

Italicized correlations are not significant

Table 14. Impact of AGCM Ensemble Size on Unsmoothed Time Series Correlations with Observations: 1979-92

Variable	sst AG r 7 runs	sst AE r 5 runs	sst AC r 3 runs	sst A r 1 run
Ch 2 T_b				
Glob	0 63	0 62	0 61	0 56
NH	0 64	0 64	0 62	0 53
SH	0 41	0 38	0 35	0 37
NH ml	0 42	0 41	0 35	0 20
Nordeste	0 76	0 76	0 75	0 61
Zimbabwe	0 41	0 36	0 37	0 22
Oceanic Ch 2R T_b				
Glob	0 58	0 55	0 54	0 53
NH	0 64	0 63	0 62	0 53
SH	0 35	0 32	0 29	0 34
NH ml	0 57	0 55	0 52	0 45
Surf Air T				
NH land	0 42	0 40	0 36	0 16
Nordeste	0 39	0 38	0 37	0 30
Zimbabwe	<i>0 16</i>	<i>0 09</i>	<i>0 11</i>	<i>-0 03</i>

Italicized correlations are not significant

Figure Captions

Figure 1. MSU channel weighting functions over a land surface emissivity of 1.0 and with a 1976 Standard Atmosphere (equivalent to a mean annual, mid-latitude atmosphere) are shown (left) relative to typical tropical and polar tropopause levels. and (right) relative to the 9 vertical layers of the AGCM.

Figure 2. Specified sea surface temperatures used to force the AGCM are shown as 3-month smoothed time series averaged over (top) the tropical pacific (20S-20N and 80W-100W), (middle) the northern hemisphere and (bottom) the southern hemisphere.

Figure 3. Stratospheric volcanic aerosols used to force the AGCM are shown in terms of the optical depth at 0.55 microns over the 1979-1999 period and over all latitudes.

Figure 4 Ozone changes used to force the AGCM are shown: (a) the zonal stratospheric ozone forcings in terms of the total ozone change over 1979-1999 and all latitudes; (b) the zonal stratospheric ozone forcing in terms of its time series for 3 pressure levels from 1979-1999, (c) the tropospheric ozone increase over latitude and longitude in terms of the total Dobson Unit (DU) from 1970-1995; and (d) tropospheric ozone increases over latitude in terms of pressure levels zonally and annually averaged for AGCM layers centered on 321 mb, 633 mb and 894 mb.

Figure 5. Sulfur and black carbon (soot) tropospheric aerosol optical thicknesses, τ at 0.55 micron, and their geographical distributions are shown for December 1970 and 1995.

Figure 6. MSU T_b anomaly time series for channels 2 and 4 from versions 'c' (6a), versions 'a' and 'c' (6b and 6c) and version d (6d) clearly show the ENSO warming and cooling of tropospheric temperatures, the volcanic aerosol warming of the lower stratosphere and the decreased-ozone abundance cooling of lower stratosphere. MSU version d is currently only

available as global and hemispheric averages for channel 2R.

Figure 7. The change to monthly mean MSU channel 4 T_b maps between versions 'a' (1982-1991 baseline) and 'c' (1984-1990 baseline) due to different sampling of high latitude variability and sudden stratospheric warming events are shown for each month.

Figure 8. The differences of calculating MSU channel 4 (top) and 2 (bottom) monthly-mean T_b from a 31-vertical layer AGCM's January and July as a combination of rescaled, averaged view angles versus as a single nadir value are shown.

Figure 9. The difference in calculating MSU channel 2 (left) and 4 (right) global and tropical pacific T_b time series as a single nadir value versus as a combination of view angles is shown. The single nadir value time series is slightly muted in terms of its extreme values but at a level less than 0.02° C for the mid-tropospheric T_b and 0.04° C for the lower stratospheric T_b .

Figure 10. The 9-layer AGCM's monthly mean T_b departures from MSU 'a' observations in the lower troposphere up into the lower stratosphere are shown in layered panels for a mean January and July in degrees Kelvin (left) and scaled by the observed MSU interannual variability (right). The AGCM control run 255, done with climatological ssts, produced these T_b departures, typical and systematic from this AGCM. The upper tropospheric channel 3R values are adjusted to match NCEP/NCAR values as detailed in Shah and Rind (1998). Note regions of inappropriate vertical static stability do occur.

Figure 11. The 9-layer AGCM departures of (a) mid-tropospheric and (b) lower stratospheric T_b seasonal means from MSU seasonal means are shown. The same AGCM control run, 255 as used in Figure 10, produced these seasonal means. Tropospheric channel 2 shows a good climate model simulation except for the common ailment of AGCMs of too-cold high latitudes. Channel 4 clearly shows the limited simulation of the lower stratosphere due to

the low, but typical, model top at 10 mb (which reflects energy unnaturally back into the troposphere) and due to the lack of gravity wave parameterizations.

Figure 12. The MSU and AGCM seasonal (a) mid-tropospheric and (b) lower stratospheric variability are shown. The AGCM variability is from the run 255F and is forced only by observed ssts. The MSU variability and the AGCM variability are for the 1980-1997 period. The MSU anomalies are from the 'c' version.

Figure 13. (a) Differences in AGCM run sst F's sea surface temperatures, precipitation and sea level pressure are shown for January 1983 and January 1998 relative to an average of 10 January from the AGCM control run. The sea level pressure changes are shown twice to examine the large shifts at the Aleutian Low location and the slight shifts over the eastern Pacific. (b) The regional responses of MSU and AGCM T_b to El Nino ssts during January 1983 and January 1998 are shown. The top rows show the lower stratospheric temperature response observed by MSU and simulated by AGCM run sst F. Local compensation and cooling in response to movement of the tropopause can be seen in both the MSU and AGCM T_b . The mid-tropospheric MSU T_b in the bottom rows show the warm dumbbell pattern documented by Yulaeva and Wallace (1994) which the AGCM did not consistently generate in discrete centers. (c) The lower tropospheric, channel 2R T_b are shown for January 1983 and January 1998.

Figure 14. The first series of AGCM transient runs forced by observed ssts and mean sea ice coverage does produce expected tropospheric warming and cooling responses across the Tropics (20°S-20°N). All seven sst-forced AGCM runs are incorporated here in terms of the range of their channel 2 T_b anomalies against the MSU 'a' channel 2 time series. The influence of varying initial conditions (and, thus, the prompting different internal variability) is non-negligible.

Figure 15. The AGCM's tropospheric response diminishes in size and has an increasing lag with distance from the tropical Pacific. The high latitudes are poorly correlated with the MSU time series, particularly in the southern hemisphere where there are few stationary waves. The warm El Nino response as observed by MSU and as simulated by the AGCM are shown (a) for 1982-85 (average of 7 AGCM runs, sst AG) and (b) for 1997-1998 (individual AGCM run sst F) as the response moves from the tropical pacific into the northern mid-latitudes. Smoothing over 3 months has been applied to all the time series shown.

Figure 16. Agreement between the AGCM's (a) mid-tropospheric, (b) lower stratospheric and (c) oceanic lower tropospheric time series and MSU observations did improve during strong events with inclusion of known atmospheric forcings. Disagreement between the AGCM's (c) oceanic lower tropospheric time series and the oceanic MSU observations remained particularly notable prior to mid-1981. Smoothing over 3 months has been applied to the time series shown.

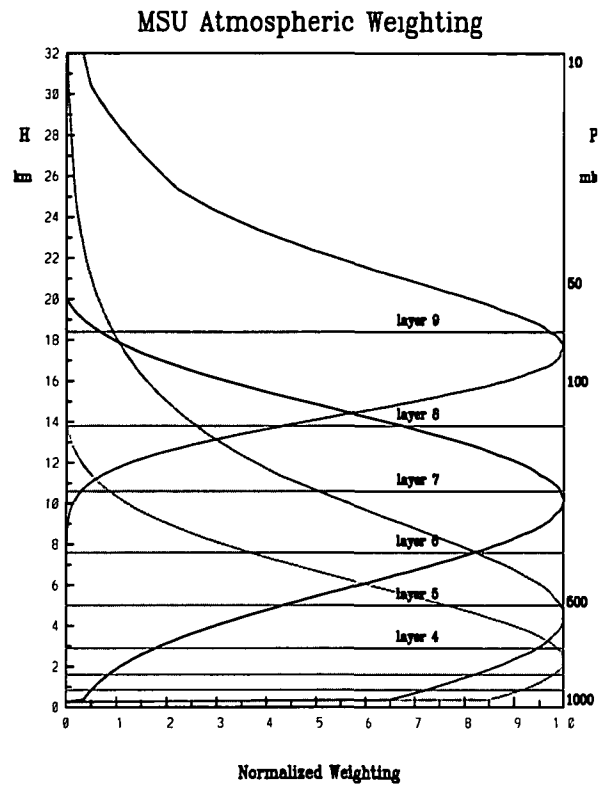
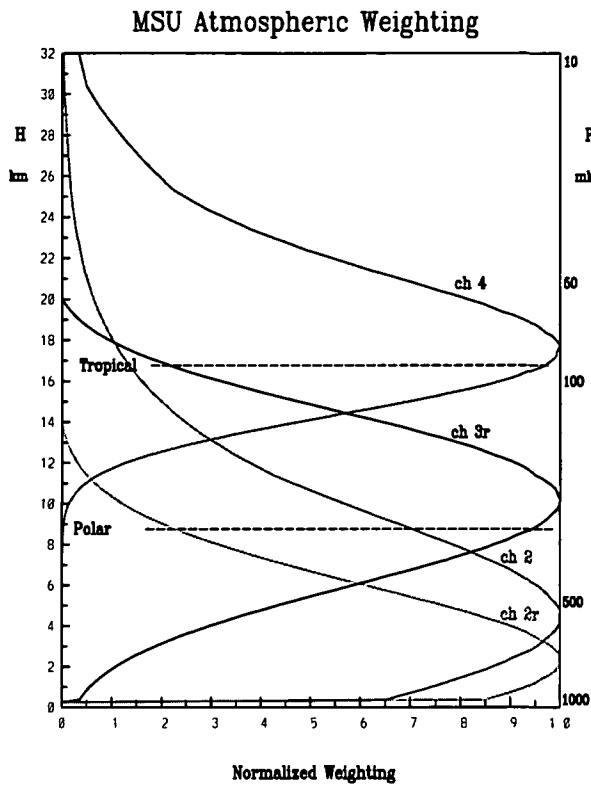
Figure 17. The ENSO signal in the MSU mid-tropospheric channel 2 anomalies becomes obscured by other sources of variability outside of the equatorial (30S-30N) latitudes (top). Consequently, while Nordeste in northeastern Brazil and Zimbabwe in Africa have clear ENSO signals in their mid-tropospheric temperatures (bottom), the US Cornbelt has a noisy mid-tropospheric temperature time series (middle). Smoothing over 3 months has been applied to these time series.

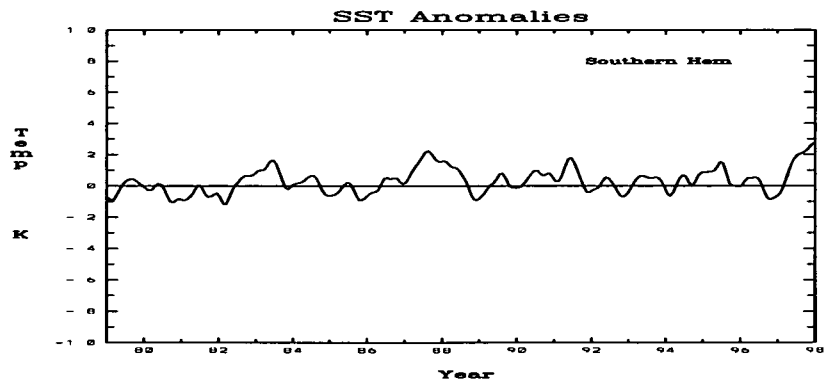
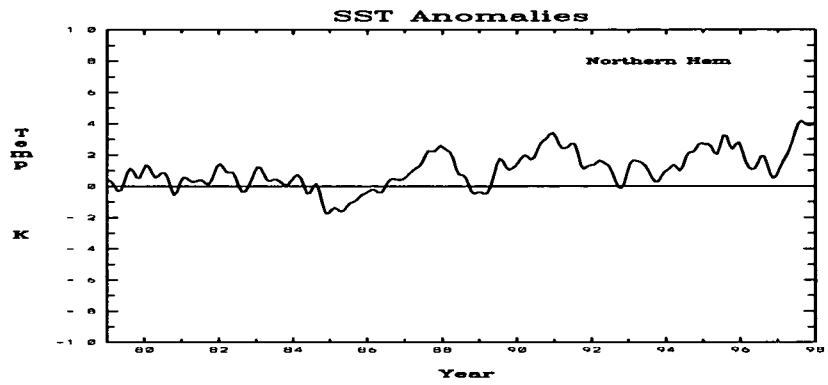
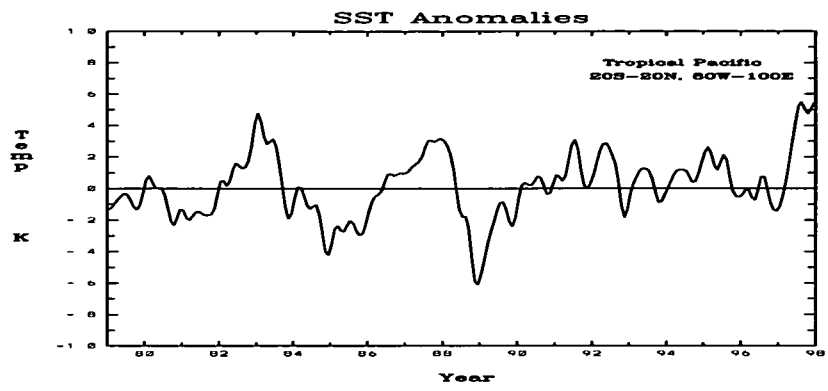
Figure 18. Agreement between the AGCM mid-tropospheric temperature time series and MSU observations over Nordeste and Zimbabwe did not notably change with inclusion of known atmospheric forcings. Different forcings improved different El Nino events (see Tables 9 and 10).

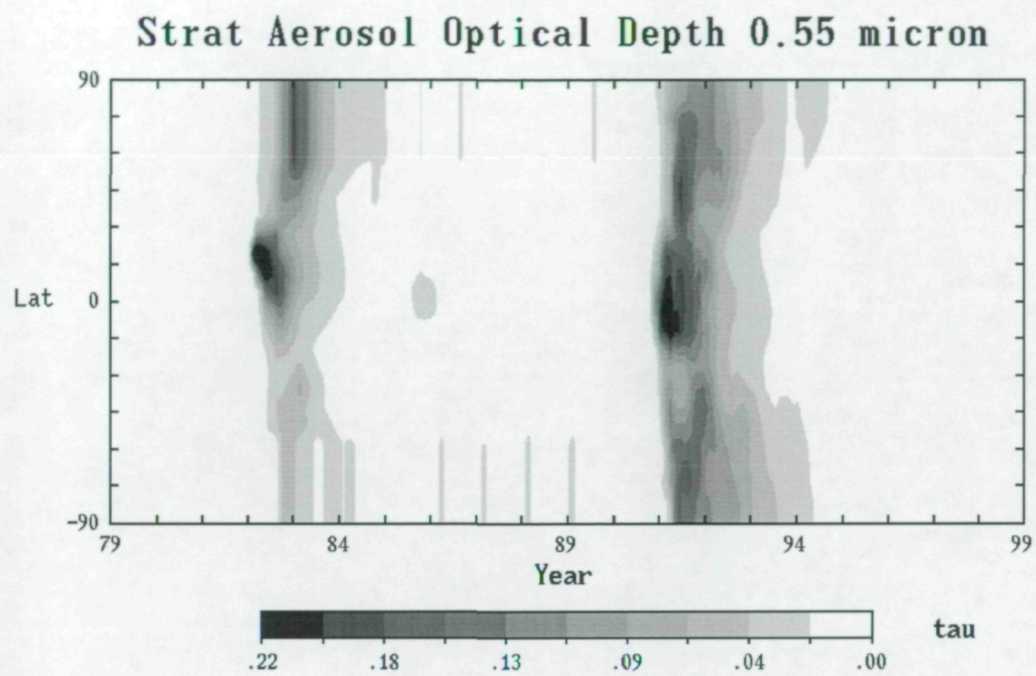
Figure 19. Meteorological station surface temperatures from the GISTEMP dataset (Hansen

et al., 1999; Hansen et al., 1996) are shown as a globally, northern hemisphere and northern hemisphere land averaged time series to emphasize the increased variability over landmasses (top left). These surface temperatures clearly show a warming trend. The ENSO signal in surface temperatures (as with the MSU mid-tropospheric, channel 2 anomalies in Figure 18) becomes obscured by other sources of variability outside of the equatorial (30S-30N) latitudes. Consequently, while Nordeste in northeastern Brazil and Zimbabwe in Africa have clear ENSO signals in their surface temperatures (bottom), the US Cornbelt has a noisy surface temperature time series (top right).

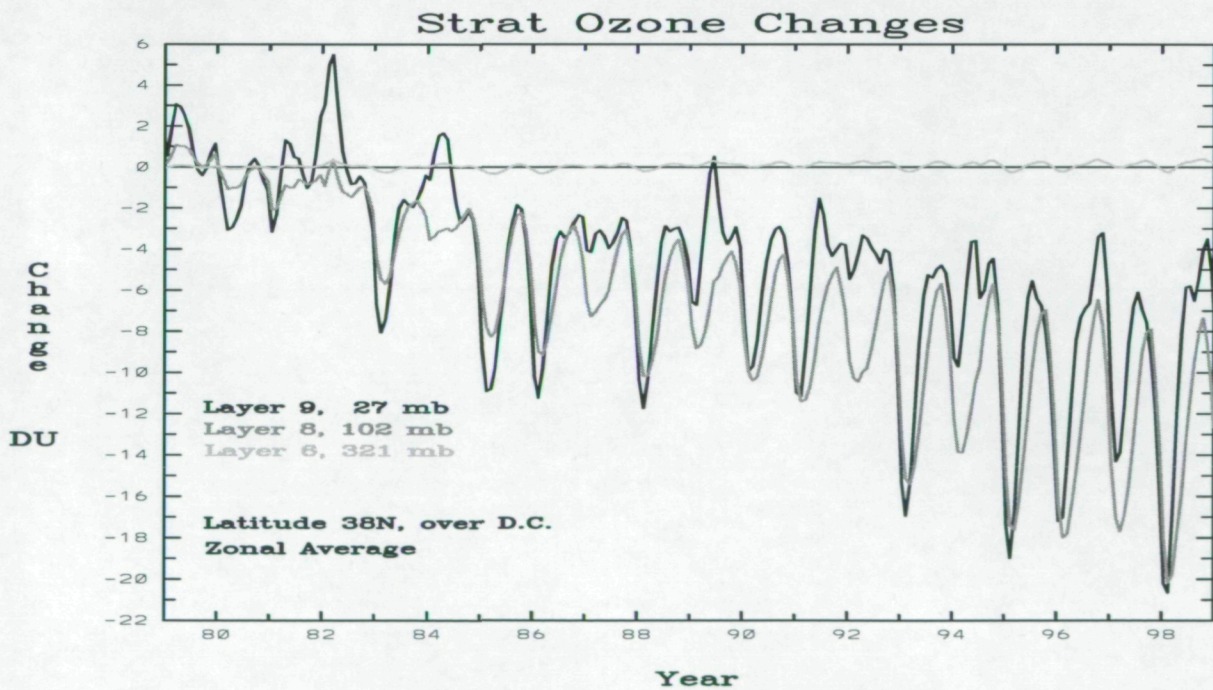
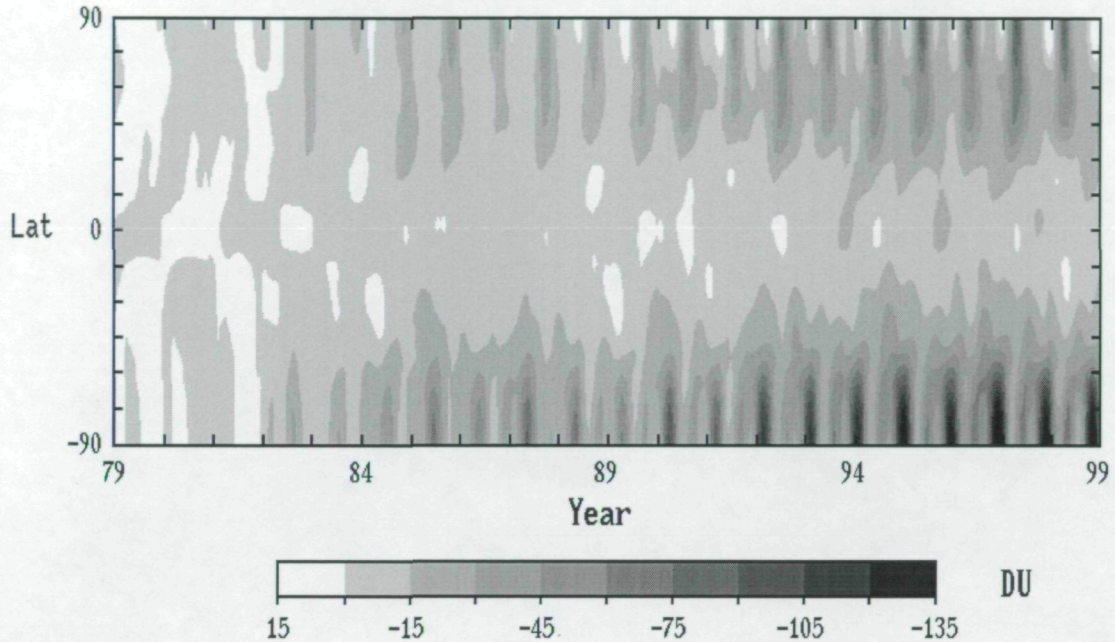
Figure 20. Agreement between smoothed surface air temperatures from meteorological station data and from the average of 7 AGCM runs, sst AG, are shown over northern hemispheric land (top left), Zimbabwe (bottom left) and Nordeste (right). Correlations for these surface air temperature time series after 3-month smoothing are 0.55, 0.51 and 0.33 respectively (see Table 11).



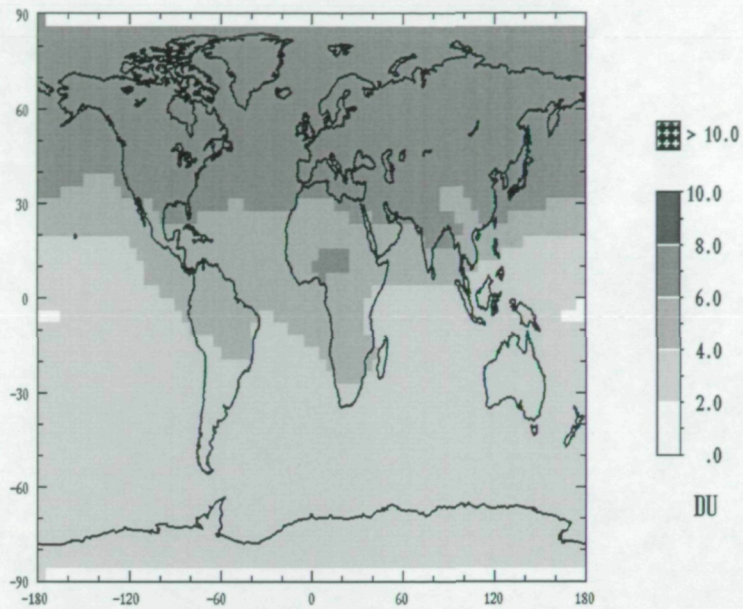




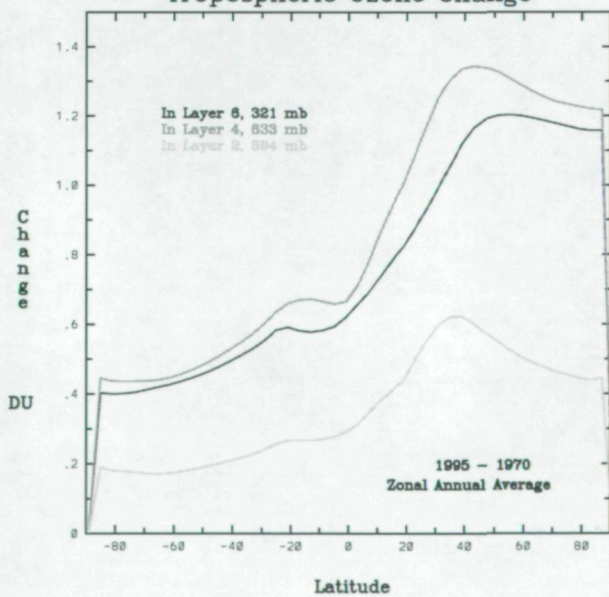
Total Stratospheric Ozone Change



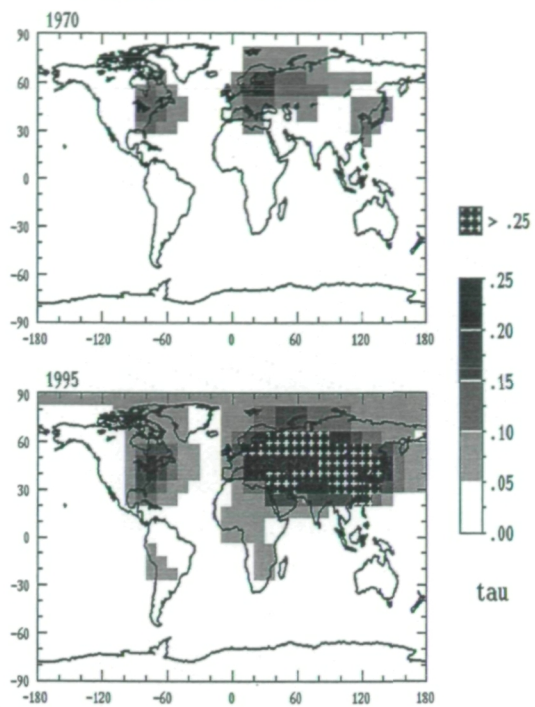
Tropospheric Ozone Change 1995-1970



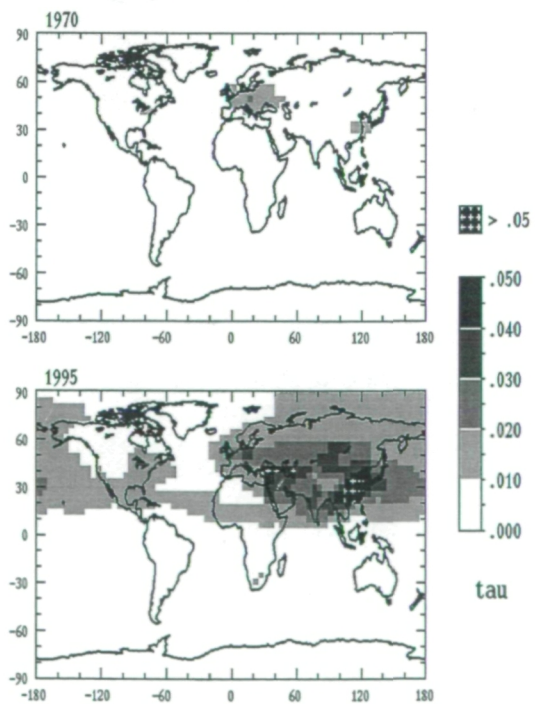
Tropospheric Ozone Change



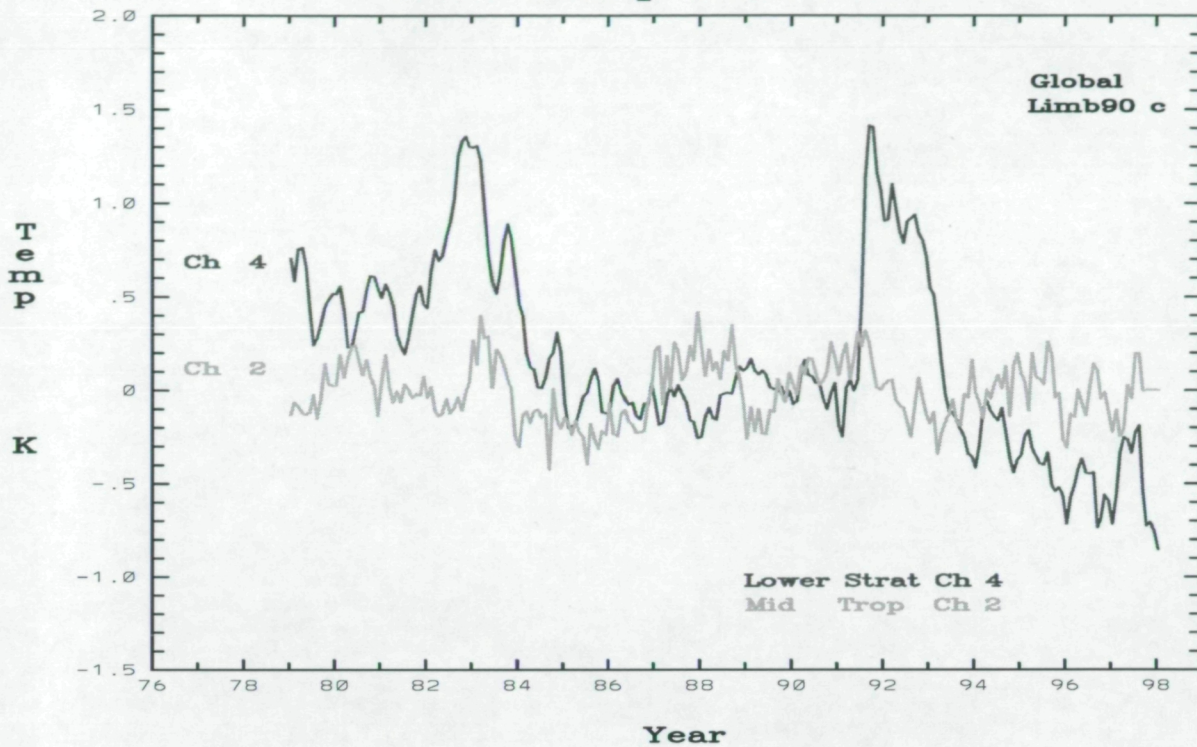
Tropospheric Sulfates



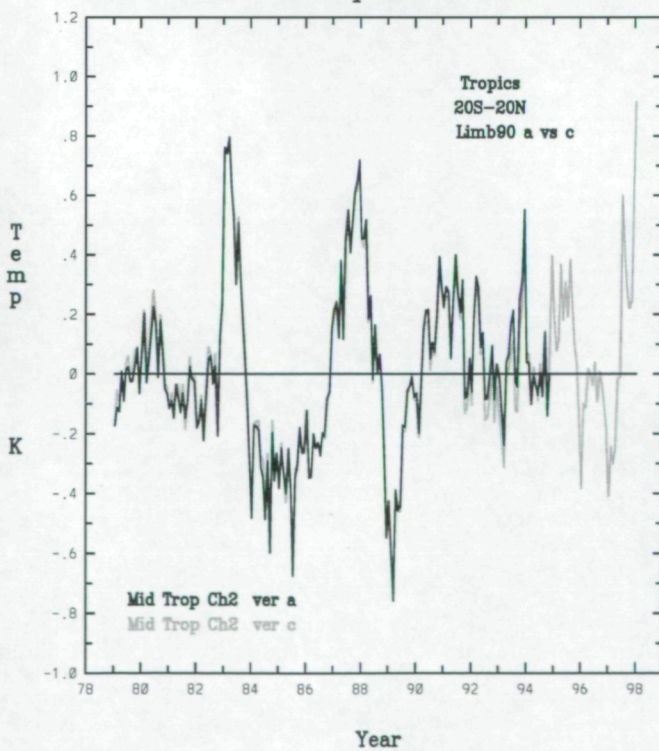
Tropospheric Black Carbon



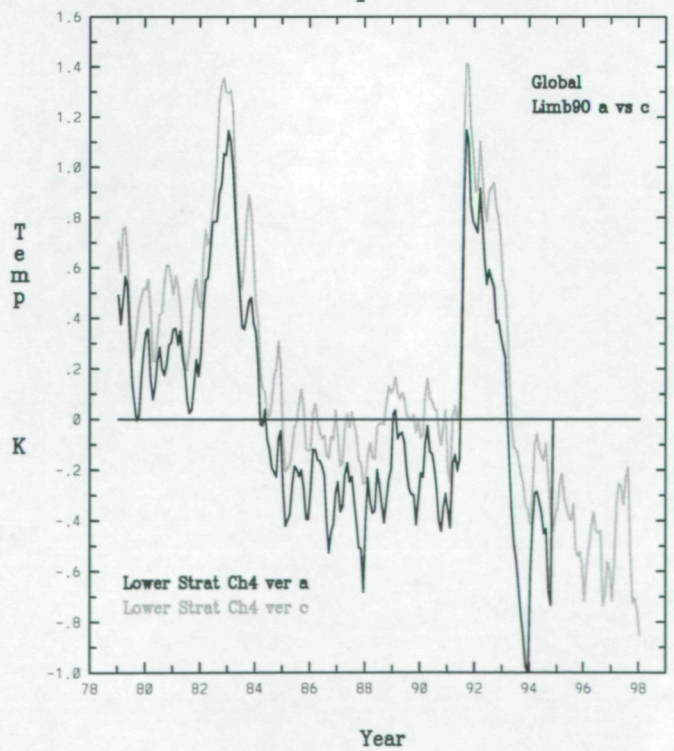
MSU Temp Anomalies

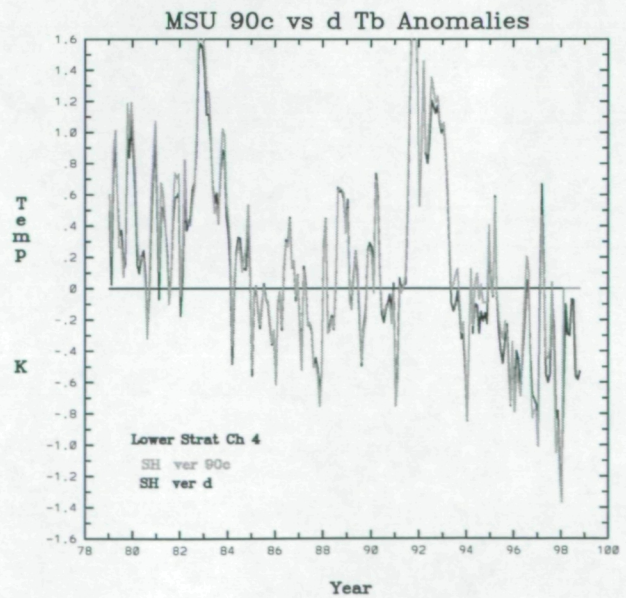
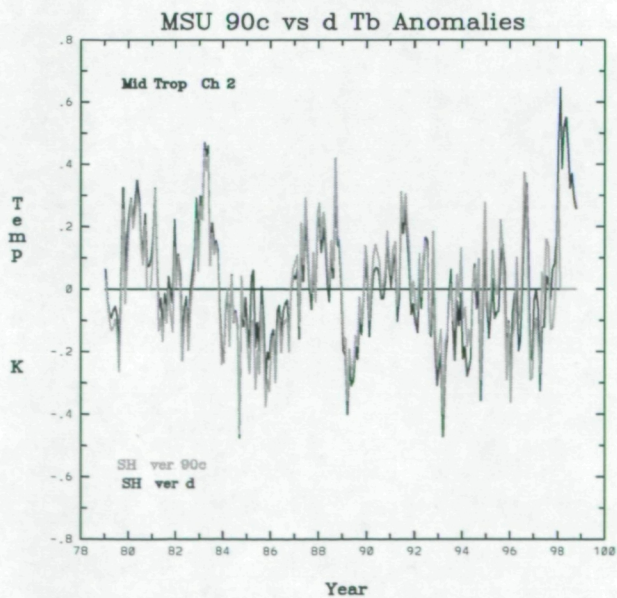
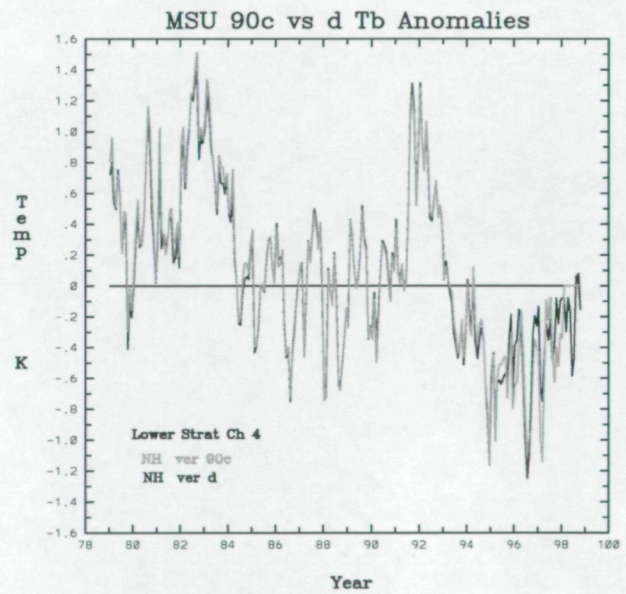
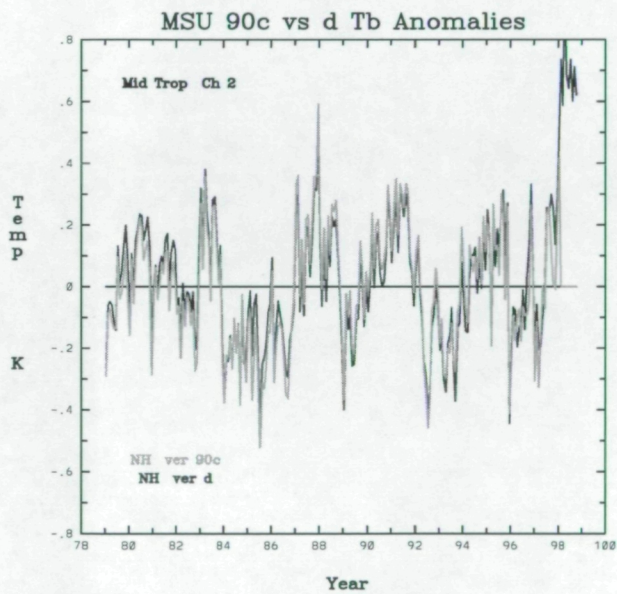
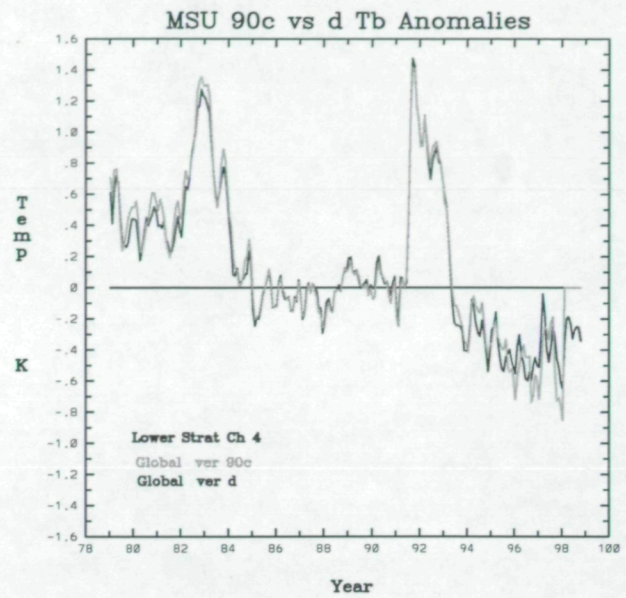
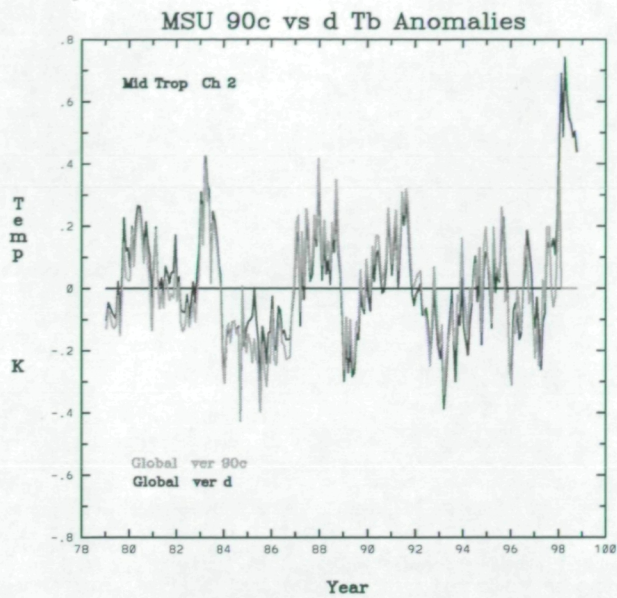


MSU Temp Anomalies

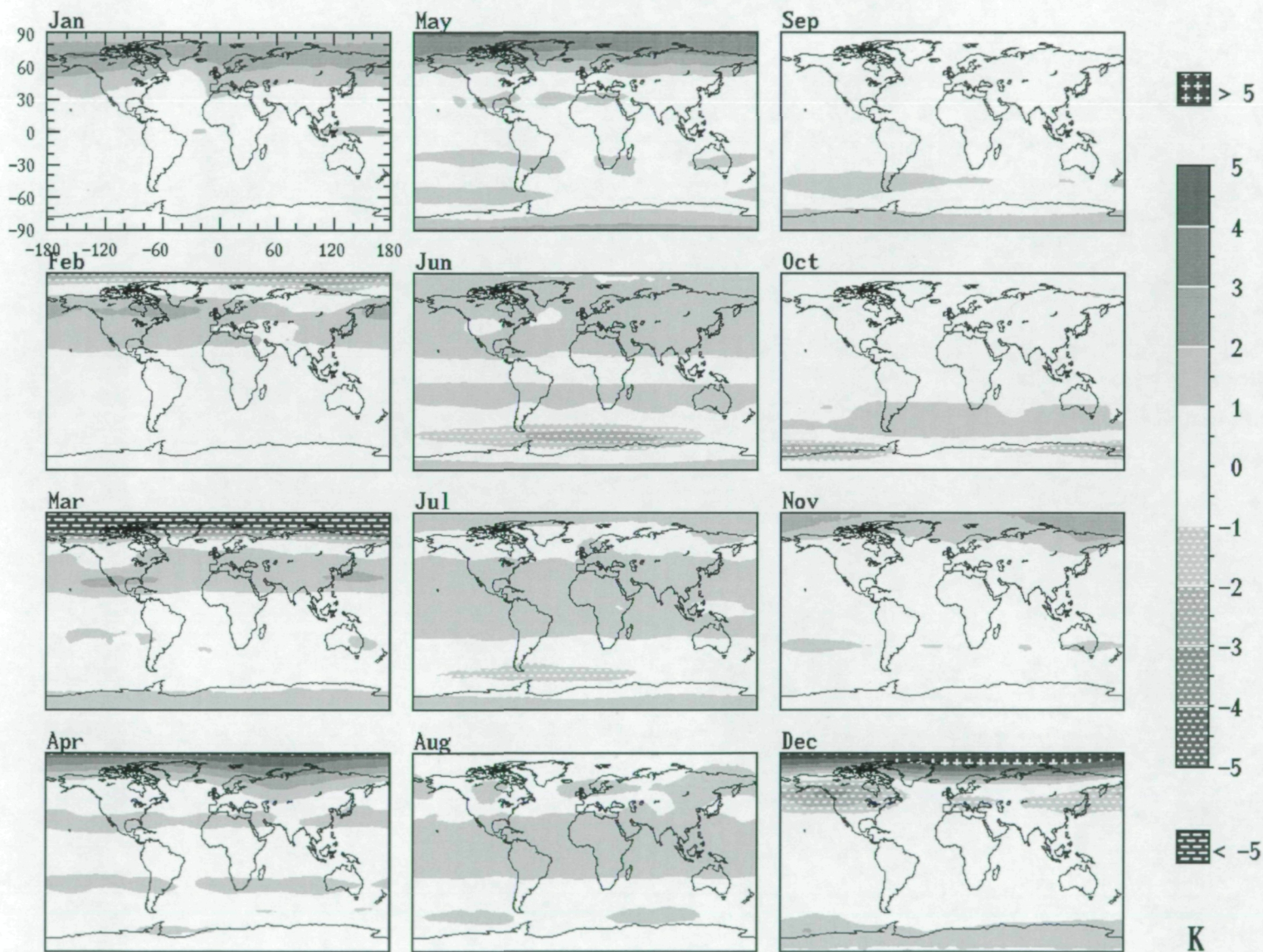


MSU Temp Anomalies

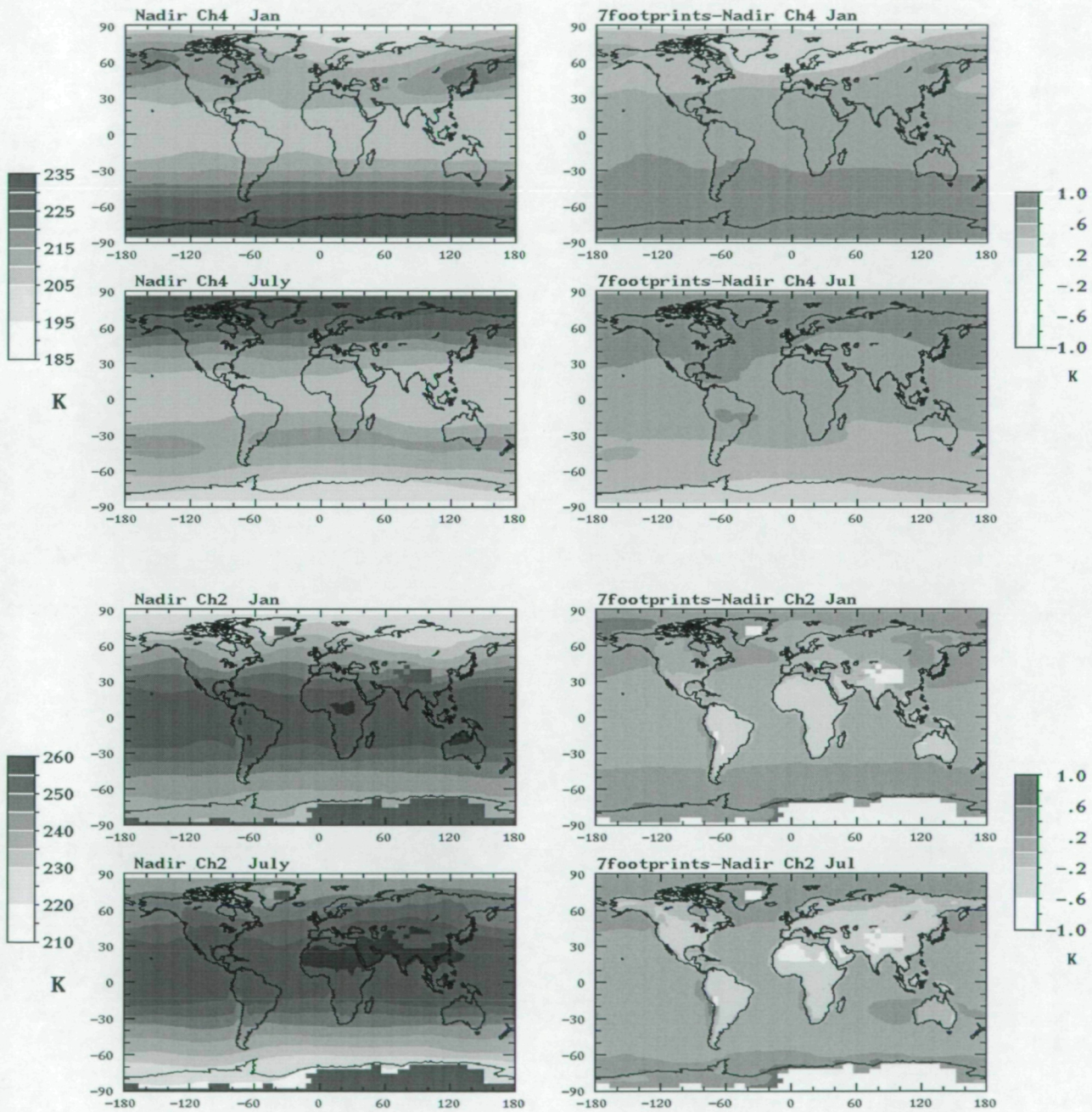


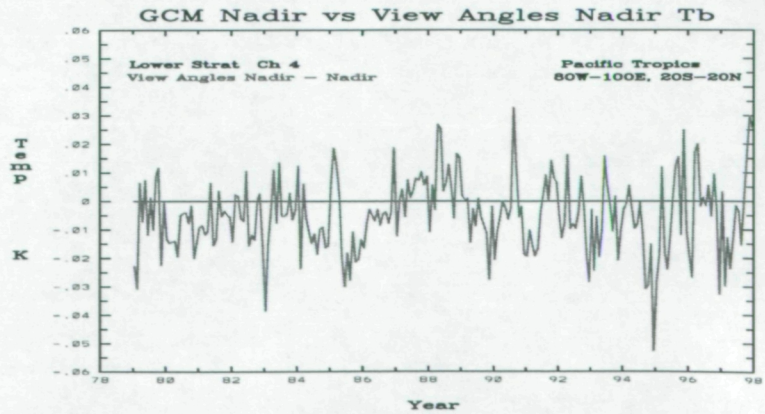
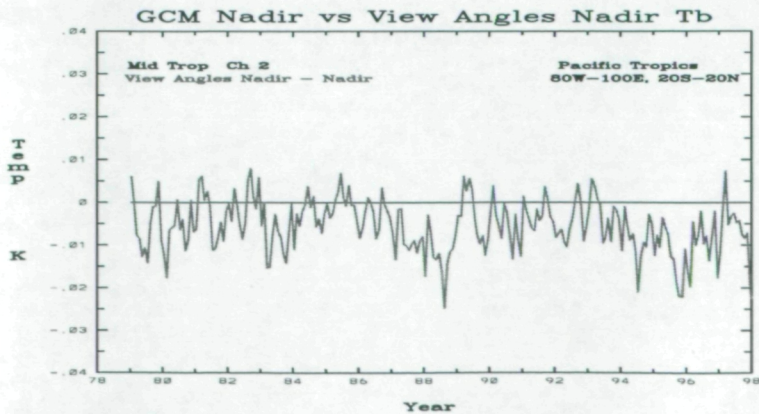
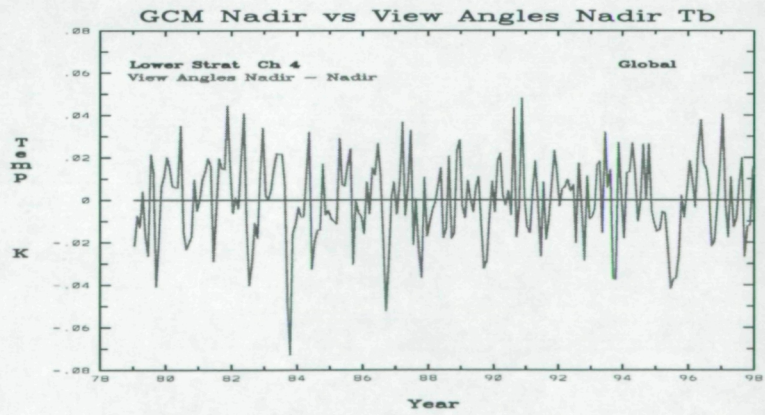
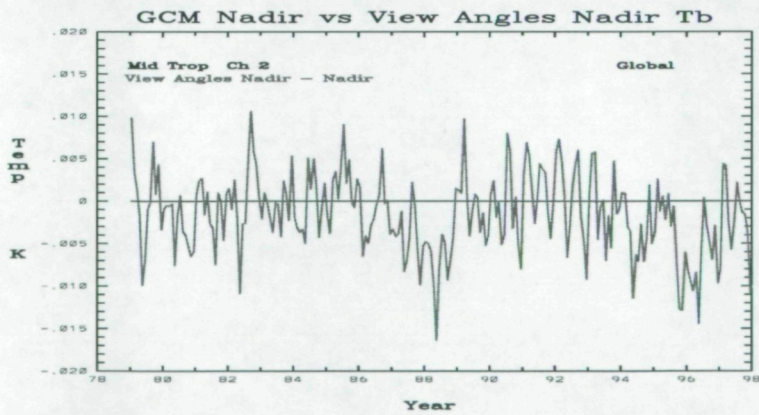


MSU Ch4 Monthly Mean Change: c - a



7 Footprints' Impact on 31-Layer GCM Tb





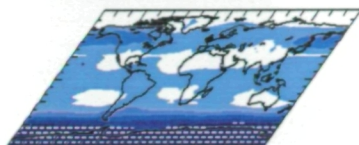
Ch 4 (80 mb)



GCM Tb - MSU Tb

B255M9
10 yr Av
Jan

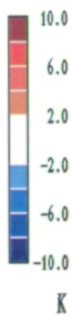
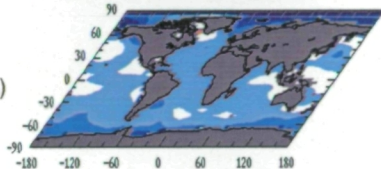
Ch 3r (280 mb)



Ch 2 (600 mb)



Ch 2r (800 mb)



Ch 4 (80 mb)

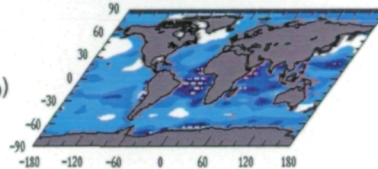


dTb/MSU std
B255M9
10yr Ave
Jan

Ch 2 (600 mb)



Ch 2r (800 mb)



Ch 4 (80 mb)



GCM Tb - MSU Tb

B255M9
10 yr Av
July

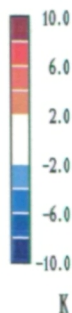
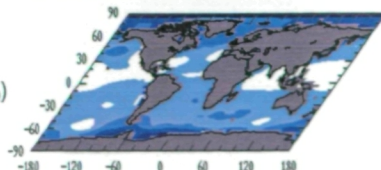
Ch 3r (280 mb)



Ch 2 (600 mb)



Ch 2r (800 mb)



Ch 4 (80 mb)

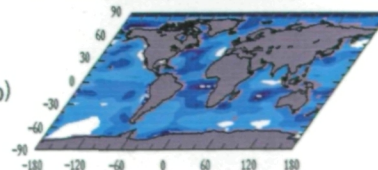


dTb/MSU std
B255M9
July

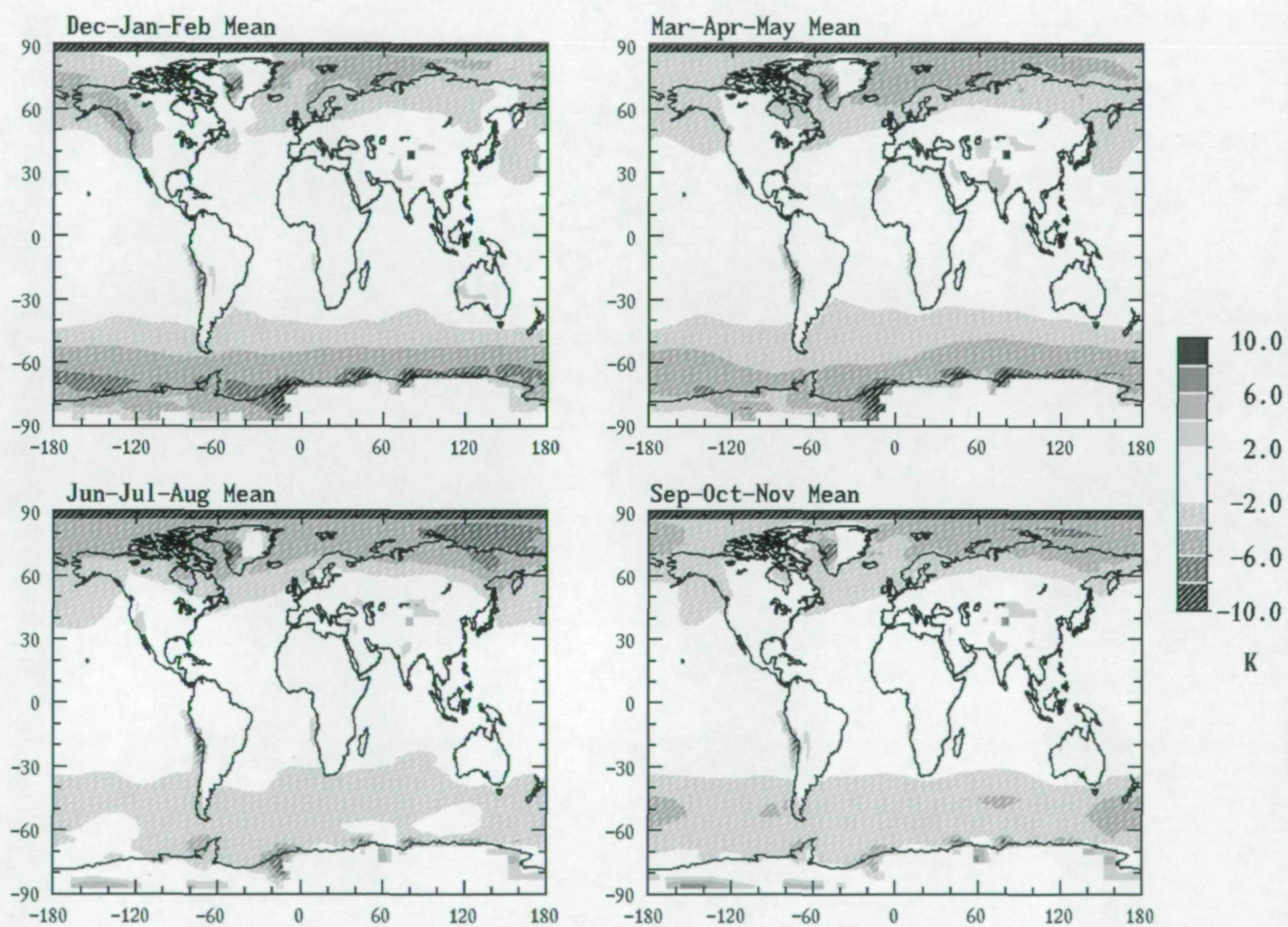
Ch 2 (600 mb)



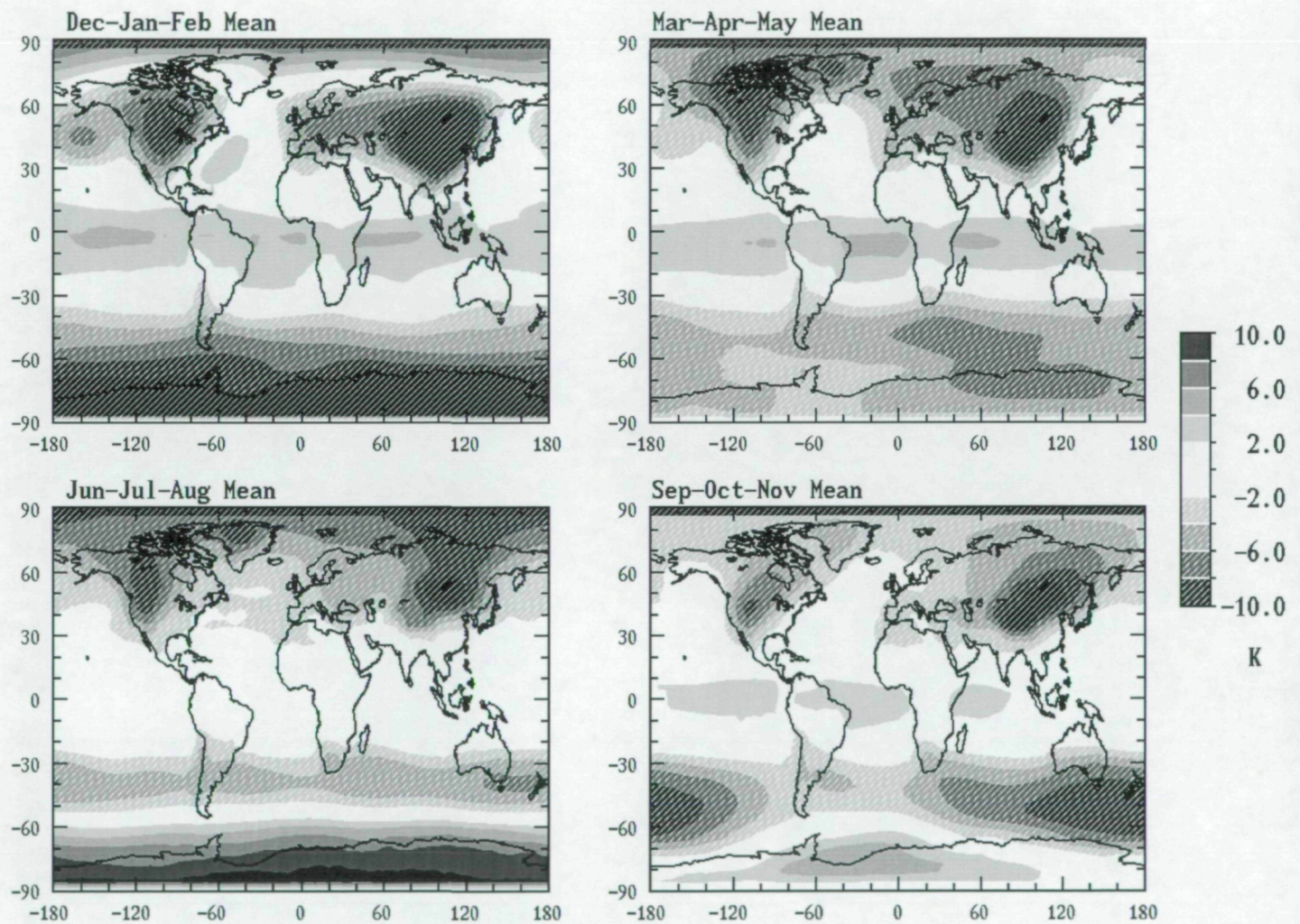
Ch 2r (800 mb)



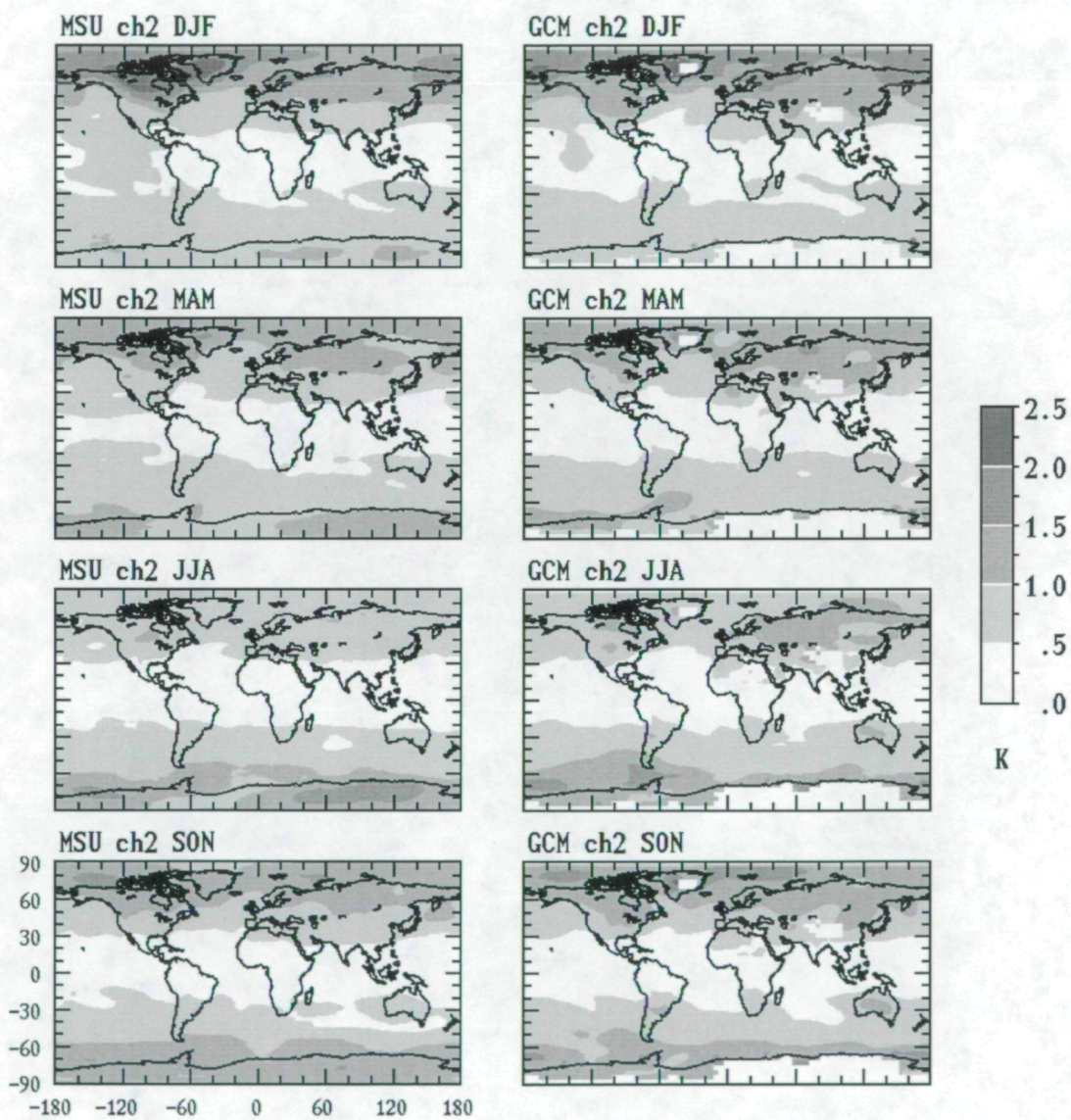
AGCM - MSU Mid-Tropospheric Ch2 Tb



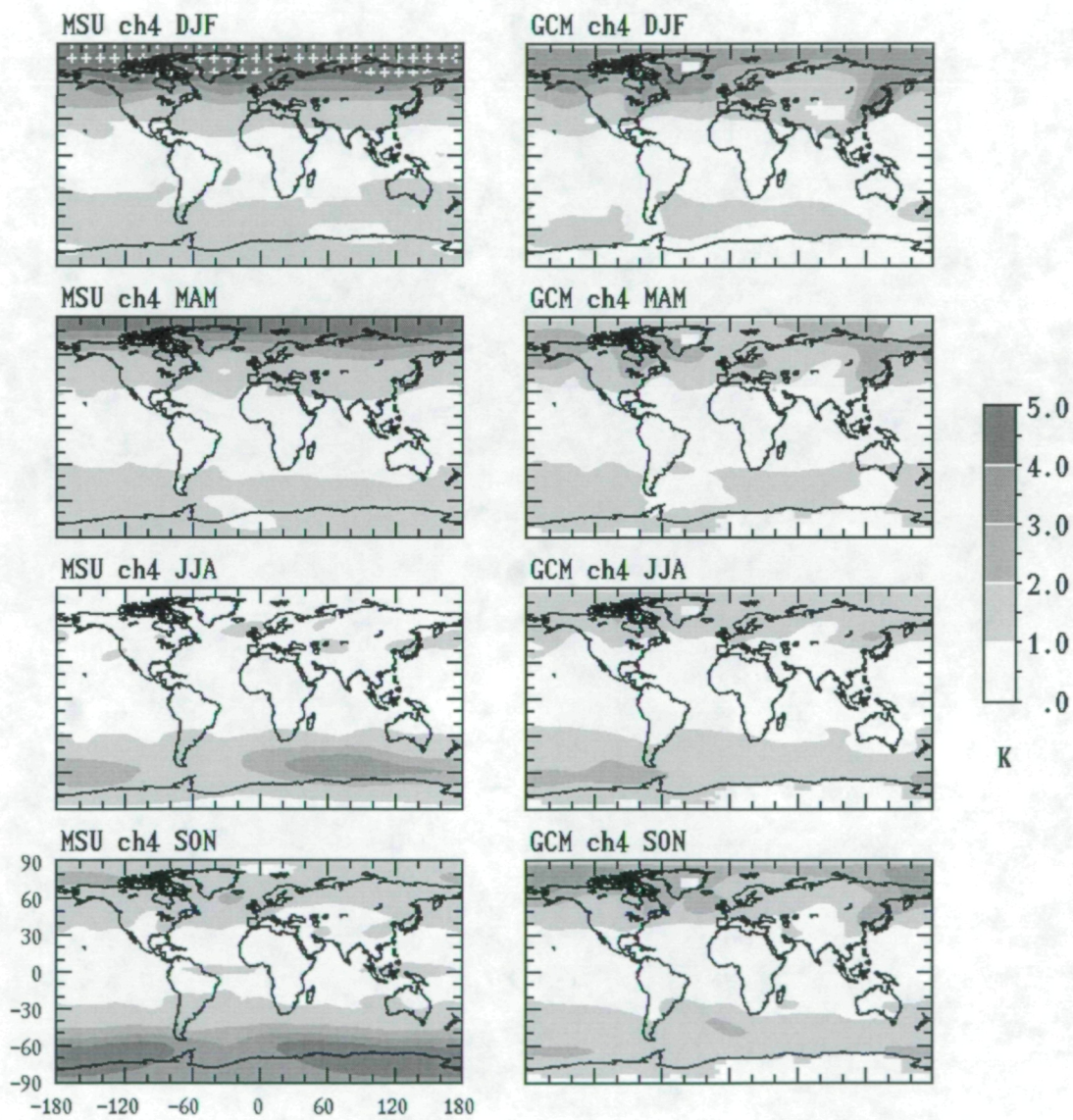
AGCM - MSU Lower Stratospheric Ch4 Tb



Mid Trop Ch2 Tb Variability



Lower Strat Ch4 Tb Variability

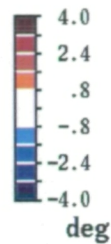
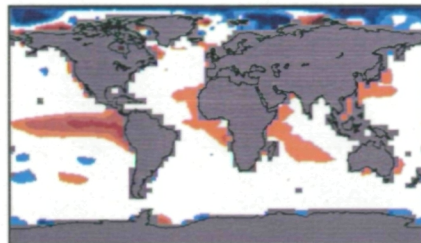
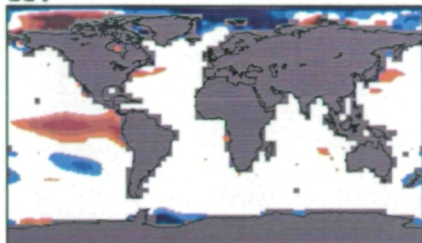


January 1983

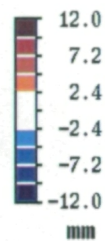
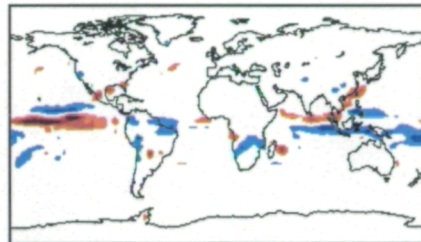
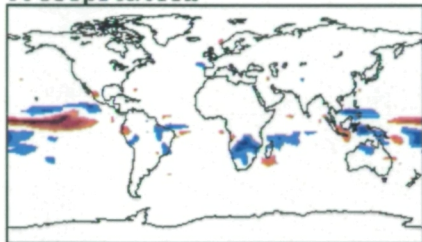
January 1998

AGCM Changes
during Elninos

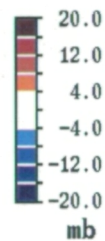
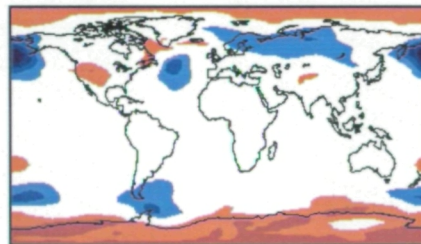
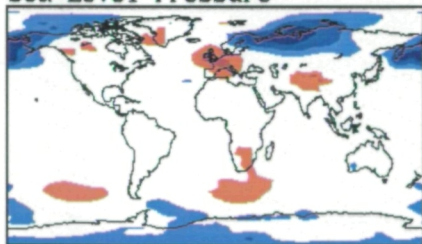
SST



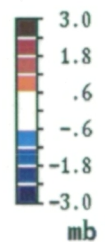
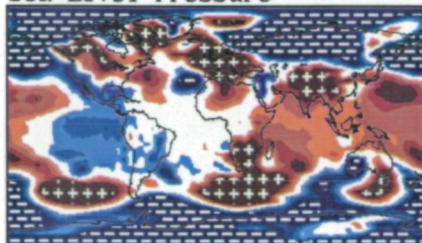
Precipitation



Sea Level Pressure



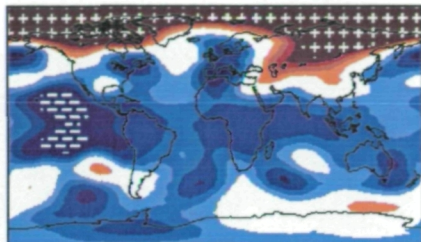
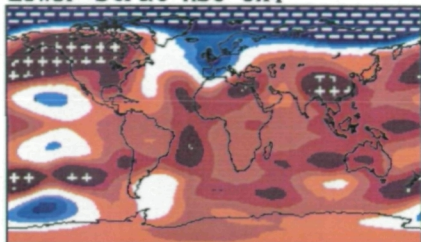
Sea Level Pressure



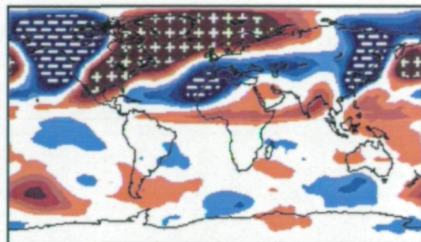
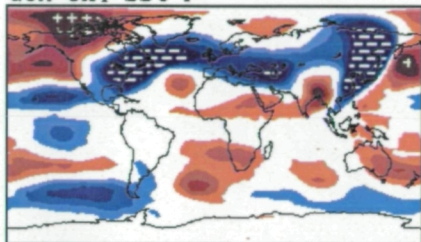
January 1983

January 1998

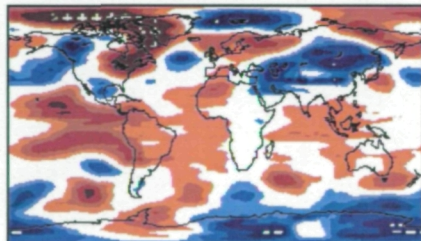
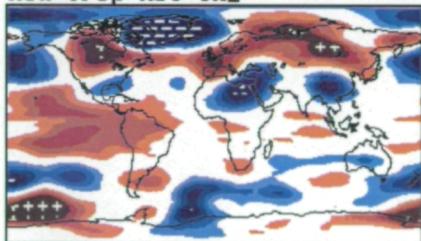
Lower Strat MSU Ch4



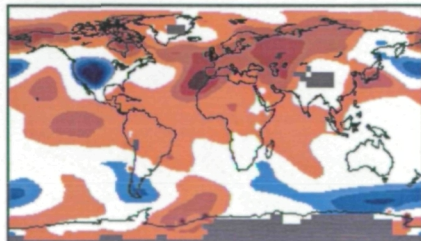
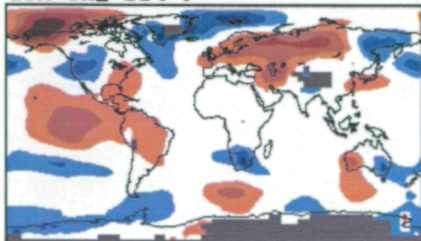
GCM Ch4 sst F



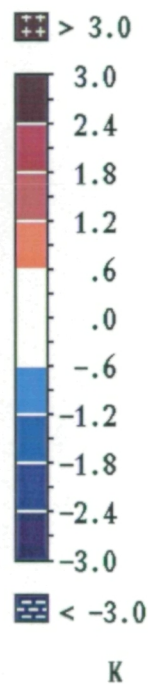
Mid-Trop MSU Ch2



GCM Ch2 sst F



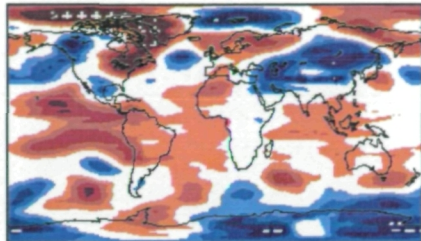
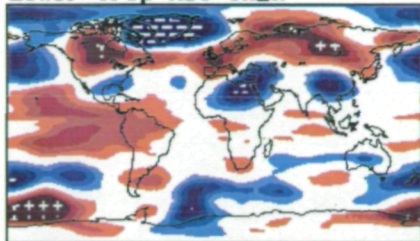
Tb Anomalies
during Elnino



January 1983

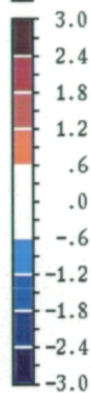
January 1998


Lower Trop MSU Ch2R



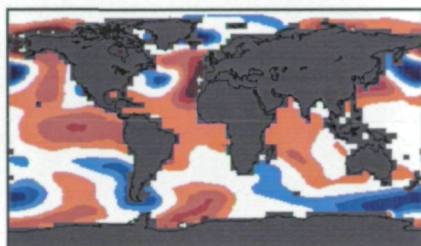
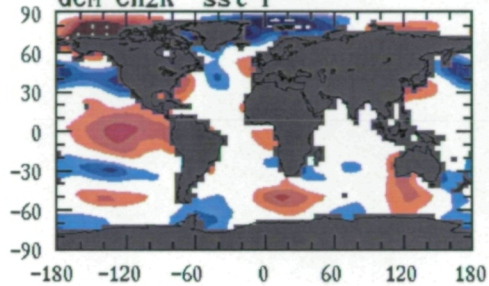
Tb Anomalies
during ElNino

 > 3.0

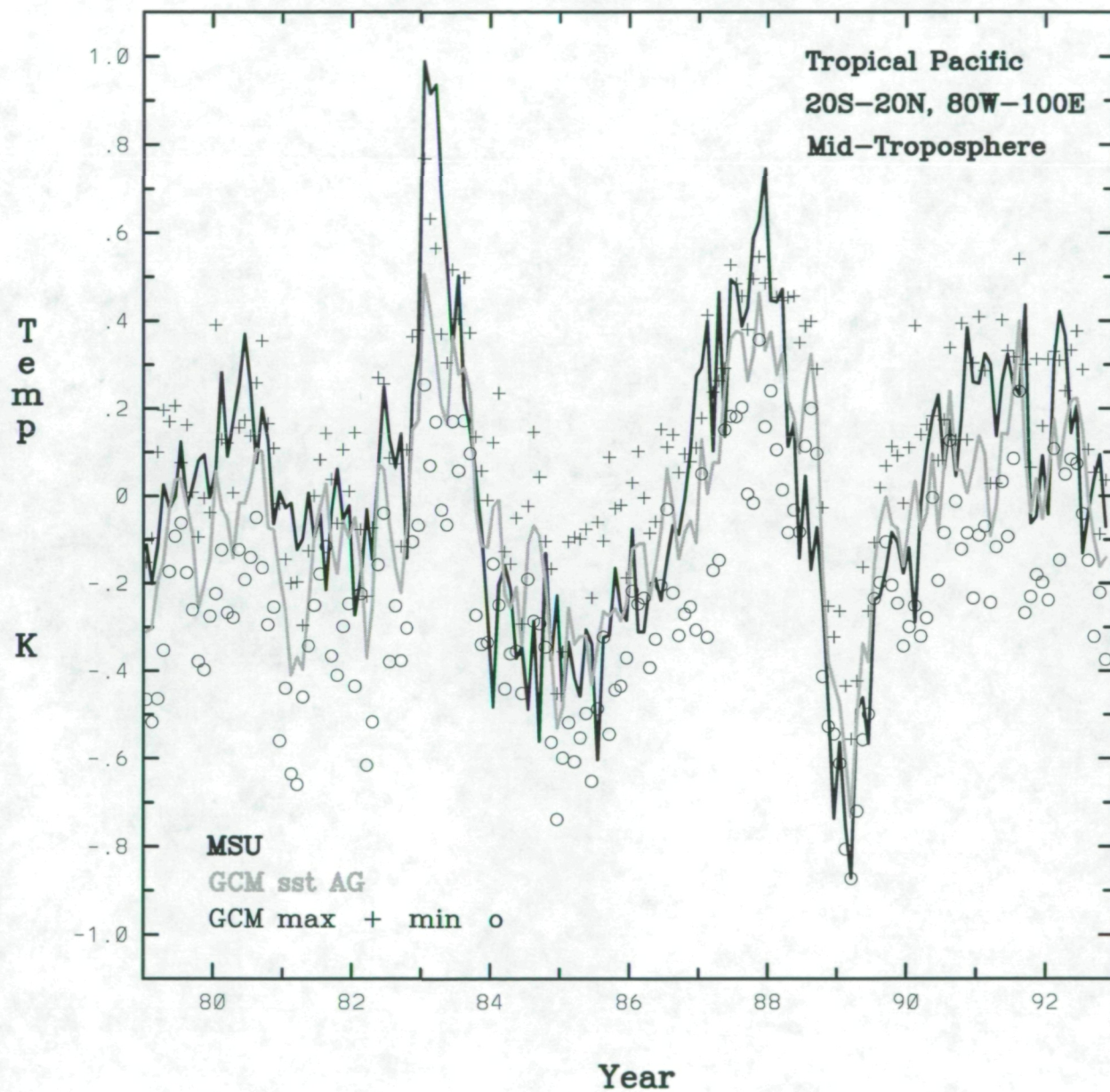


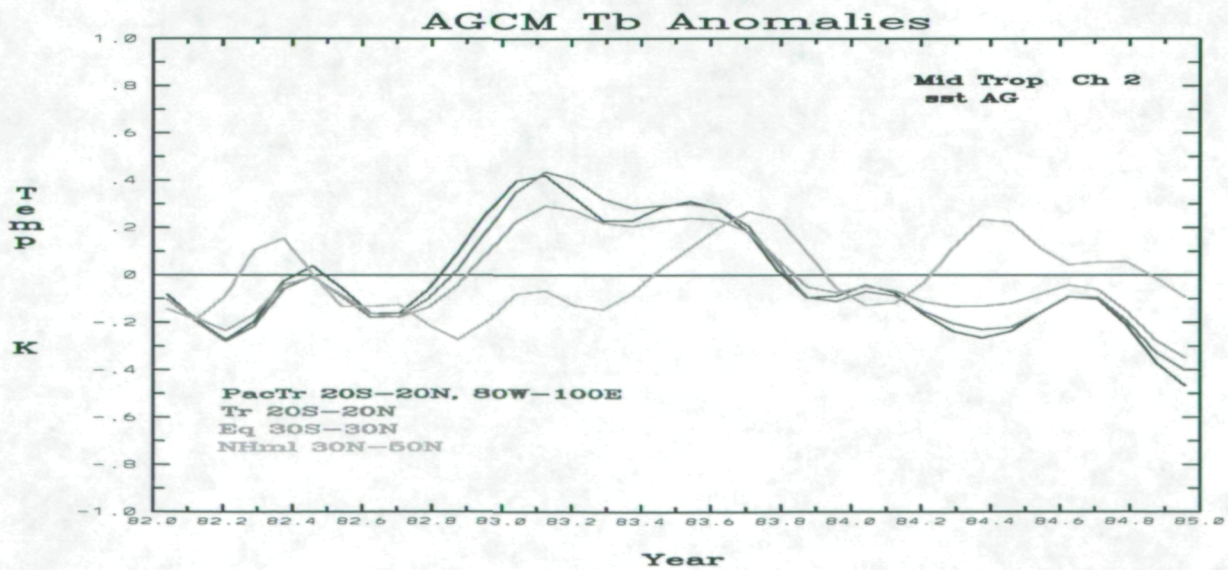
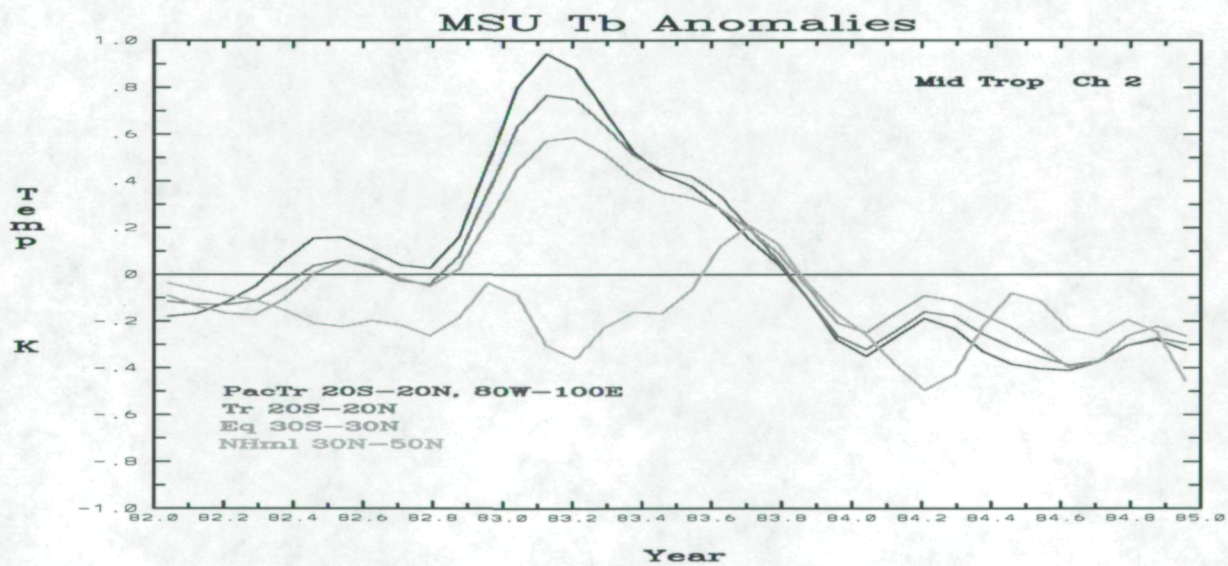
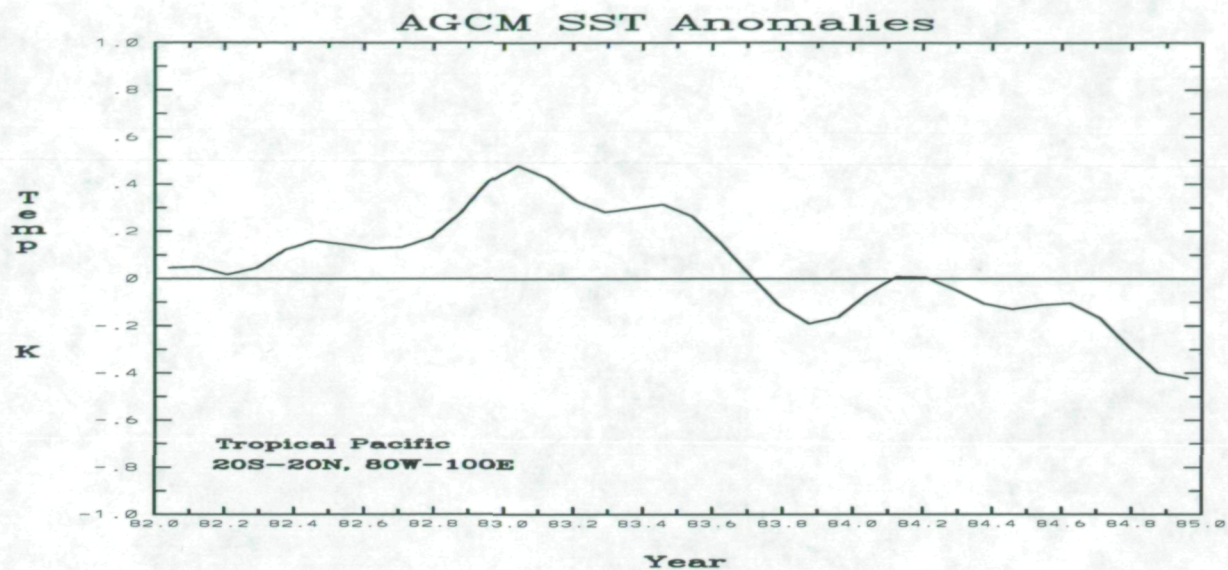
 < -3.0 K

GCM Ch2R sst F

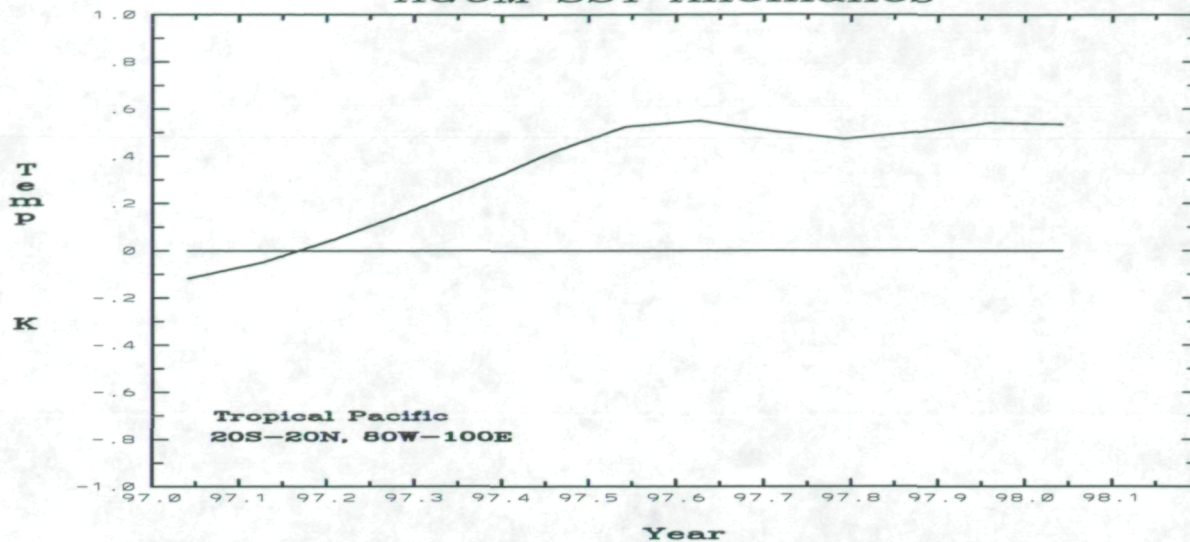


GCM vs MSU Ch 2 Tb Anomalies

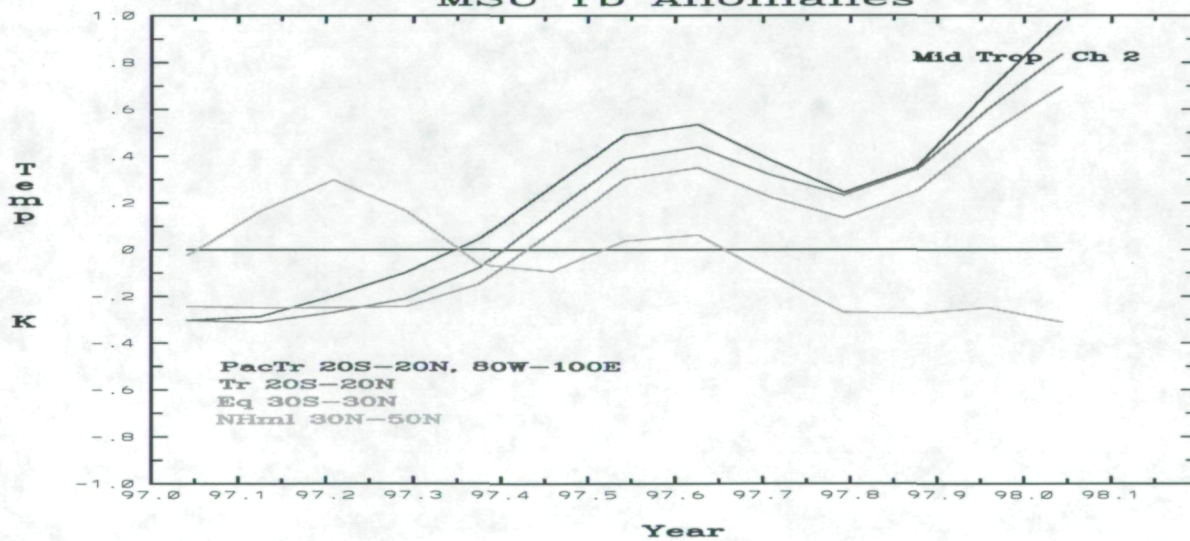




AGCM SST Anomalies



MSU Tb Anomalies



AGCM Tb Anomalies

